ABSTRACT

Title of Document:	COMPARISON OF INTERCONNECT FAILURES OF ELECTRONIC COMPONENTS MOUNTED ON FR-4 BOARDS WITH SN37PB AND SN3.0AG0.5CU SOLDERS UNDER RAPID LOADING CONDITIONS.
	Patrice Belnora Gregory, Doctor of Philosophy, 2010
Directed By:	Professor Donald B. Barker, Department of Mechanical Engineering

Electronic circuit boards can experience rapid loading through shock or vibration events during their lives; these events can happen in transportation, manufacture, or in field conditions. Due to the lead-free migration, it is necessary to evaluate how this rapid loading affects the durability of a leading lead free solder alternative (Sn3.0Ag0.5Cu) assemblies as compared with traditional eutectic lead based solder Sn37Pb assemblies. A literature review showed that there is little agreement on the fatigue behavior of Sn37Pb solder assemblies and Sn3.0Ag0.5Cu solder assemblies subjected to rapid loading.

To evaluate the failure behavior of Sn37Pb and Sn3.0Ag0.5Cu solder assemblies under rapid loading conditions, leadless chip resistors (LCR), ball grid arrays (BGA),

small outline integrated circuits (SOIC), and small outline transistors (SOT) were subjected to four point bend tests via a servo-hydraulic testing machine at printed wiring board (PWB) strain rates ≤ 0.1/s. The PWB strain was the metric used to evaluate the failures. The PBGAs and LCRs were examined with both Sn37Pb and Sn3.0Ag0.5Cu solders. There was no significant difference found in the resulting test data for the behavior of the two solder assembly types in the high cycle fatigue regime. PBGA assemblies with both solders were also evaluated at a higher strain rate, approximately 1/s, using drop testing. There was no discernable difference found between the assemblies as well as no difference in the failure rate of the PBGAs at this higher strain rate.

The PWB strain was converted to an equivalent solder stress index using finite element analysis. This equivalent solder stress value was used to compare the results from the LCR and BGA testing for Sn37Pb and Sn3.0Ag0.5Cu. Independently generated BGA data that differed with respect to many testing variables was adjusted and incorporated to this comparison. The resulting plot did not show any significant differences between the behaviors of the two solder assemblies under rapid loading outside of the ultra low cycle fatigue regime, where the assemblies with Sn37Pb solder outperformed the assemblies with SnAgCu solder.

COMPARISON OF INTERCONNECT FAILURES OF ELECTRONIC
COMPONENTS MOUNTED ON FR-4 BOARDS WITH SN37PB AND
SN3.0AG0.5CU SOLDERS UNDER RAPID LOADING CONDITIONS.

By

Patrice Belnora Gregory

Dissertation submitted to the Faculty of the Graduate School of the
University of Maryland, College Park, in partial fulfillment
of the requirements for the degree of
Doctor of Philosophy
2010

Advisory Committee:
Professor Donald Barker, Chair
Professor Abhijit Dasgupta
Professor Peter Sandborn
Associate Professor Charles Schwartz
Dr. Michael Osterman

Dedication

To my dad, James K. Gregory, my mother Patricia W. Gregory, and my sister, Jasmine K. Gregory. Each of you has provided me with so much support and encouragement during this stage in my life. Thank you so very much and I love you all so very much.

Acknowledgements

I must first acknowledge God and how He has blessed along this journey. "The steps of a good man are ordered by the LORD: and he delighteth in his way." Psalms 37:23

- ➢ To my parents:

Mom and Dad, I wonder if,
You know how much I care.
I got the good things, all I have,
Because you both were there.
I thank you for the time you spent,
Doing all you did.
You help me now;
you helped me then
When I was just a kid.
Unselfish, giving, loving, more...
You gave so much to me.
Without you, Mom and Dad, I don't
Know what on earth I'd be.
Thank you for the way you are,
Like angels from above;
I thank you both for everything,
And give you all my love. - *Joanna Fuchs*

- ➢ To my sister:

"Like branches on a tree we grow in different direction, yet our roots remain as one. Each of our lives will always be a special part of each other" –Anonymous
You are such a special part of my life. I want you to know how love you and value you. I have learned so much from you about thoughtfulness, giving and life. You are my sister and more important, my friend. I love you.

- ➢ To my advisor:

Dr. Barker, thank you for your wonderful guidance, support, and patience during this process.

- ➢ To my committee:

Dr. Dasgupta, Dr. Sandborn, Dr. Schwartz and Dr. Osterman, thank you for all you feedback and help with my dissertation.

- ➢ To my grandparents:

Grandma Emily, I thank you for always giving me words of encouragement and your concern for my happiness. You are a pillar of strength for our family and a true example of love and unselfishness. You are a joy to all that know you. I love you.

Tim, I do wish you could be here to see this. I want you to know that yes I finished and that "Sweet Pea" is doing great. Thank you for investing in me, caring for me, and supporting me through the years. I love you.

Mama, I too wish you could see this day. You empowered me and served as a model for the importance of education that has lasted three generations. You exemplified grace and compassion while always keeping family first. I love you.

➢ To my family
Aunt Rose, Aunt Yvonne, Aunt Gwen, Uncle Chris, Uncle Robert, Uncle Arturo, Aunt Rheva, Uncle Bennie, Uncle Raymond, Aunt Naomi, Uncle Albert, Aunt Delana, Aunt Carmen, Papa, and all my cousins especially, Julia, Nachell, Jody, Michelle, Jerry, Myles, Chrisonne and Christina, I say thank you for your prayers, well wishes and support for me. You are a large part of why I have made it to this point in my life and I am blessed have you in my life. I love you all!

➢ To my fellow *Team Barker* members (and friends too):
Jamie, Morrigan, Aaron, Mei-ling, Gil, Alan, Rachel, Saifa, and Beth---Thanks for all your support of me. I could not have asked for a better group of people to have to opportunity to work with. Gil I also want to thank you for all your help with the FEA modeling.

➢ To my friends:
Carey, Happy, Charles, Sophoria, Gleneesha, Bralyn, Taquina, Corey, Kendra, Byron, Bryon, Sean, Joi, Maureen, Nikki, Randall, Shantisa,
And my Girlfriends (Hey Girl!), Nicole, Anica, Calandra, Carmen, Renita, Bianca, Danielle, Fanta, Laneisha, Tracey, Celia, Tondra,

Thanks for the laughter, the prayers, the food, the weekend retreats, the phone calls, text messages, BBMs, ---all the good times. You all have been blessings in my life and I am thankful for you all!

➢ Special thanks you to
   o Morris Berman at ARL, for your assistance with the drop tower experiments
   o The David and Lucille Packard Foundation and AAAS, for your support
   o The mechanical engineering staff, especially Felicia, Fitz and Amarildo for your help and support
   o The Center for Minorities and Engineering: Ms. Parker, Ms. Hamilton, Mr Burhane, Mrs. Kamalidiin, and Ms Young—for being there
   o The Black Engineer Society, for allowing me get involved.
   o Dr. Gillyard, Dr. Streator and Dr. Ehme, for mentoring of me during undergrad and helping make this possible
   o The Promise Peer Mentoring Program, Maryland's Alliance for Graduate Education and the Professoriate, for the support

Table of Contents

List of Tables

List of Figures

Chapter 1: Introduction

The goal of this dissertation is to gain a fundamental understanding of the failure behavior of Sn37Pb and Sn3.0Ag0.5Cu solder assemblies under rapid loading conditions where any creep effects can be considered negligible. Electronic circuit boards can experience this rapid loading through shock or vibrations events during its life; these events can happen in transportation, manufacture or in field conditions. Obtaining this fundamental understanding will allow for better design of electronic assemblies to aid in their survivability during these rapid loading events.

This dissertation initially uses the PWB strain as the critical metric for determining failure. Using the PWB strain will allow for the prediction electronic component life regardless of the printed wiring board boundary conditions as long as the board strain in the vicinity of the component is known. The printed circuit board strain was chosen as the failure metric because it can be directly measured through quick calculation or simple finite element models and it makes no assumptions as to the exact location of the attach failure. Later analysis in the dissertation will use FEA modeling to obtain and equivalent solder joint stress to assess the durability relationships between SAC305 and Sn37Pb solder assemblies.

1.1 Motivation

The motivation behind this project is to assess the inclusion of electronic devices into artillery rounds for guidance purposes. A typical launch acceleration profile includes

an initial setback with a peak value of 10,000 – 100,000 G's applied over a timeframe of milliseconds, followed by muzzle exit buffeting ranging from 1,000 – 5,000 G's applied over a timeframe of microseconds. Such large accelerations can produce stresses and deformations that can exceed the structural limits of packaged electronic hardware. A basic understanding of the behavior of electronic assemblies under rapid mechanical loading is necessary before the project is ramped up to a high-G environment.

1.1.1 Project overview

The assessment of fatigue of electronic systems under rapid loading through vibration or shock events is very important. Current generation electronics are being used everywhere and in a way that may experience higher shock and vibration load levels than previous generations. Having a better understanding of the fatigue behavior can be used to determine the life expectancy of sets of electronic components used in electronic systems.

This dissertation will be discussing the development durability fatigue models based on PWB strain. In order to understand the approach taken, some general background of fatigue needs to be reviewed. Fatigue can generally be separated into high cycle and low cycle fatigue. Classically high cycle fatigue is understood to be driven by the stress level in a part, while low cycle fatigue is understood to be driven by the strain level in a part. High cycle fatigue failures involve elastic deformation and thus are easily expressed in terms of the stress in the part of interest. Low cycle fatigue failures involve plastic deformation and the stress levels in the part are generally

above the tensile yield strength of the material, thus it is easiest to express the fatigue in terms of the strain in the part.

Traditionally, experimental measurements of time to failure, or fatigue data, are plotted as stress or strain vs. life. Fatigue data is traditionally plotted in log-log space with the abscissa being the log of the time to failure and the ordinate being the log of the stress level in the part for high cycle fatigue, and the log of the strain in the part for low cycle fatigue, or the combined case where both high and low cycle fatigue can be present. This plot is typically know as an S/N plot standing for stress or strain versus life, N. It is recognized that in fatigue the dependent variable is life, which one would normally plot on the ordinate. The form of the plot in this thesis will use the traditional format for S-N plots where the life is plotted on the abscissa. When plotted in log-log space, low cycle fatigue and high cycle fatigue is recognized as a linear region of the fatigue data. There is also a transition, though not a sharp or distinct transition, between the behavior of materials in the low-cycle regime and the high-cycle regime. This transition typically occurs somewhere around 10^4 cycles. The linearity of the plot in the high cycle regime, above about 10^4 cycles is commonly referred to as the Basquin's power law relationship. Similarly there is commonly seen a low cycle linear region, below 10^4 cycles that is commonly referred to as the Manson-Coffin relation. If a parameter that is directly proportional to the stress or strain is plotted versus life in log-log space then a plot with this parameter will also be linear. Such a power law relationship will be used to relate board strain to cycles to failure for the rapid assessment model. The printed circuit board strain is

3

directly proportional to the stress in the component solder joint and can be easily demonstrated in finite element simulations. Hence, using board strain on the plot will yield the same slope as using the stress in the component; only the intercept will change. Board strain can be easily measured or predicted in the area near the component. The board strain can be converted to a board curvature using the printed circuit board thickness if a more generic quantity is desired. This PWB strain will also be converted to an equivalent solder stress for the development a master SN durability curve for the failure of Sn37Pb and SAC305 solders.

1.1.2 Component selection

To assess the behavior of electronic components under bending loads a list of likely used components was made. These components were evaluated for suitability in high-G environments. To first assess the survivability of the likely used components they have to be evaluated with respect to the types of motions they will experience. There are three types motions that components mounted to printed circuit boards can experience, transverse, normal, and bending. Of these three, bending is the most damaging because it will cause damage much sooner than transverse or normal loading. However, the potential of the components of shearing or pulling from the board was evaluated to initially narrow the component list To assess the potential risk of failure due to either normal or transverse motion, a simple calculation can be performed by dividing the load due to acceleration by the total cross sectional area of the package attach. This is illustrated in Figure 1.2.1. The load is equivalent to the package mass multiplied by the proposed acceleration. The intention is to see which

packages survive a maximum acceleration of 100,000 G's in the transverse and normal direction to ensure package does not shear or pull from the board. The 100,000 G's includes a dynamic amplification factor of 2, which gives a maximum quasi-static load of 50,000 G's. Finite element analysis done in previous work by CALCE [1] determined that components in a projectile may see loads of up to 50,000 G's during launch. This design goal is labeled in Figure 1.1, and based on this criterion certain packages can be deemed unfit for use in the intended application. It must be noted that the figure accounts for normal and transverse loading only; bending was not included in the component selection phase. The component types were narrowed down to four types, surface mount resistors and capacitors, ball grid arrays (BGA), small outline transistors (SOT), an small outline integrated circuits (SOIC). Surface mounted resistors were chosen because of their simplicity and their ability to give us a large data set per board due their small size. The surface mount capacitors are being studied in another project [37]. BGA packages were chosen because they are increasingly being used on PCBs because of the high I/O count they allow. SOIC and SOT components were chosen to examine leaded components. SOICs are more of a flexible leaded component, while SOTs are a stiffer leaded component. Including both will allow us to look at the different ends of the leaded components family.
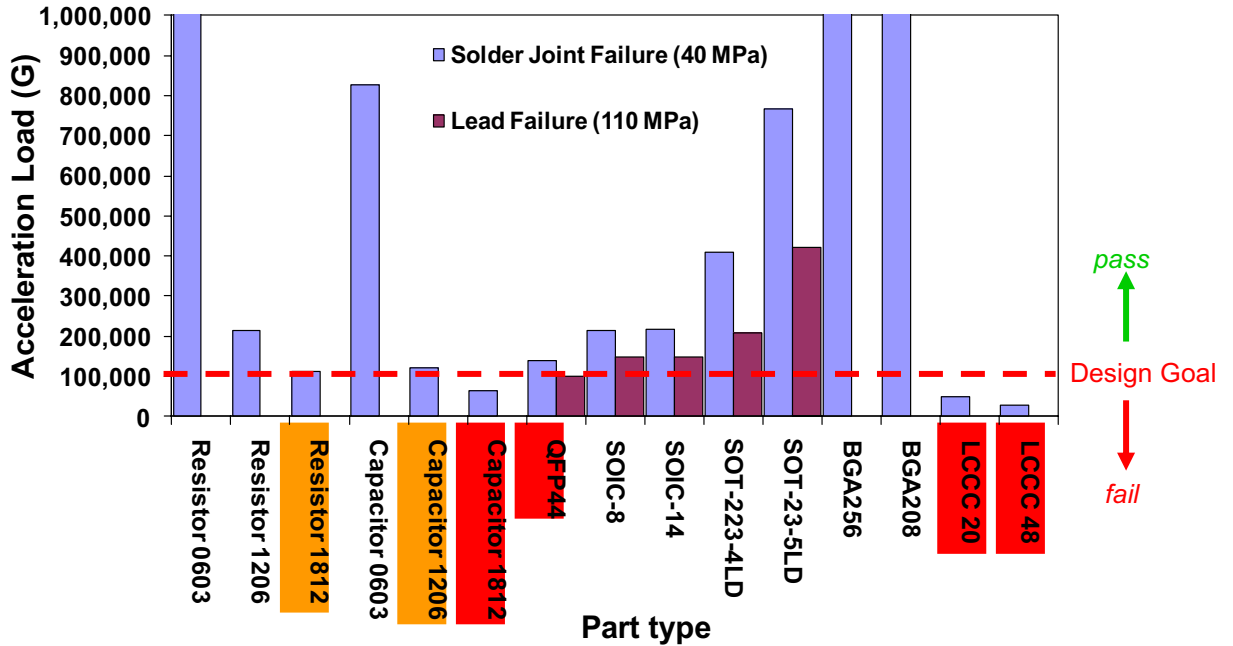
Figure. 1.2.1 Component Selection Diagram

1.1.3 Types of testing

This dissertation will use bend testing to aid in studying the behavior of electronic assemblies under rapid loading. Bend tests, specifically four-point bend tests, will be used to mimic the loads printed circuit boards see during shock and drop events. Four-point bending allows for a uniform PWB strain in the test region of the board. This uniform strain value will allow for testing of a relatively large set of components at the same time at the same strain levels, unlike testing done on a shaker table or in three-point bending. Testing a large number of components will increase the confidence of our model by allowing us to develop and use failure distributions in lieu of single failure data points.

1.2 Project objectives

In addition basic understanding of the fatigue behavior of the selected components and the creation of a master SN durability curve, this dissertation also will also create PWB strain based models for each of the selected components. This dissertation will use data generated by this project and data collected from studies not related to this project to create this master durability curve. The location of the failures will also be recorded and analyzed and any trends found will be noted.

1.3 Organization

A review of the current durability trends and available fatigue models for electronic assemblies is reviewed in chapter 2. Chapters 3, 4, and 5 are organized as separate data and related data. Each chapter will be re-written as a standalone, but related journal paper. Chapter 3 will explore the behavior of LCRs and SOIC under bending loads. Chapter 4 focuses on the bend and drop testing of PBGAs. Chapter 5 will bring the data of chapter 3 and 4 together, along with additional data from other tests to create a single master durability curve for Sn37Pb and SAC305 solder under rapid PWB bending. Chapter 6 will summarize the results from all three chapters of the dissertation and offer suggestions for future work.

Chapter 2: Literature Review

Much testing has been done on the failure of electronic components under bending and shock loading conditions. This literature review seeks to explain what models are currently available to estimate the fatigue life and show how bend testing can be an important tool in the evaluation of electronic components. It will also explore the need of including high strain rate testing in the study of the reliability of electronic components.

2.1 Current fatigue modeling/assessment techniques

Fatigue-life models can typically be divided into four main categories. Failure models that are based on equations, models that a based on analytical methods, models that are based on numerical or finite element techniques and models that are based on experimental results.[2] These categories are often combined with some studies, but generally there tends to be a dominant method or category used in the model creation. A full review of the literature based on each model type can be found in the appendix.

2.2 Bending

This section will focus on the bend testing that has been conducted and explore the trends that other have found through the bend testing of PWAs. Bend testing has been found to be a crucial part of understanding how electronic components fail under fatigue. Four point bending is the most preferable bending type testing. It allows for a less complex analysis of failure and for the testing multiple components

at the same strain level at the same time unlike three and five point bending which can allow for an individual component to experience different strain level along the component during a test. Four point bend testing has also been shown to be relatively insensitive to misalignment issues.[15] Therefore, bend testing will be one of the main tools this project will used in the model development along with drop testing.

Bend testing is a good tool to use for mimicking the loads electronic see in their lifetime, in lieu of using shaker tables. During bending the loading rate can be changed to mimic dropping or the magnitude and rate can be lowered to mimic more everyday conditions.

Four point bending has been shown to be useful in the testing of electronics because of the earlier mentioned reasons. The results of some four-point bending experiments are detailed here. Harada et al [16] used four-point bending to verify the reliability of flip-chip BGAs. Two groups of components were tested, those mounted for three weeks and those mounted for one-hour. Failure occurred sooner in the one-hour after mount packages. The strain ranges were from 2000 microstrain to 9000 microstrain. A strain rate dependence on the strain value to failure was found. Cracking in the solder ball was observed as the package substrate side.

 Ilho et al [17] compared fatigue life of 95.5Sn4.0Ag0.5Cu to 63Sn37Pb using plastic ball grid array, PBGA, 256 I/O packages using four-point bend testing. The bend testing was done using a special bend tester made using an electromagnetic coil.

When the applied load to the specimen is small, the Pb-free solder has a longer fatigue life than Pb solder. The fatigue life of lead-free solder was found to be less sensitive to applied loads. As the applied load decreases, the relative fatigue life of lead-free solders increases. A visco-plastic deformation analysis was used to quantitatively examine the resistance to creep, plastic and inelastic deformation of solder.

Bending has also been used as a tool to study shock loads. Keat, et al [65] developed a method to characterize the solder joint performance using board surface strain. It employed the use of a specially designed shock test board. This board, a BGA, and rigid masses were used for dynamic bend testing. Linear solder joint behavior was assumed due to the high strain rate loading and the strain rate effect was neglected because the solution scheme only pronounced for non-linear material response. The strain response was found to be directly related to the stress in the solder joint through modeling. The board thickness is the coordinating factor between the two. The board strain measured at the corner of the package correlated with the stress in the corner joint.

This section illustrated the use of PWB strain as a viable option for describing failure. It was shown to relate to the stress in the solder. The tests described here also conflict on the effects of thermal ageing on the survivability of electronic assemblies.

This section will explore the high rate testing of PWAs and what types of component have been investing at high loading rate and the trends that have been seen. Drop testing is a common tool used to test for survivability of electronic under high strain rates. This subject has been studied using various test methodologies and models have been developed to explain the behavior of electronic under higher strain rates. Wong et al [11] found there to be three main causes of board level drop impact failure, elongation and bending of the interconnect from the difference in the flexing of the board and package, the inertia force from the package, and the longitudinal stress wave from impact. Lall, et al [19] developed a methodology "to determine the damage progression versus number of drops by studying the transient strain history of the test boards" [19]. They developed drop and shock survivability model using wavelet transforms and damage proxies. 63Sn/37Pb and lead-free solder balls and 95.5Sn4.0Ag0.5Cu solders were studied using 10 mm, 100 I/O BGAs and 8mm 132 I/O BGAs. Failure was observed at the solder interconnect at the package and the board interface, copper-trace, and printed circuit board resin cracks under the copper pads. The majority of the failures, however, were in the solder. They also developed a transient strain based damage index to measure damage in aged and unaged samples. Board strain was converted into solder interconnect transient strain history using Hexahedral Reduced Integration Element Models with Timoshenko-Beam Element Interconnects. 63Sn37Pb and 95.5Sn4.0Ag 0.5Cu solders were tested with board finishes of immersion silver, ENIG, and HASL. Failure was observed in the solder interconnect as the package and board interface, in the copper trace, and in the

board under the bond pads; though most were in the solder for both solder types. The aged lead-free samples had a lower survivability under shock and vibration loads.

Darveaux, et al [20] explored interface failures using impact testing. A ductile to brittle transition strain rate was used to explain interface failures using tensile testing to measure performance. It is defined as a metric to quantify the performance of a specific joint relative to interface failure. Samples were tested at 22ºC and strain rates were calculated from the equation, $d\varepsilon/dt = \dfrac{\left(dz/dt\right)}{h}$, where h is the solder joint height and dz/dt is the displacement rate of the testing machine crosshead. Solder joint array tensile testing was employed to understand how intermetalic failures affected performance. The strength of the solder joint was found to be rate dependent.

The impact surface finish has on the failure rate of electronic has also been investigated. [20] Chong, et al. studied the drop impact solder joint reliability of plastic ball grid array packages, no leaded very-thin quad flat, and plastic quad flat pack packages. A lead based and a lead free solder, 62Sn36Pb–2Ag and Sn4Ag0.5Cu and two different pad finishes, organic solder preservative and electroless nickel immersion gold were tested. The type of surface finishes was found to have a significant impact on the solder joint reliability between a package and the board. The lead-free solder joints on ENIG finish revealed weaker drop reliability performance than the OSP finish. From simulations, they found the peel stress in the direction of drop to be the driving force behind drop failures. The integrity of the copper traces, vias and resin were found to be equally important in the drop/impact

reliability. The PQFP did not fail in their study due to the compliancy of its leads. The most robust part however was the VQFN, because of its small size. Through FEA, they found that using only on elastic model can overestimate the stress by 50%; hence the plastic behaviors of the materials must be accounted for in drop/impact loading.

Chong, et al [21] also examined the effect of surface finish under drop condition. They tested leaded components (PQFPs) and non leaded components (PBGAs and very thin profile quad flat no-lead-VQFN) using 36Pb62Sn2Ag and Sn4.0Ag0.5Cu using OSP and ENIG finishes. The packages were dropped in a position face down, parallel to the drop surface and the board had clamped-clamped boundary conditions. The majority of the PBGA failure sites were detachment from the copper pad. Copper trace and resin cracks were found to be second cause of the PBGA failure. No failures were found in the PQFPs and VQFNs. OSP was also found to be a better choice in surface finish than ENIG. This project will be using OSP as the board finish avoiding the early failures seen in the ENIG samples.

The failure mechanisms in impact tests have been explored. Seah, et al [23] tested SnPb, SnAg and SnAgCu solder joints on ENIG pads and they were found to exhibit combinations of bulk solder and intermetallic failure, and SnPb, SnAg and SnAgCu on OSP exhibited almost complete IMC failure at the pads under drop impact. The fatigue failure of solder joints in drop impact was dominated by the crack initiation phase. For SnAg, SnAgCu and SnPb on ENIG pads, failure was observed to initiate

in the bulk solder at the joint corners for most cases. This initiation was not observed for the SnAg and SnAgCu and SnPb solders on the OSP pads. The crack initiation was thought to have occurred in the intermetallic region for the OSP pads. Low strain-rate and low strain tests were also found to produce considerably different failure modes than drop impact or high speed bend testing.

These failure mechanisms have also undergone a root cause analysis to determine why they failed. Wong, et al. [24] found that high strain rate tends to raise the fracture toughness of ductile materials while it lowers the fracture toughness of brittle materials. This makes the drop impact reliability of interconnects to be controlled more by the fracture toughness of the brittle intermetallics than by its bulk creep strength. It is noted that the solder alloys and pad finishing that are ideal for temperature cycling may not be ideal for drop impact and that some report SnAgCu solder performs worse under impact than SnPb eutectic solder but SnAgCu was said to have higher impact fracture energy. Using D'Alembert's Principle, it was shown that the interconnection strength due to board bending is two orders of magnitude higher than the stress due to acceleration. This accounts for the different failure rates under drop and bending loads. It is clear that the fracture strength of the IMC and IMC-solder bond depends both on the types of solder as well as the pad finishing.

They tested the behavior of Sn37Pb, Sn3.5Ag, Sn3.8Ag0.7Cu, Sn2.5Ag0.8Cu0.5Sb, and Sn58Bi solders on electroless Ni-P/Au (ENIG), HASL, OSP, and Immersion tin (Tin) under static shearing and impact shearing. The impact fracture strength of

solder joint was found to be higher than its static fracture strength in most cases. SnAg solder had the highest impact strength and BiSn solder had the lowest. SnPb solder showed mainly bulk solder failure. The lead-free solders showed a mixture of intermetallic and bulk failure. The SnAgCu solders had comparable impact fracture strength to SnPb solder but had much lower impact fracture energy. OSP and Tin finishing outperformed ENIG and HASL in both impact fracture strength and impact fracture energy.

Testing has shown that vibration can be used to obtain drop testing like conditions. This was used by Marjamäki, et al [25]. By applying harmonic vibrational loads to printed circuit boards at their resonance frequencies, they achieved similar loading to drop testing, in spite of difference in the bending behavior of the boards. The failure modes found were the same as those Lall et al. [19] discovered and were determined by the vibration amplitude. The shift in failure mode from bulk solder to intermetallic cracking was noticed with an increase in the vibration amplitude. By using vibration to study the failure modes under shock loading instead of drop testing, life prediction can be more easily made because of the constant bending amplitudes during the test, tests can be carried out in less time and the more control of the environment is possible. The most important difference between vibration and drop test was found to be that the bending of the printed circuit board is constant during vibration testing, and in drop testing the amplitude is reduced after each impact. Vibration testing uses the resonance phenomenon to generate large constant bending amplitude with a small harmonic force. Drop testing employs the use of

higher frequency modes and their interaction with the lower natural frequencies complicate the stress histories in solder interconnections. This vibration testing done to achieve drop-like conditions is similar to the testing presented in this work. Using bending, the loading rate can be set to fast with a steady and slower unloading rate but eliminating the higher frequency content which can lead to resonance issues.

There have also been studies into how consumer portable electronic are affected under drop conditions because of their increasing smaller size and wide-spread use. Seah, et al [23] assessed how to best test these products under drop conditions by evaluating what measurement to take and where and how to get them from board level testing conditions. They determined that strain and acceleration measurement were both key in evaluating the reliability of these electronics. Tests were done to understand the relationship between acceleration, strain, and drop orientation and another set to obtain data on portable electronics under drop conditions. BGAs and CSPs were tested.

This section has demonstrated the benefits and performing drop testing on PWAs. Drop testing is very important in the study of the reliability of electronics because of the harsh conditions that electronic components can experience. As electronics become more and more portable, there is an increased likelihood of electronics experiencing a high rate loading event, whether it be an accidental drop to the ground or the a breaking apart of boards during assembly. SnAgCu based solders have been shown to have the highest survivability rates for the reviewed lead-free solders.

However, there is no consensus among the papers on whether strain rate affects the durability of electronic assemblies or the survivability difference between lead and lead free solders.

2.4 Failure analysis

The investigation of the location of the failure site and any trends seen this location over the test range is an important part of testing electronics. The typical failure sites of electronic component are in the bulk solder, in the solder intermetallics, through the copper trace, and in the board material underneath the bond pad (at the interface). Interface failures occur due to rapid loading of the solder joint and a tensile component to the loading. Under rapid loading the bulk solder must bear the stress of the high strain rate. The solder's compliancy allows for strain relief. Stresses build up in the joint interfaces causing failure in the interfaces. [26] Much analysis has been done of the location of the failure to understand the root cause of the failure. Rooney et. al [27] performed a detailed failure analysis on micro-, flex, and laminate BGA packages, ceramic chip scale packages (CSP), and central packet switches (CPS) that had been tested under three-point bending. Four failure modes were found through cross-sectioning. The first was through the solder along the board side. This failure type is attributed to the solder joint being solder mask defined in this area and the solder fillet not extending around the side of the pad. This was the most common failure mode. The second failure type was through the solder on the package side. This failure type is said be caused by solder fatigue. The third failure mode consisted of board material failures, i.e. cracked laminate, delamination of the printed circuit

board from the solder pad, and fracture of the solder mask. The fourth mode was copper trace cracking where there was no cracking of the solder mask or printed circuit board laminate. This failure type was only noticed in more severe bending stress conditions.

2.4.1 Failure site transitions

From the failure analysis there has also been noted the existence of a transition in the location of the failure depending on the loading rate and stress level. Jonnalagadda, et al [28] made note of this phenomenon while testing, Sn62Pb36Ag2 and Sn95.75Ag3.5Cu0.75, under three point bending. In low cycle failure (high load levels), all of the observed failures were on the printed circuit board side and PCB failure was most dominant. In high cycle failure, solder failure was observed. In medium cycle failure, PCB and solder failures were found. Darveaux, et al [26] explored interface failures and suggested a failure mode transition occurring where the bulk solder strength has increased past that of the intermetallic based on strain rate because the intermetallic portion of the solder balls have lower strength as strain rate increases because they have higher melting points. Varghese et al. [29] also found this rate dependence in the location of the failure. The failure site transitioned from the solder to the copper trace/board interface as the strain rate increased. This dissertation will perform failure analysis to note if any such transitions exist during the bend and drop testing.

2.5 Lead-free solder

There has been a great deal of interest on the effect transitioning to lead solder will have on component life. A consortium between the Joint Council on Aging Aircraft, JCAA, and the Joint Group on Pollution Prevention, JG-PP, was formed to evaluate the suitability lead-free solders and finishes in their applications.   They studied thermal, cycling, thermal shock, vibration, mechanical shock, and combined vibration/thermal cycling. For the purposes of this discussion only the vibration and mechanical shock studies will be reviewed. A total of 55 components were tested in the families of ceramic leadless chip carriers (CLCC), plastic leadless chip carriers (PLCC), thin small outline packages (TSOP), thin quad flat packs (TQFP), BGAs, and plastic dual inline packages (PDIP). The board finish was immersion Ag. The solder types tested were Sn3.9Ag0.6Cu, Sn3.4Ag1.0Cu3.3Bi, Sn0.7Cu0.05Ni, and Sn37Pb. Two groups were tested, as manufactured and reworked. The reworked sets were boards that were originally lead-based and had the components replaced with some lead and some lead free ones. The vibration studies were performed by Boeing For example, in the case of the BGAs the SnPb outperformed the SAC.   The orientation of the TSOPs determined how the solder performed. On the reworked boards the lead solder outperformed the lead free solder in most cases. The differing results may be attributed to the small amounts of lead that may have remained on the board after rework. [30] The mechanical shocks were performed by the American Competitiveness Institute. In these shock tests, it was found that the solder was not root cause of any of the recorded failures.   The recorded failures were due to packaging or wiring defects (copper trace failures and failures at the trace BGA land

neck area) and these failures were found only at very high shock levels. [31] These tests demonstrate the importance of examining how component orientation in leaded components affects time to failure.

2.6 Durability trends

There is myriad of information available on the durability of different solders as noted in some of the aforementioned studies. This information can vary based on test conditions like vibration or shock, whether aging was used and how long the samples were aged, board finishes, etc. Many studies found that lead free solders were more durable than lead based solders in a low cycle vibration environment. [6,12,13,14]

Park [6] found that Sn3.5Ag0.75Cu solder has a longer fatigue life than 63Sn37Pb solder in all of their testing conditions. Zhang [14] found that Sn3.9Ag0.6Cu solder behaved better than the Sn3.5Ag solder. Zhang, et al [32] also continued their testing to add for creep analysis. Sn3.9Ag0.6Cu shows much larger creep resistance the Sn37Pb. This difference became smaller as the equivalent stresses decreased. The lead free alloys were shown to have a superior durability. The results showed that the durability of the SAC305 was better than the SnPb eutectic in low cycle fatigue. The opposite was found to be true for high cycle fatigue. [12,13]

Other studies have found that lead free solder are not as durable as lead solders. The 95.5Sn4.0Ag0.5Cu solder interconnects had a lower shock and vibration survivability compared to 63Sn37Pb interconnects. [19] Qi, et al [33] tested dual in-line packages in random vibration conditions and found the durability of SnPb eutectic solder to be

20

better that that of Sn3.0Ag0.5Cu. The SAC solder was tested with four different board finishes, OSP, immersion silver, immersion tin, and ENIG. The SnPb was tested with a HASL finish. The SAC solder was also found to be more sensitive to aging temperature and duration of aging; their performance decreased as the time and temperature increased. The immersion tin board finish was found to perform best.

Seah, et al. [34] developed a high speed bend tester to bend test printed circuit boards at the high flexing frequencies of drop impact and used this testing to develop a constant amplitude power law fatigue curves. The lead free solders were found to fail in much fewer cycles than the SnPb solders on both ENIG and OSP pads. Solder joint reliability was found to be strain rate dependent. A decrease in reliability with frequency was found for SnPb on both OSP and ENIG and SnAg on OSP, but not for SnAg on ENIG.

Darveaux [20] found mixed results in his testing based on the different pad finishes. For the nickel/gold plated pad, the 63Sn37Pb was better than SAC305, which was better than SAC405. Multiple passes through reflow was found to help the SAC alloys perform better. For the electroplated nickel/gold pads in the aged condition, the order of robustness against interface failure was SAC305 followed by SAC405 followed by 63Sn37Pb. For the copper pads in the unaged condition, the order of robustness against interface failure was 63Sn37Pb better than SAC305, which was better than SAC405. The final conclusions were that Ni/Au is the most robust pad finish and Cu-Sn was the least robust pad finishes. Robustness was measured against

interface failure by looking at the interaction of solder alloy, pad finish, reflow conditions, and thermal aging.

Other trends were also found involving durability and failure sites. Shetty et al [5] found that the durability of the components lower by 65% under negative curvature than under positive curvature. Varghese, et al. [29] found that the failure site depends on the loading conditions, the board design and the dynamic properties of the materials in the printed wiring assembly. A power law durability model was developed in terms of the printed wiring assembly strain and strain rate to explain fatigue failure envelopes. The durability of the solder was found to be variable with solder plastic strain but not on plastic strain rate. Qi et al [35] tested 2512 chip resistors under step-stress random vibration. Sn3.0Ag0.5Cu was tested with four different board finishes OSP, immersion silver, immersion tin, and ENIG and Sn37Pb was tested with HASL. He found no significant difference in the time to failure between the lead and lead free solders.

2.7 Summary

There is a lot of research being done to study the fatigue of solder. Bend and drop testing were shown to be valuable tools in the studying of electronics. There are ample failure models for different solders and component types. These models, however, are typically based on a limited data from one specific testing condition and board configuration. There is no consensus on the durability trends between lead and lead free solder, though there is agreement that OSP is the best board finish for use in mechanical loading. Most of the testing was done in on specific failure region (ultra

low cycle, low cycle, high cycle, etc.) with conclusions based on sparse data This work presented in this dissertation will gain a fundamental understanding and overcome this lack of agreement for a rapid loading assessment of SAC305 to Sn37Pb solder assemblies by combining a significant amount of data from different mechanical testing methods (drop, mechanical cycling, and vibration), different test coupons and configuration, component types, and solders over a wide range of failure regions to create a master fatigue curve.   The PWB material (FR-4) and PWB thickness, however, will be constant between each of the tests.

Chapter 3: Isothermal Fatigue Behavior for Surface Mount Components Assemblies with SnPb and SAC305

The following components were chosen for an experimental test program to study solder fatigue properties; 2512 leadless chip resistors (LCR), small outline integrated circuits (SOIC), and small outline transistors (SOT). The 2512 LCR was chosen due to its relatively large size to ensure fatigue failure would occur in a reasonable amount of time. The SOT and SOIC components were chosen to investigate the behavior of leaded components on solder failure and to serve as a comparison for the LCRs.

The overall purpose of these experiments is to obtain more confidence in the solder fatigue exponent and to investigate whether leaded components could affect the value of this fatigue exponent. The tests are run at a frequency that results in a loading rate that basically negates any solder creep effects.

3.1 Approach

A MTS servo hydraulic material testing machine was used for the bend testing. This machine allows for variation in the loading rate and level. This permits the testing of the effect of different loading rates on the time to failure. The MTS also allows for single load testing and cyclic testing. Four-point bend testing was done to allow for a constant bending moment in the middle of the board. This is illustrated in Figure 3.1.

The coupon was tested such that the components were between the inner supports. This ensures they will experience a constant bending moment during the test. Each coupon was tested at a specific displacement. The coupons were tested as-reflowed, meaning no thermal ageing was done. Darveaux [20] studies the effects of pad metallization, solder alloy, reflow conditions, and post reflow thermal aging on interface failure. The study found that thermal ageing (24hrs / 125ºC) increased the fatigue life of SAC305 and Sn37Pb on copper pads but Lall [18] found exposure to thermal aging reduced shock and vibration survivability of 95.5Sn4.0Ag0.5Cu solder interconnects because the microstructure of SAC alloys makes it more susceptible to ageing than SnPb. The test assemblies used in this project were not thermally aged but the testing ran the course of one year. As a result some test coupons were aged at room temperature over the duration of the testing. The microstructure of SAC alloys makes it more susceptible to ageing than SnPb.
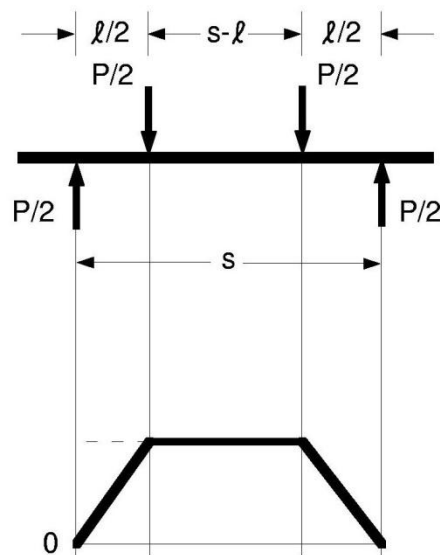

Figure 3.1 Four point bending illustration

Printed wiring board strain was recorded along with continuity during each test. The continuity monitoring was achieved using a resistance network. When the resistance increased above 300 Ω, the component was considered to be failed as per IPC SM785. A Labview based software program was used for the data collection.

3.2 2512 LCR board

2512 leadless chip resistors (LCR) were chosen to evaluate the high cycle fatigue failure properties of lead and lead-free solder assemblies. The test coupon consisted of 24 resistors and had one strain gage site, as shown in Figure 3.2. It was 14 by 3.65 cm and 1.65 mm thick, four layer FR-4 board. The test coupon is shown in Figure 3.2. The coupon had bare copper pads to limit the board finish and solder interaction effects. The test coupons were stored in a desiccant jar to prevent any oxidation of the copper pads before reflow. Two sets of test coupons were built, one set with Sn37Pb solder and one with Sn3.0Ag0.05Cu (SAC305). The test coupon also has two different pad sizes to investigate the effect of a larger bond pad size on time to failure. The pad dimensions are 1 mm and 1.6 mm wide, with a constant length.
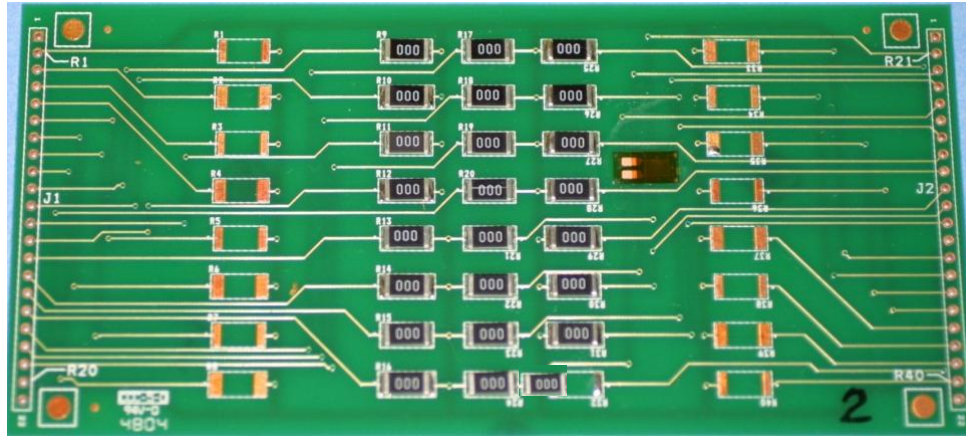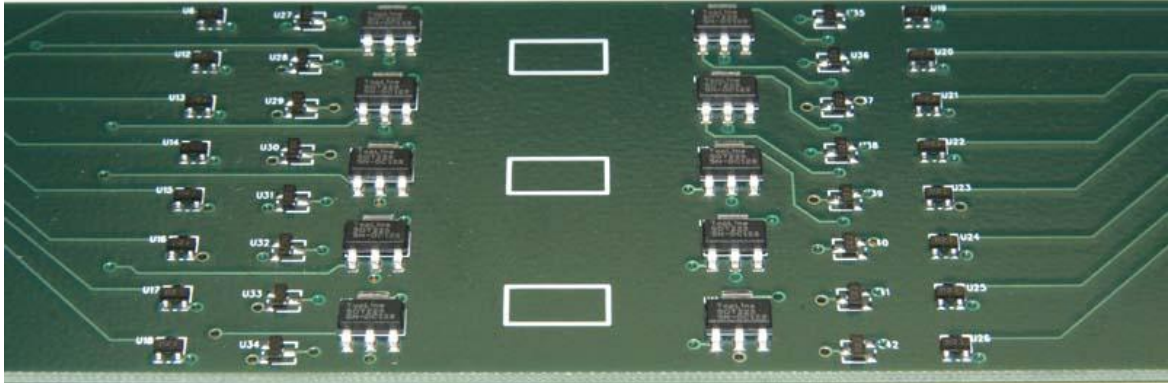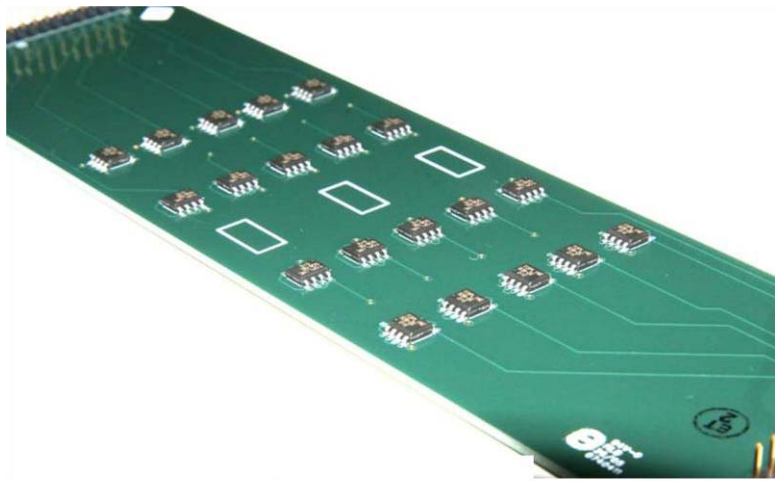
Figure 3.2 LCR Test coupon

3.3 SOIC & SOT boards

To examine the behavior of leaded components, SOIC and SOT were chosen. The SOT coupon has a combination of SOT-23 and SOT-223-4 components. This coupon is shown in Figure 3.3. There are a total of ten SOT-223-4 components on the coupon and thirty-two SOT-23 components. Sixteen of the SOT-23's are oriented parallel to the longest side of the board; the other sixteen are perpendicular to the longest side. The SOT-223-4's have dual monitoring; failure in the smaller leads and larger lead was monitored separately. Figure 3.4 shows the SOIC coupon. Ten of the SOIC parts are parallel to the longest side of the board; the other ten are perpendicular to the longest side.

The SOIC and SOT boards are constructed with SnPb eutectic HASL finish on the copper pads. Each coupon also has three predetermined strain gage locations. During the testing, however, only the center strain gage location was used.

Figure 3.3 SOT test coupon


Figure 3.4 SOIC test coupon

3.4 2512 LCR Testing/ Results Discussion

Basquin's power law relation, $\sigma^b N = \text{constant}$, can be used to model high cycle fatigue. The ordinate can be any parameter deemed proportional to the stress or strain at the failure site. Printed wiring board strain range was used as the ordinate in this study. The slope given by using the PWB strain range will be the same as the slope given using the strain or stress value at the failure site with the PWB thickness as the coordinating factor [57].

There are many SnPb eutectic solder high cycle fatigue exponents. Bulk solder samples give a range of b between 9 and 10[44]. For lead and solder combined, the value of b is equal to 6.4 according to Steinberg[3]. Mil-Std-810G, Section 514.6A, for accelerated testing says values of b are commonly between 5 and 8 and a value of 6 is commonly used for sinusoidal environments. CALCE's previous experimental experience gives b between 4 and 6 [44].

A sample strain plot for the four point test coupon is shown in Figure 3.5. It can be seen that the amplitude ratio, s_{min}/s_{max}, is nearly zero for this test, as only tension to near zero tension testing was performed. The testing was continued until approximately 75% of the components registered a failure. This was done for failure analysis purposes so as to not completely destroy any cracking evidence in the failed components.
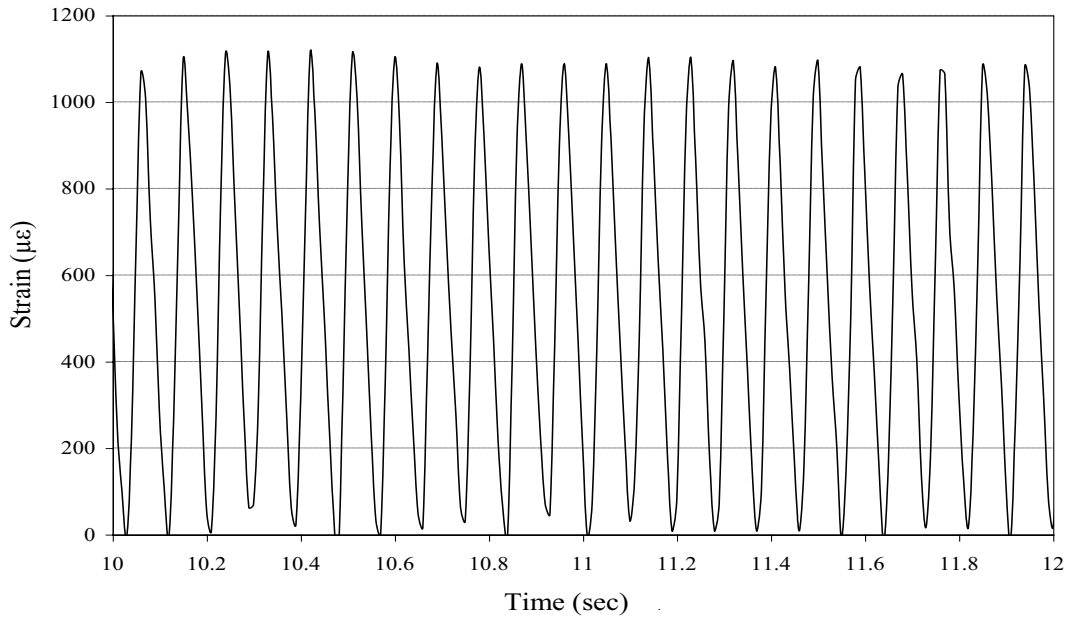
Figure 3.5 Sample strain plot

A two parameter Weibull distribution was used in analyzing the data. A typical Weibull distribution can be seen in Figure 3.6. It is important to note that the shape factor, β, is 3.5 for this coupon. The Weibull shape parameter for mechanical loading is not as high as one would see in thermal cycling fatigue. The shape parameters in these test range between 2 and 4. The Weibull distributions for all of the data points can be found in the appendix. The characteristic life, η, for 63.2% failure is plotted in log-log space. This gives a linear correlation for the printed wiring board strain range vs. cycles to failure. The failure data is plotted in a classic SN like durability plot in Figure 3.7. Each failure point represents one part. The plot represents 240 failure parts (24 coupons per board and 10 boards). The cycles to failure for each of the 24 components on the board were used to obtain a Weibull distribution.

Figure 3.7 shows the durability plot for the 2512 SnPb eutectic solder assemblies. The regression gives a fatigue exponent, *b* value of 5.9. Note that this is the inverse of the exponent shown in the above plot because the trendline equation is in the form $\sigma = CN^{-1/b}$. The 90% confidence interval of this *b* value is from 4.3 to 9.8. The data points for this plot are given in Table 3.1. The 90% confidence interval for the fatigue exponent spans all the common values for the referenced fatigue exponent.
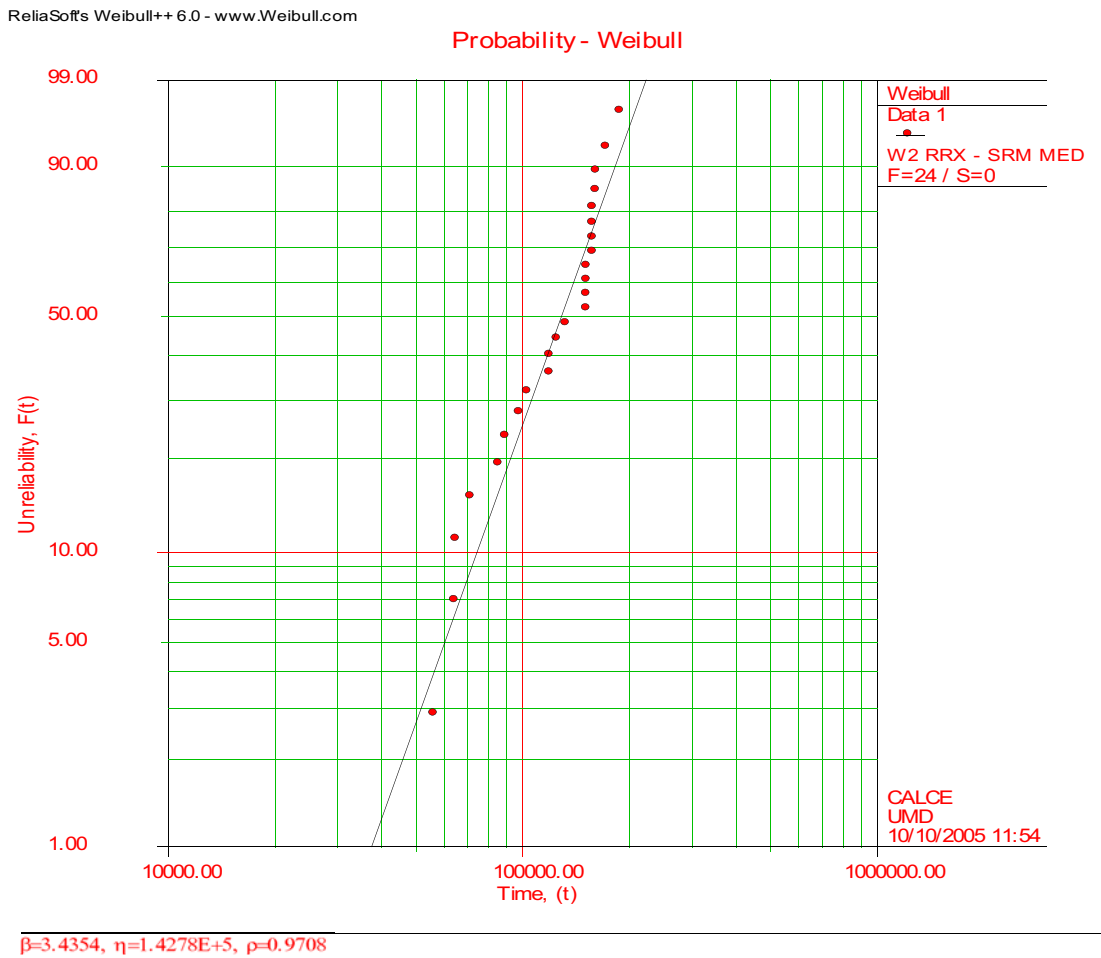
Figure 3.6 Typical Weibull distribution
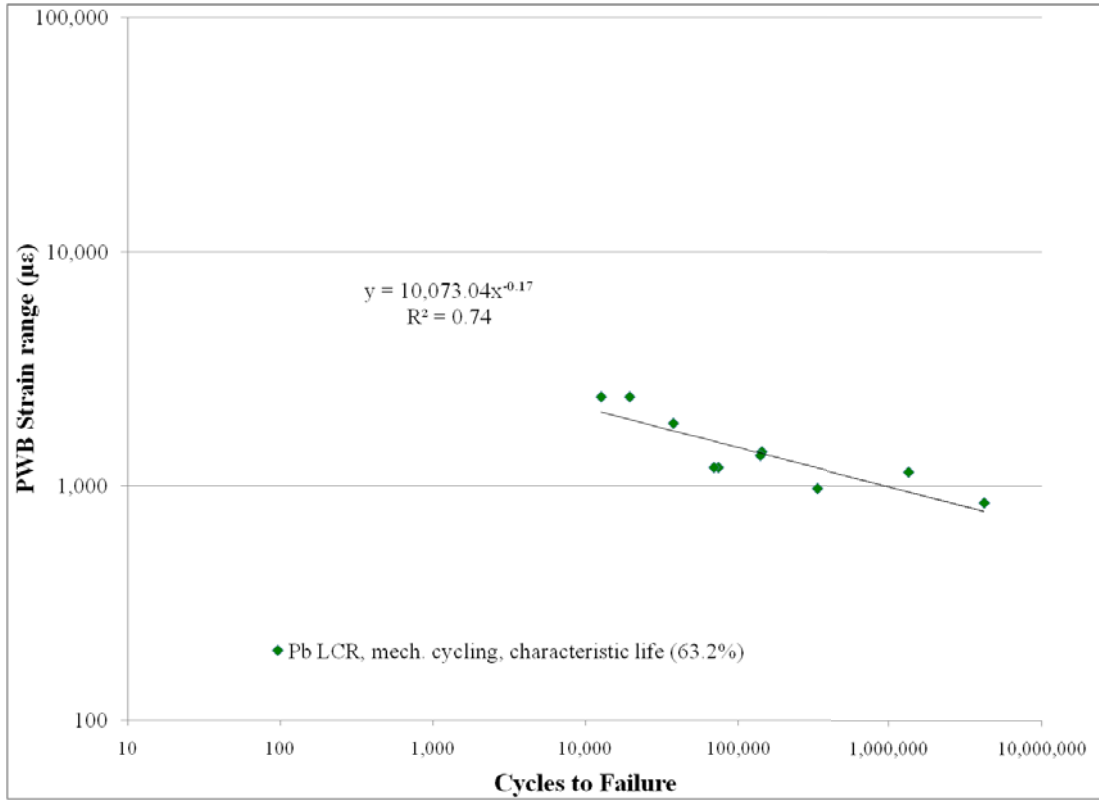
Figure 3.7 2512 LCR failure plot for Sn37Pb

Table 3.1 SnPb Data for LCRs

Strain	Cycles to Failure (Characteristic Life)
2400	12,680
1200	74,125
850	4,181,500
1400	142,780
1350	139,460
1150	1,344,300
975	330,000
1200	69,340
2400	19,485
1850	37,620

The effect of characteristic life on the slope, *b*, of the fatigue curve was also evaluated. Increasing the percent failure gives a larger value for the fatigue exponent, and vice versa. This is illustrated in Figure 3.8. The value of the fatigue exponent is plotted versus the percent failed as calculated from the Weibull parameters. This demonstrates the importance of knowing what percent failure is being used when describing the fatigue exponent because small variations in the fatigue exponent will give large changes in life. The fatigue exponent is also shown to have linear relationship with the failure percentage. This linear relationship is not surprising because it just illustrated the well known observation in high cycle fatigue. With low stress or strain, the failure distribution becomes wider than observed under higher stress or strain and shorter life. A common assumption is often made in extrapolating accelerated test data to field conditions is that the failure distribution remains similar. The experimental evidence indicates that this is clearly a poor assumption made by the common user.
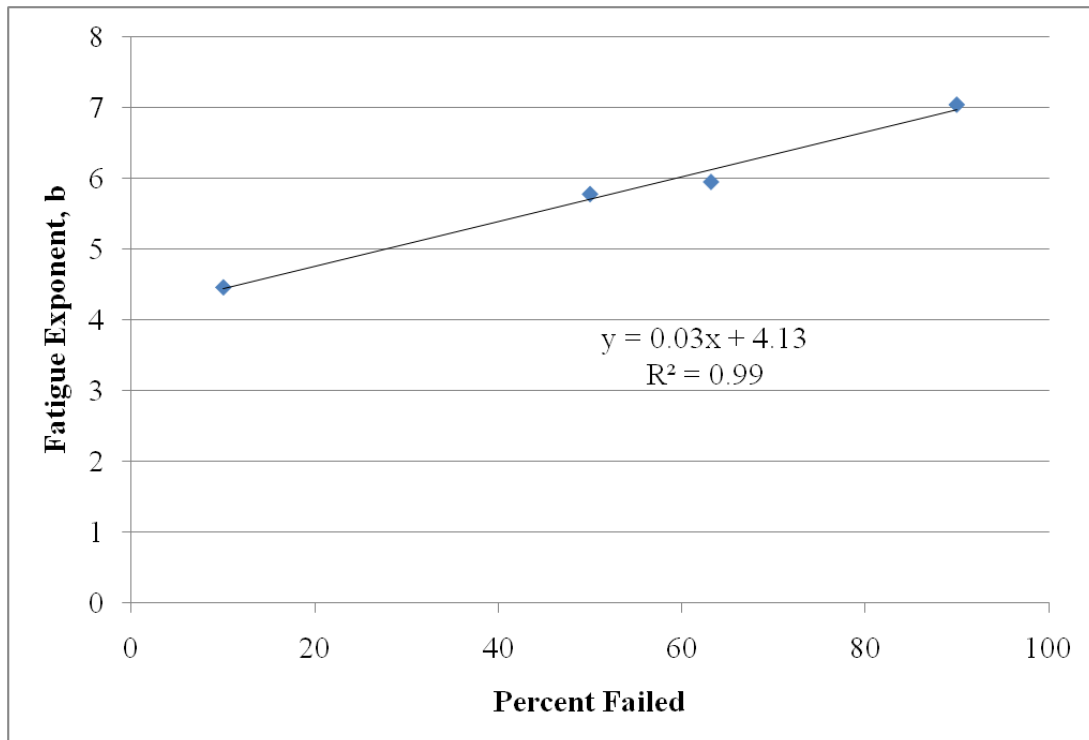
Figure 3.8 Fatigue exponent vs. failure percentage

It is very important when extrapolating from accelerated testing to field conditions for mechanical loading to calculate the Weibull distributions at each stage. As the number of cycles to failure increases, the shape parameter decreases which increases the spread in the distribution, as demonstrated in the schematic shown in Figure 3.9. For example, the figure shows two lines. The solid line assumes the same distribution being present from acceleration testing to use conditions for ~10% failure. This over predicts the failure life. The dashed line demonstrates the proper use of extrapolating from testing to field conditions because the distribution for the field conditions has been adjusted to account for the decreased shape parameter.
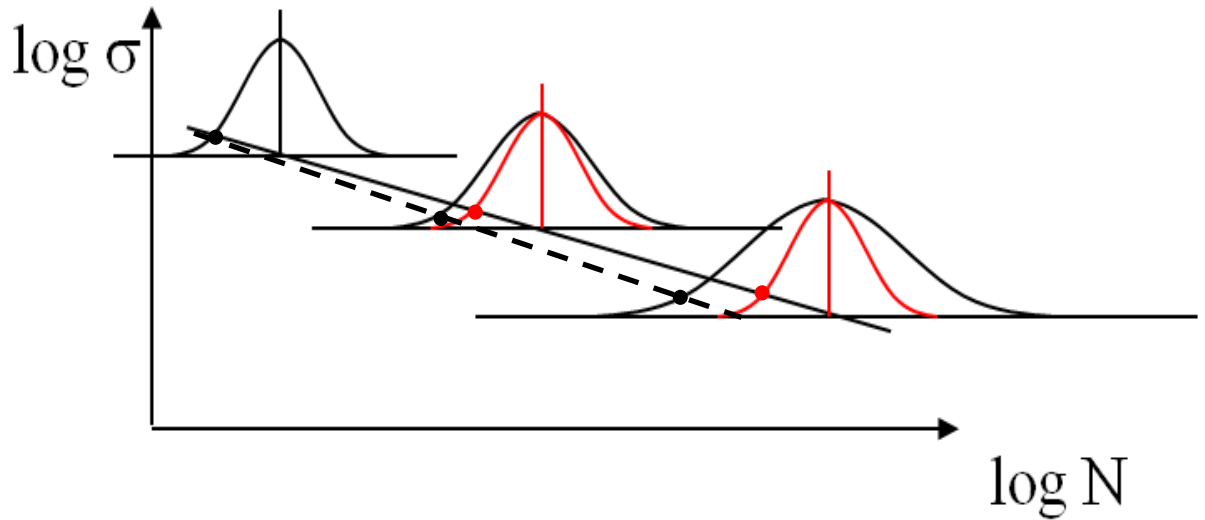
Figure 3.9 Extrapolating from Accelerated to Life Conditions

Bending of LCR assemblies with Sn3.0Ag0.5Cu solder (SAC305) was also done. The characteristic life for each test coupon is shown in Figure 3.10 along with the SnPb eutectic data. The solid trend line plotted is for the SAC305 data only. Here the value for the fatigue exponent, b, is 5.1. The 90% confidence interval about b is 4 to 6.6. Since the 90% confidence interval of b for the SAC305 assemblies fatigue exponent overlaps with the 90% confidence interval of fatigue exponent for b for the Sn37Pb solder assemblies, there is no statistical difference between the fatigue exponents of the two solders assemblies. This can be further illustrated by performing a z-test where,

$$z = \frac{(\overline{x_1} - \overline{x_2}) - (u_1 - u_2)}{\sqrt{(\sigma_1{}^2/n_1) + \sigma_2{}^2/n_2}}$$

Assuming the means $u_1 = u_2$ i.e. the two fatigue exponents are the same and for a 90% confidence

$$-1.645 \leq z_{.05} \leq 1.645$$

from the standard normal table [61]. These equations give

$$-1.645 \leq z_{.} = -0.0127 \leq 1.645$$

Therefore it can be said that, there is no statistically significant difference between the durability of resistor coupons with SAC305 and Sn37Pb.
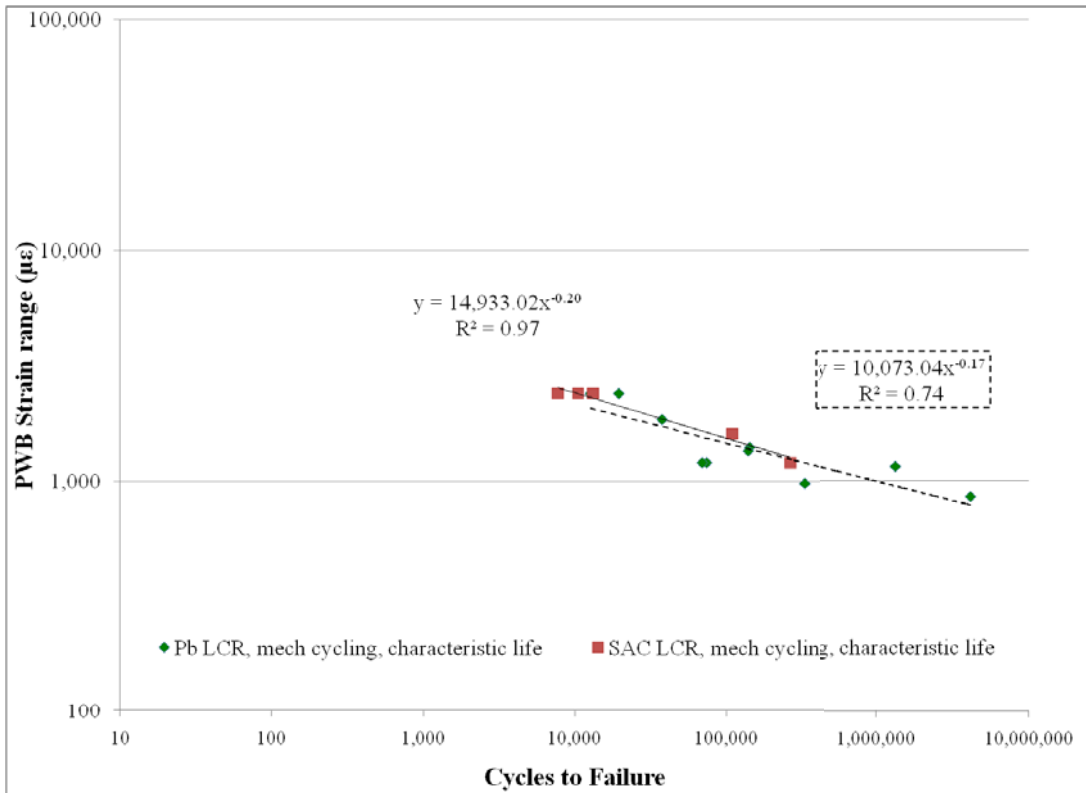
Figure 3.10 2512 LCR Failure data for SAC305 and Sn37Pb

The effect of bond pad size was also examined. The larger bond pad size (1.6 mm) did not contribute to a longer or shorter fatigue life as compared to the standard size (1 mm). The failure data for each size bond pad can be seen in the Appendix.

The samples were cross-sectioned and the only failures seen were fatigue cracks in the bulk solder as seen in Figures 3.11.

Figure 3.11 Solder Fatigue Crack

3.5 SOIC Testing/ Results Discussion

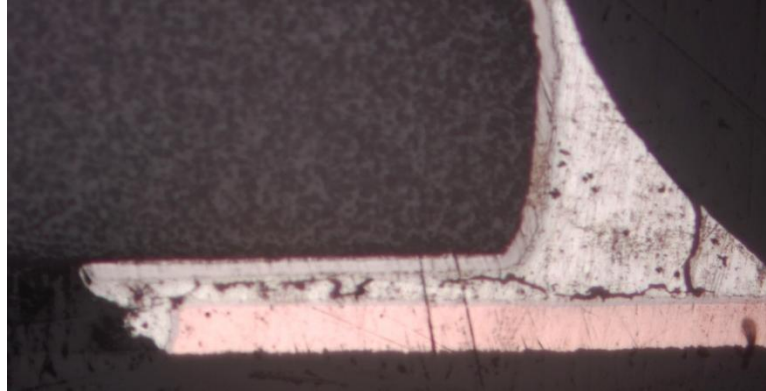The SOIC failure data is plotted in log-log space in shown in Figure 3.12. Like the LCR data, each point on the plot represents the characteristics life of one test board, which consists of 20 SOIC components. The 12 data points represent 240 failures. The data appears to be best fit along a single straight line. This line is the dashed line in Figure X. However, when the data is examined further another trend emerges. It appears that one could consider the latter part of the data is in the high cycle fatigue regime, which agrees with other observations for Sn37Pb fatigue testing, where the failure is in the solder. This transition from low cycle fatigue to high cycle fatigue is shown in the same figure with the solid lines. The data point around 10,000 cycles to failure was used in the plotting of both the HCF and LCF line because it lies in the typical transition region. This gives a low cycle fatigue coefficient of 4. The fatigue exponent for the combined high cycle and low cycle fatigue is 4.8 for a single straight line. Both fatigue exponent values are not considered unusual.
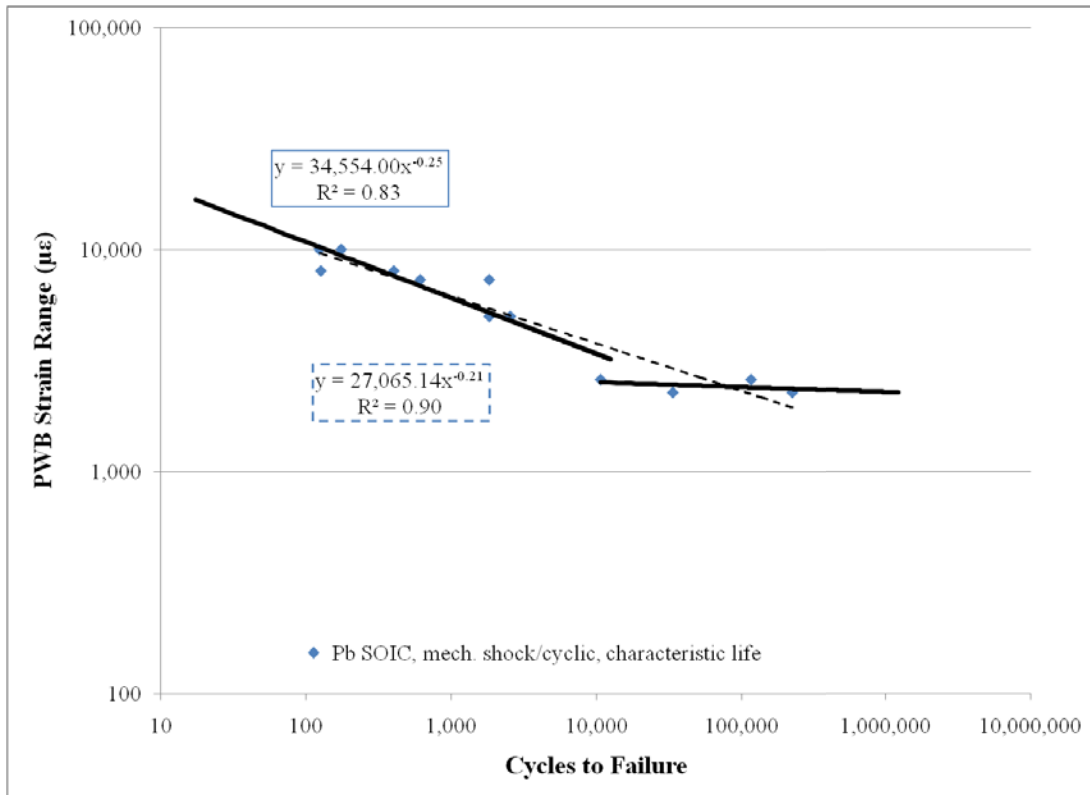
Figure 3.12 SOIC Durability Plot

The effect of component orientation was also examined. The results are plotted in log-log space in the Appendix. The SOIC components with their leads oriented perpendicular (transverse) to the longest side of the coupon survived longer than the SOIC components with their leads oriented parallel (longitudinal) in the low cycle regime but the opposite is true for the high cycle regime. The above observation on influence or component orientation is not a strong trend, and does not make any physical sense. Thus, the results may be just a function of the sparse data.

Failure analysis was also performed on the SOIC coupons. The only failure mode observed was bulk solder failure. This is illustrated in Figures 3.13 and 3.14.
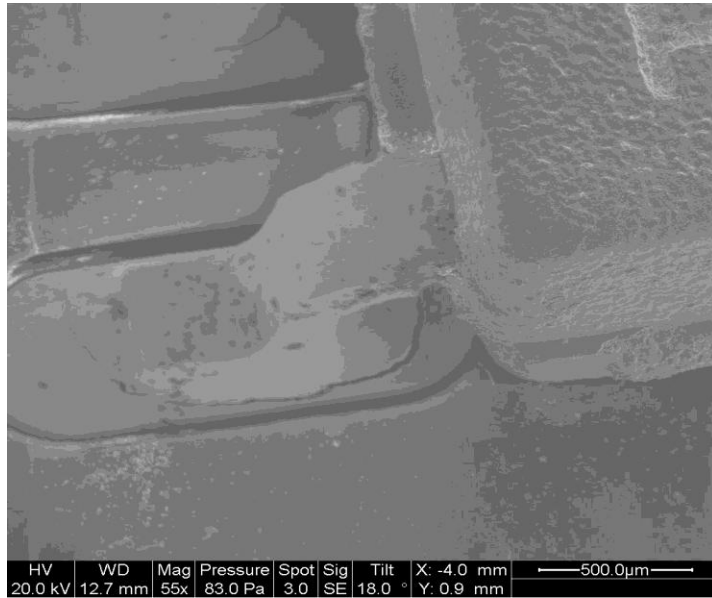
Figure 3.13 SOIC Solder failure picture
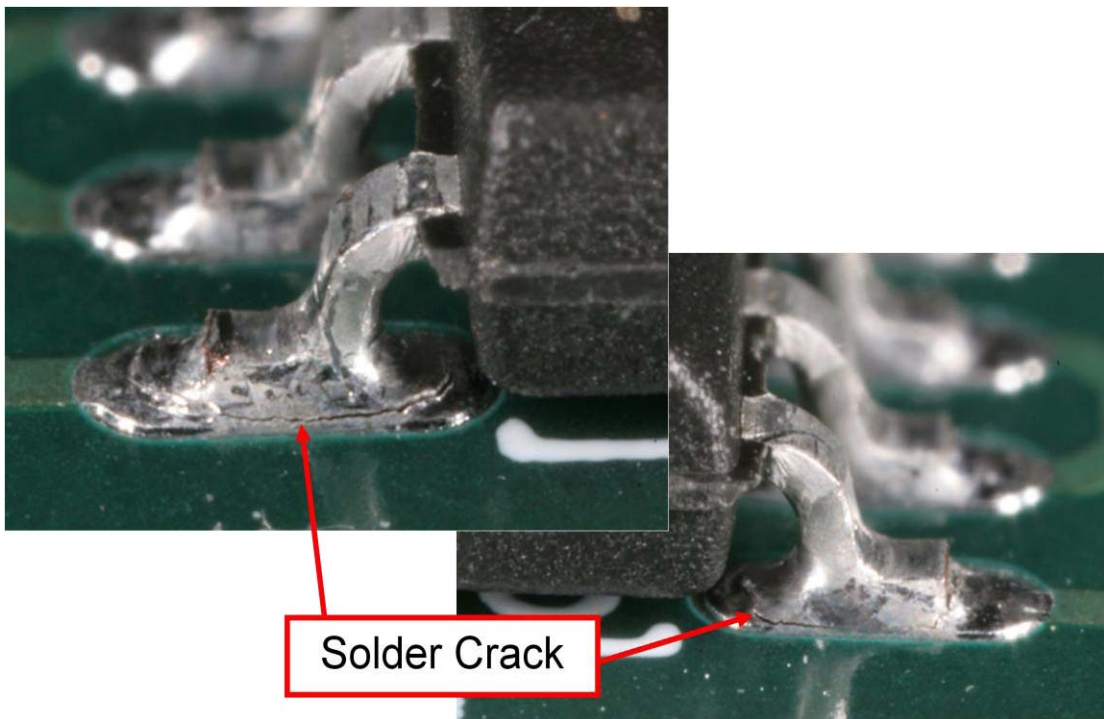
Solder Crack

Figure 3.14 SOIC solder cracking example

A limited amount of failure data was also obtained from the mechanical cycling of the larger SOT-223-4 component. The smaller SOT-23 component was simply too small to fail with our test coupon design. The data is shown in Figure 3.15, along with the data from the SOIC failure. Each data point here also represents a failure distribution and not a single component failure. With this limited data, it appears as though the SOT 223-4 component would outlast the SOIC component. This is plausible because the SOT 223-4 components are physically smaller and have much thicker leads (more solder attach) than the SOIC components. The SOT-23 components did not fail in the tests.
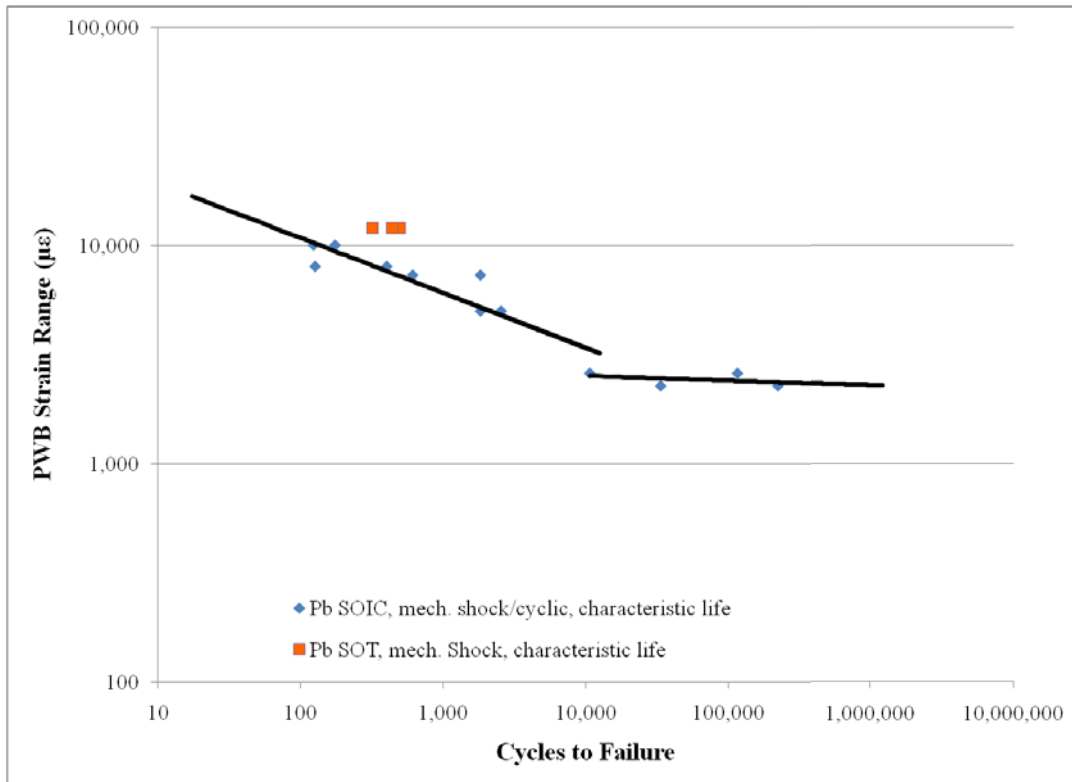
Figure 3.15 SOT failure data with SOIC failure data

Figure 3.16 compares the failure data (characteristic life) from the LCR, SOT, and SOIC assemblies. Despite the differences in the components, the characteristic life data illustrates a common trend. Unfortunately, the tests were not run at low enough stress levels to generate many failures in a ultra high cycle fatigue environment ($N > 10^6$ cycles).
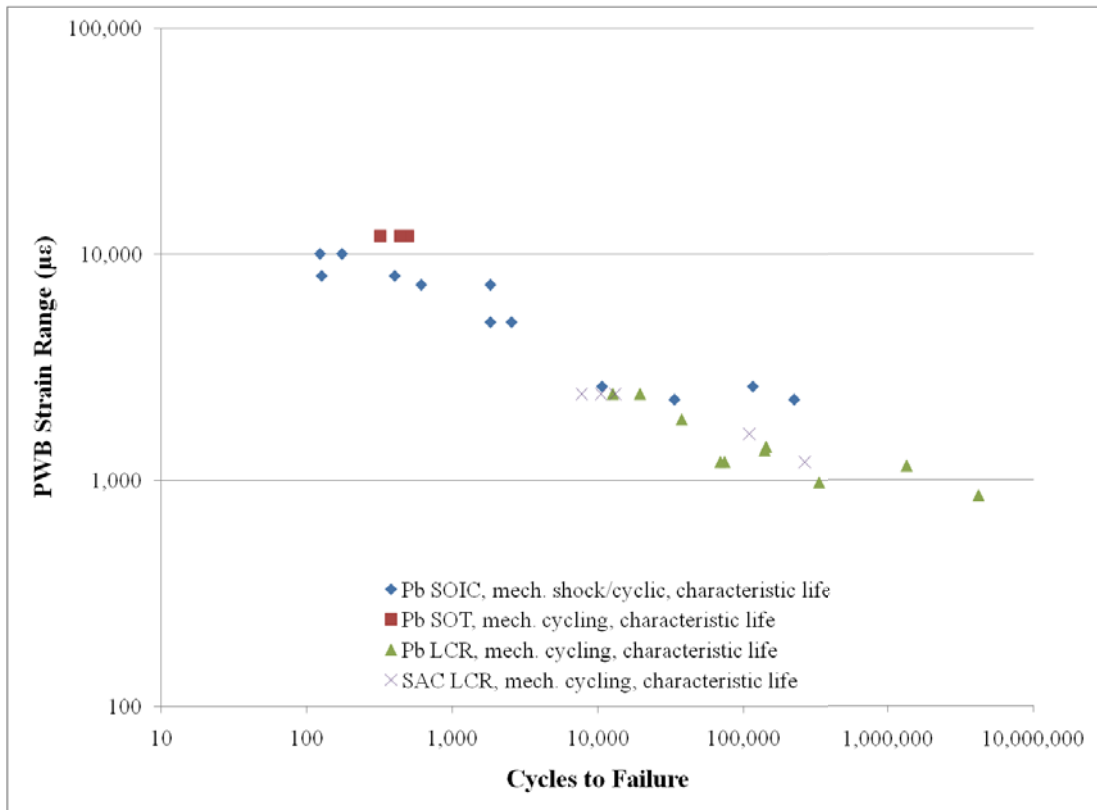
Figure 3.16 LCR, SOIC, and SOT failure data combined (Weibull 63.2% failure data)

3.6 Conclusion

This study used 2512 leadless chip resistors (LCR), small outline integrated circuit (SOIC) packages, and small outline transistor (SOT) packages to evaluate the fatigue performance electronic assemblies of traditionally used Sn37Pb solder and a leading lead free alternative solder Sn3.0Ag0.05Cu (SAC305). The packages were assembled onto printed wiring boards with the different solders and mechanically cycled in a 4 point bend fixture at loading rates were solder creep could be considered negligible. The PWBs and 4 point bend fixture were designed to simultaneously subject many similar packages to the same loading. Continuity monitoring of the packages provided

time to failure information. At different load levels as determined by the printed wiring board strain, the failure distributions were fit to a 2 parameter Weibull.

The printed wiring board strain was used as the "stress" parameter in an SN failure plot. The printed wiring board strain was a simple parameter that allowed easy fatigue comparison between the different assemblies. The 2512 LCRs were the least durable components, followed by the SOIC components. The SOT-223 components were more durable. Due to the limited loading that the bend fixture could apply. The small SOT-23's were the most durable and did not exhibit any failures.

No significant difference was found in the fatigue behavior between SAC305 and Sn37Pb soldered assemblies as evidenced by their calculated fatigue exponent and the fact that the failure data basically fell on top of each other in a durability plot. It was found that the common assumption that the failure distribution remains constant is a poor assumption. The failure distribution gets broader, Weibull shape parameter decreases, as the load is reduced and fatigue life gets longer. This fact influences the value of the fatigue exponent. The value of the fatigue exponent turns out to be a function of the percent of parts failed. If one is interested in the mean time to failure, 50% of the parts failed, the fatigue exponent is higher than if one were interested in the time to failure where only 1 or 10% of the parts had failed.

Chapter 4: Study of PBGAs under Bending and Drop Loading Conditions

Typical drop motion is quantified by number of drops to failure per the JEDEC JESD22-B104-B standard for mechanical drop testing. This section seeks to use PWB strain during drop to quantify failure in lieu of number of drops.

It has been well documented how PBGAs react under bending loads. Most of these studies, however, focus on strain or stress in the solder joint. The failure models developed by these studies use the maximum stress in the solder joint. As determined by FEA models, the location of this maximum stress is often in the corner solders balls. However, failure does not always originate in the solder. Studies done by Zhou et al [39] and the consortium between the Joint Council on Aging Aircraft, JCAA, and the Joint Group on Pollution Prevention, JG-PP [31] found that failures in copper traces were often prevalent in long term durability testing. Copper trace failures were often found along with failure in the bulk solder. Without knowing which failure mode came first, it can be very difficult to create a failure model based on maximum stresses or strain in the component or component attach. The approach used in this paper is to develop a failure model based on PWB strain under different loading rates. The PWB strain is an easily determined metric for the evaluation of when failures will occur. This section will first discuss the higher rate mechanical cycling PBGA testing and then discuss the high rate drop testing of PBGAs.

4.1: PBGA Bend Testing

PBGAs are being increasingly used in electronic designs due to their higher I/O count. As capacitors become smaller and with the evolution of flexible termination capacitors, BGAs are increasingly becoming the component of concern for evaluating failure of printed wiring assemblies subject to mechanical loading.   PBGA bend test samples were made to determine when they would fail under bending loads. The test coupon, shown in Figure 4.1.1, has two lead-free PBGA components soldered with Sn3.0Ag0.5Cu solder with OSP on the copper pads. The PWB was 1.59 mm (1/16") thick FR-4. The PBGAs were 256 I/O, 1 mm pitch, Practical and Topline components. The board has three strain gauge locations in the center of the board. The strain was measured during the test using the center location. A close up picture of the mounted components is shown in Figure 4.1.2. The PBGAs were internally daisy-chained and monitored individually for continuity. The package was daisy-chained as a whole because this project's main goal is the determination of when the package failed not the location of the failure. Post-test failure analysis was done to determine the location of failure. Probe test pads are located around each BGA to aid in the finding the location of the failure site. Each PBGA contained a dummy die of size 7mm by 7mm. The die can be seen from x-ray analysis shown in Figure 4.1.3.
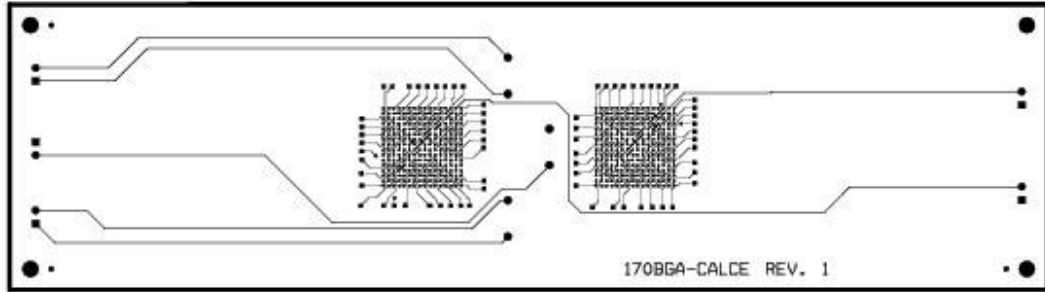
Figure 4.1.1 PBGA Test Coupon
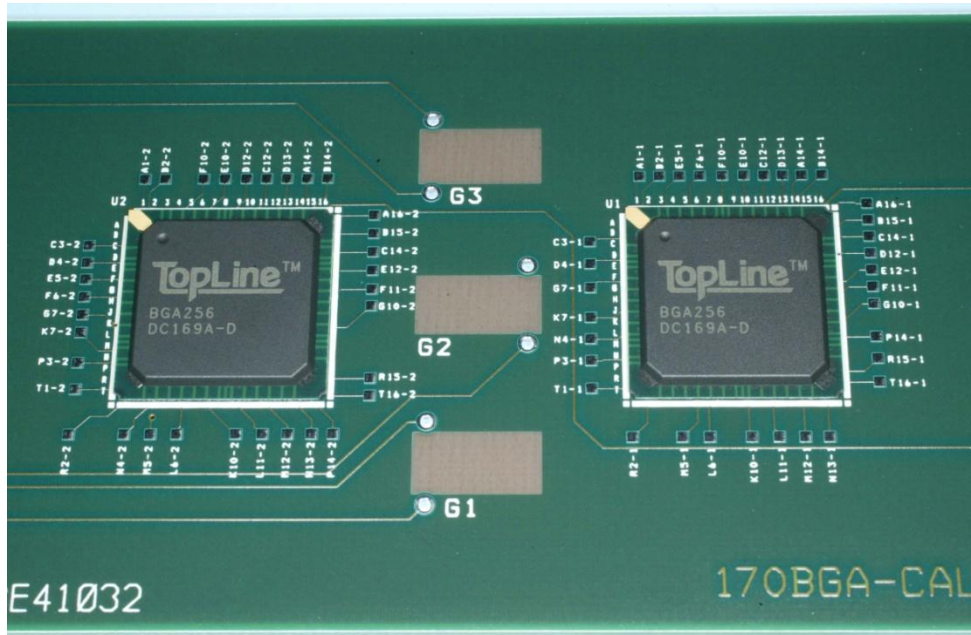
Figure 4.1.2 PBGA test coupon close up
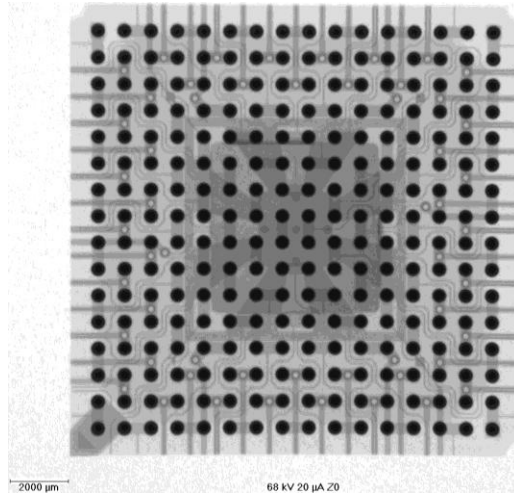
Figure 4.1.3 X-ray of PBGA with die showing

Four-point bend testing was done to allow for a constant bending moment in the middle of the board. This is illustrated in Figure 4.1.4. The coupon was tested such that the two PBGAs were between the inner supports to ensure they experience a constant bending moment during the test. A MTS servo hydraulic material testing machine was used for the testing. Each coupon was tested at an increasing level of displacement until both components on the coupon failed. The coupons were tested as-reflowed.
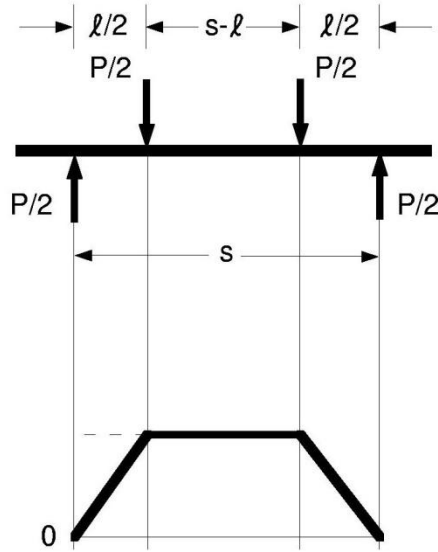
Figure 4.1.4 Four-point bending illustration

Printed wiring board strain was recorded along with continuity during each test. The continuity monitoring was achieved using a resistance network. When the resistance increased above 300 Ω the component was considered to be failed per IPC SM785. Two types of load profiles were employed. One profile was a continuous sinusoidal profile. The other was a single rapid loading pulse that was repeated if failure did not occur. Both profiles only loaded the coupon and PBGA in tension. Both profiles start from zero strain and increases to a certain PWB strain level before returning to zero. A sample of the strain values and continuity monitoring are shown in Figures 4.1.5 and 4.1.6 for each load profile. Figure 4.1.5 shows the rapid loading profile. The board was loaded rapidly and unloaded at a slower rate. The maximum PWB strain on this test was 7000$\mu\varepsilon$. The secondary axis shows the continuity plot. The value of 0 represents a closed circuit i.e. a functioning component and 1 represents an open circuit. On this run both components failed. Figure 4.1.6 shows the sinusoidal

loading. The maximum PWB strain on this run was 4000µε. In the run shown, only one of the two components failed. For the rapid loading, the PWB strain rate was about 10^{-1} /s, for the slower cyclic loading the PWB strain rate was about 10^{-2} /s. Both of the tests were rapid enough that any solder creep could be considered negligible.
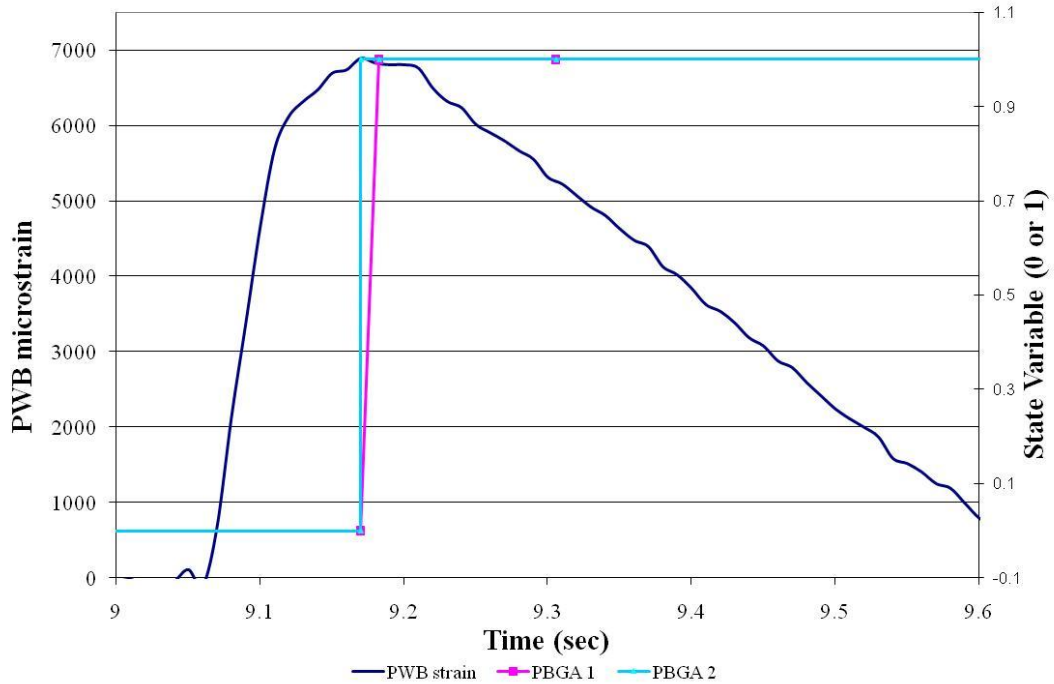
Figure 4.1.5 Sample rapid loading profile
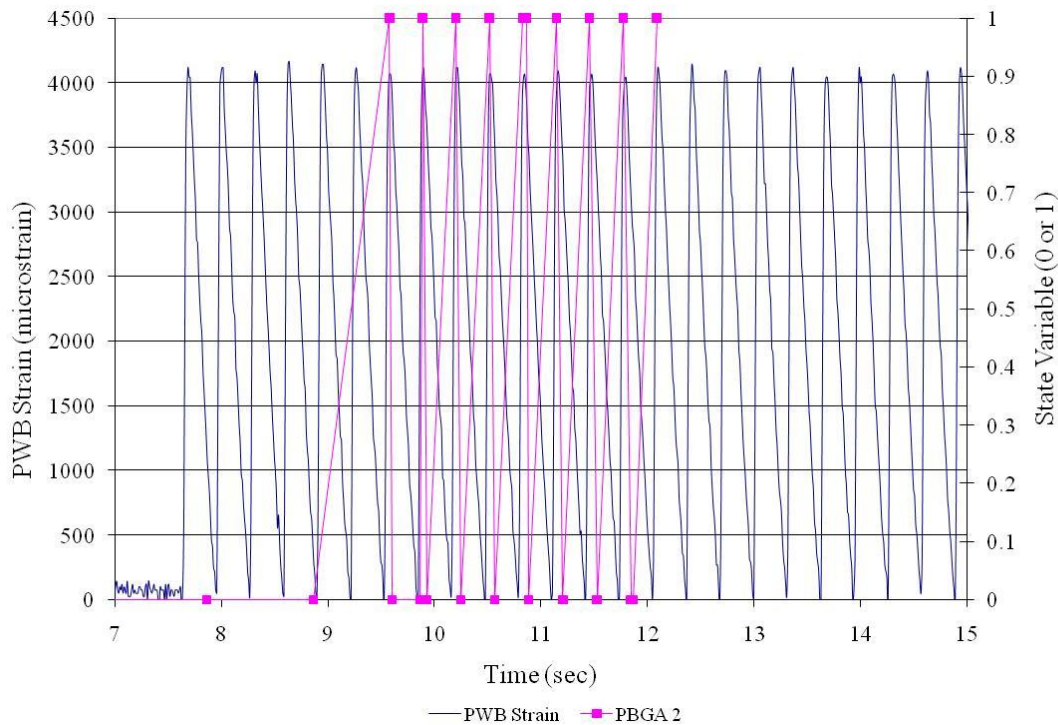
Figure 4.1.6 Sample sinusoidal loading profile

The results of the tests are shown in Figure 4.1.7 where the rapid loading is labeled mechanical shock and the sinusoidal loading is labeled cyclic. The PWB strain range is plotted versus the number of cycles to failure. Normally when plotting high cycle fatigue and low cycle fatigue data, there is a noted transition between the two regimes as evidenced by a change in slope of the failure data. This transition is not apparent in this case and a single straight line seems to best fit the data. It is important to note that the failures plotted in the graph are simple loss of continuity, which can be caused by PWB trace failures or cracks in the solder attaches. One would expect that if this were only solder attach failure data, the transition between the LCF and HCF data would become evident. This non-delineation between high cycle and low cycle fatigue could also be due to the use of the PWB strain and not the stress in the solder.

Large plastic deformations of the solder present in LCF would cause the low cycle end of the regression line to curve upward.

The linear line in the plot is a power law regression to the failure data with the regression equation and R^2 indicated. The exponent in the equation is the inverse of the Basquin fatigue exponent. As seen, the fatigue exponent is 1/0.109 or approximately 9. Due to the regression analysis, this fitted line corresponds to the mean time to failure at a given load, or where 50% of the components have failed. In Chapter 3 we noted that the value of the fatigue exponent is a function of the percent of components that have failed.
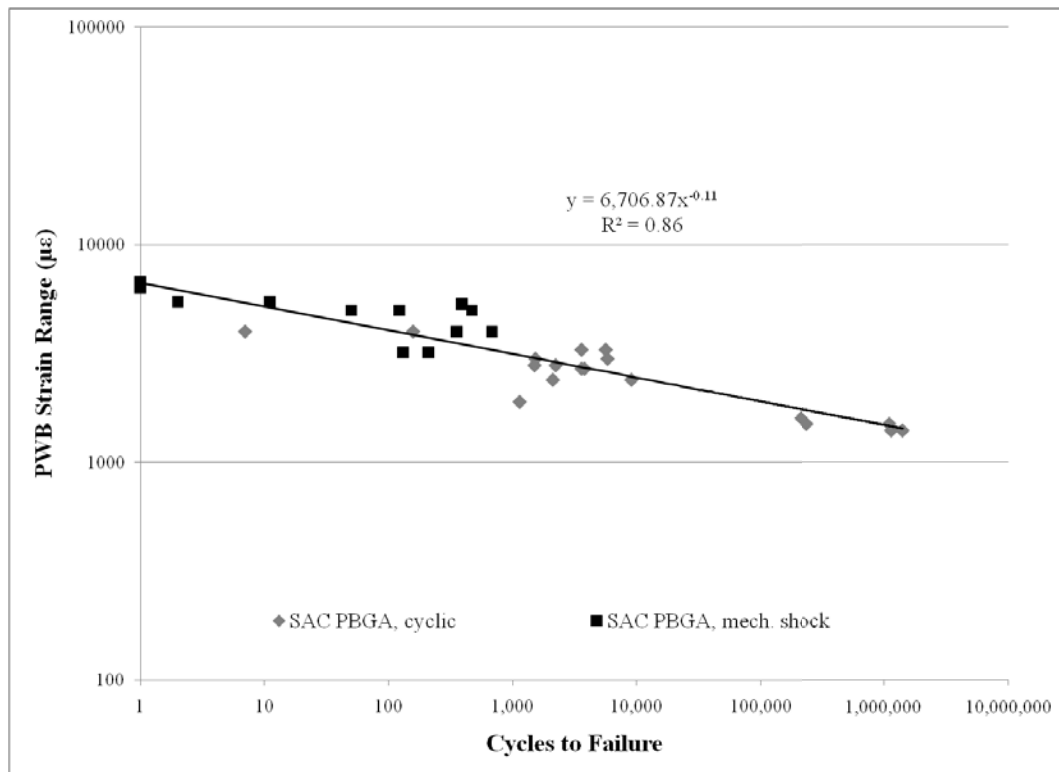
Figure 4.1.7 SAC305 Bend test results

During failure analysis of the PBGAs, there were distinctly different failures noted based on the printed wiring board (PWB) strain level. In what can be called the high PWB strain regime (0 to 10 cycles to failure), the failures were all in the PWB (copper trace cracking and copper pad pullout). An example of the copper pad pullout can be seen in Figure 4.1.8. In medium PWB strain regime (10-100,000 cycles to failure), the failures were either in the PCB or in the solder joint intermetallics, as shown in Figure 4.1.9. In the low strain region (100,000+ cycles to failure or in the classical high cycle fatigue regime), the failures were mainly in the bulk solder and intermetallics, as shown in Figure 4.1.10. It must be again noted that despite seeing these varying failure locations in each of these areas, no noticeable transition was seen in the failure data when viewed in a durability fatigue plot.
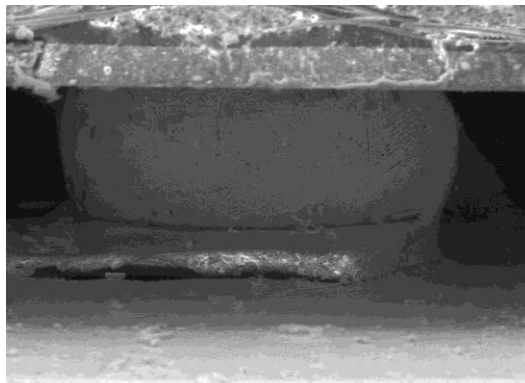
Figure 4.1.8 High strain regime (0 to 10 cycles) failure example
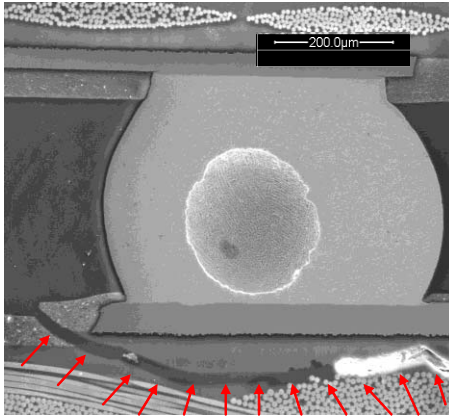
Figure 4.1.9 Medium strain regime (10 to 10,000 cycles) failure example
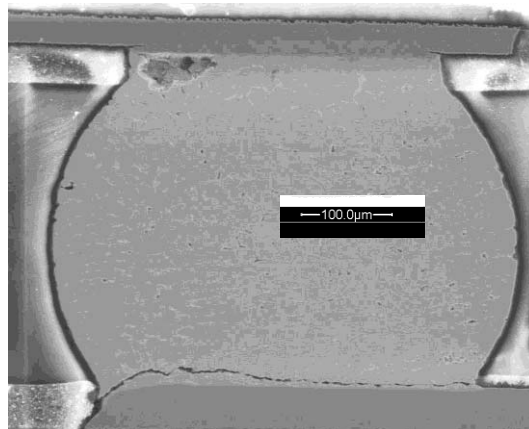
Figure 4.1.10 Low strain regime (10,000+ cycles) failure example

The data collected by this study was correlated with independently gathered data from literature. Zhou et al [39] conducted narrow band harmonic excitation tests on a PWB populated with 256 I/O PBGAs and other components. Sn3.0Ag0.05Cu solder was used with an OSP board finish. Strain gages were located immediately outside the footprint of a component, on the underside (non-populated) side of the PWB. The samples were aged for either 100 or 350 hours at 125°C before testing. The recorded

failure sites in this study were in the bulk solder and copper traces. This data was added to the original failure data and is plotted in Figure 4.1.11. Despite the differences in the two studies, the data correlates very well. Conducting a simple power law regression analysis of the data gives a R^2 value of 0.91 for the combined studies, which indicates that it is a good fit. This demonstrates that a simple power law model (straight line in log-log space) is a good model for predicting the failure of 256 I/O PBGAs mounted with SAC305 and OSP. The two studies had different boundary conditions, testing methods, ageing constraints, PWB layouts, and manufacturers. The only similarity in the two studies other than the use of 256 I/O, 1 mm pitch PBGAs was the board thickness. Both studies used 1.6 mm (1/16 inch) thick FR-4 board material. It must be noted the PWB strain measurements from Zhou were taken at the edge of the component (the location of PWB highest strain), whereas this study measured strain at away from the component. The PWB strain values will fall lower on the plot than their current position when this data is adjusted to account for the difference in where the strain is measured. This adjustment, however, should only be minor in the log-space of the plot.
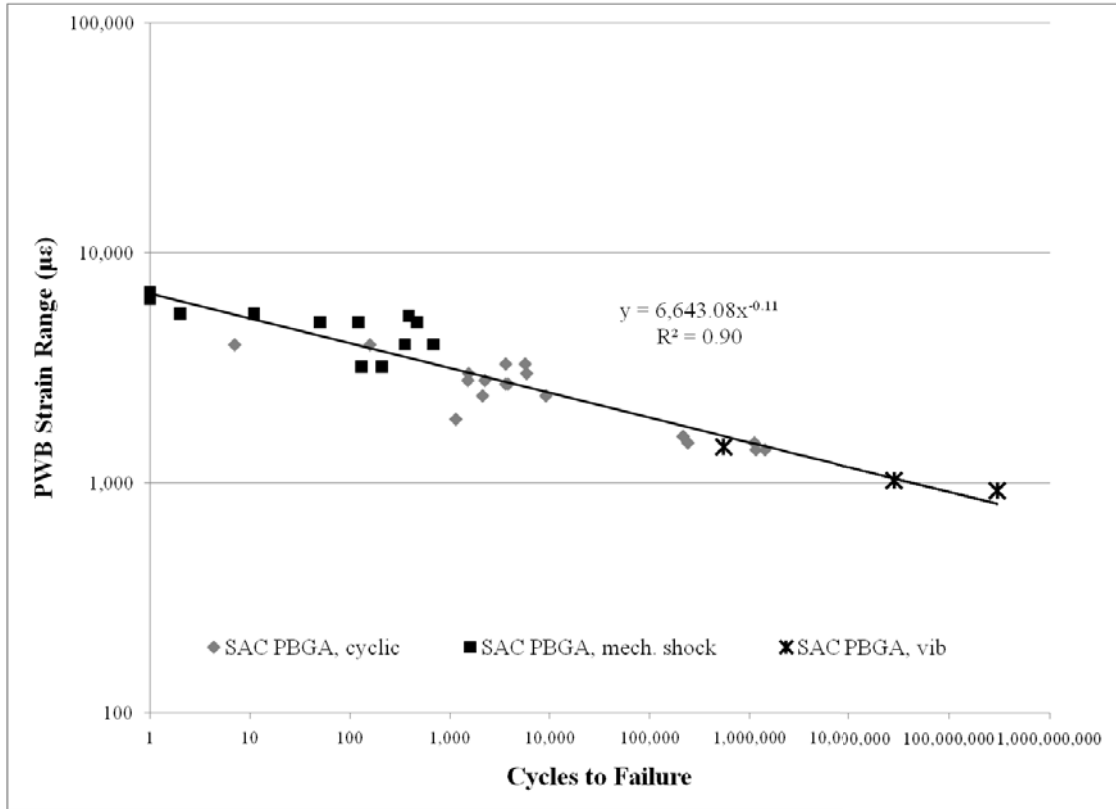
Figure 4.1.11 Plot of failure data with additional source

These results for SAC 305 solder assemblies were compared to studies of the behavior of SnPb eutectic solder assemblies. Data for 256 I/O PBGAs from previous testing by the author, Watkins et al [42], Varghese et al [40], Yu [41], Song [43], and Zhou et al [39] for Sn37Pb are shown along with the SAC data in Figure 4.1.12. The regression line plotted is for the SAC305 data only. The PBGA assemblies with the SnPb eutectic solder are shown to outperform SAC305 assemblies in ultra low cycle regime (below 100 cycles). In the ultra high cycle area (above 1 million cycles), the SnPb solder assembly data appears to be above the SAC data line, but any definitive conclusion in this region is questionable due to the small number of data points. The

PBGA failure modes shown in each of these studies were consistent with the findings of this study. Board failure (pad pullout, copper trace failure) was the dominant failure mode in the low cycle regime while bulk and intermetallic solder failure dominated failure seen in the high cycle fatigue region.
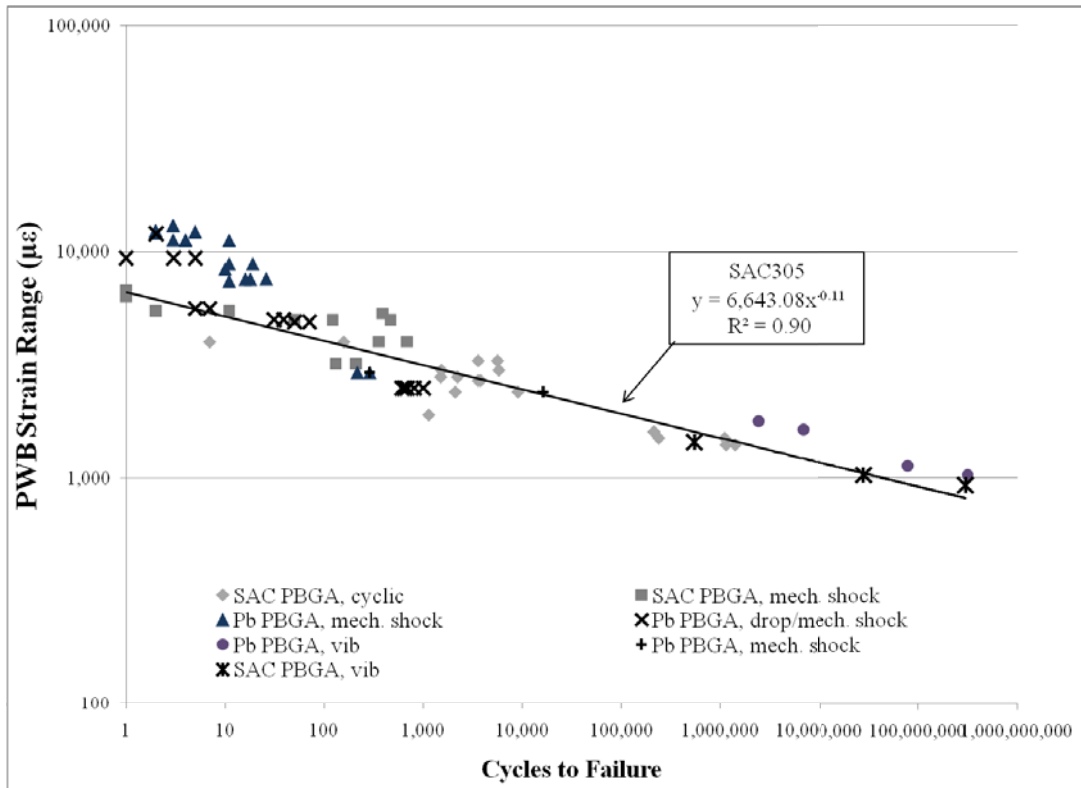
Figure 4.1.12 SAC305 Failure data with Sn37Pb data

4.2: PBGA High PWB Strain Rate Test

After evaluating the behavior of PBGA assemblies in the quasi-static (PWB strain rate 10^{-2}-10^{-1} 1/s) regime, their response to a faster loading rate was evaluated. To achieve this condition, a six inch diameter round test coupon was designed for drop testing. The outer ½ inch of the coupon was clamped. This produced a diaphragm

motion with an axi-symmetric strain distribution. The coupon is double sided. The top side of the coupon was designed for 4 PBGA to be placed along radial lines. Each PBGA was located a different distance from the board center and the PBGA's diagonal was aligned along the radial line. The bottom side was designed for 6 PBGAs. One PBGA was located exactly at the board center and the other 4 were located at different distances from the center along orthogonal radial lines. The bottom side PBGAs were all aligned with each other so that edges of the PBGAs were parallel to the 4 alignment radial lines. This is illustrated in Figure 4.2.1, where each of the radial lines is drawn. The board has three strain gage sites and pin-out locations for continuity measurements. Photos of the actual test coupon can be seen in Figures 4.2.2 and 4.2.3. There are a total of 11 PBGA 256 I/O 1 mm pitch Practical brand packages per board. Due to the clamped outer edge the test region of the board is 5 inches in diameter. It is a four layer, 1/16 inch thick FR-4 board. Two different solder types were used on the board, 96.5Sn3.0Ag0.5Cu (SAC305) and 63Sn37Pb. Both types had organic solder preservative (OSP) as the board finish. A commercial vendor was used for the board assembly and reflow.

Outer Ring

Pinouts

| Yellow- top side |
| Red- bottom |
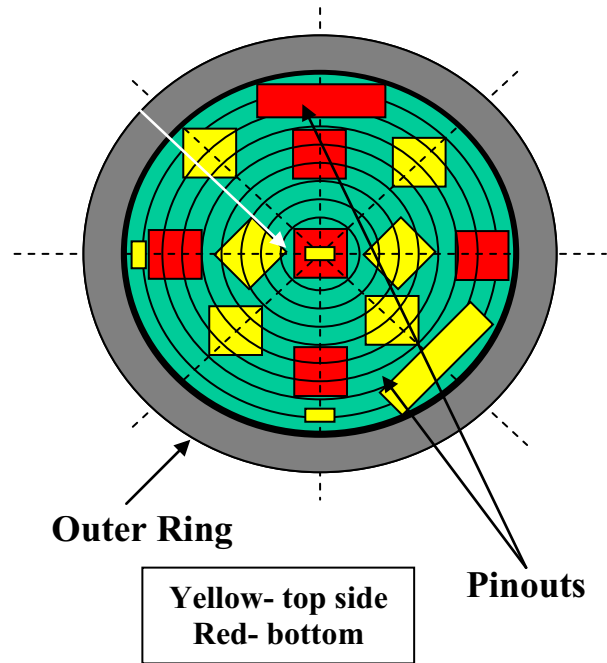
Figure 4.2.1 Round PBGA test coupon
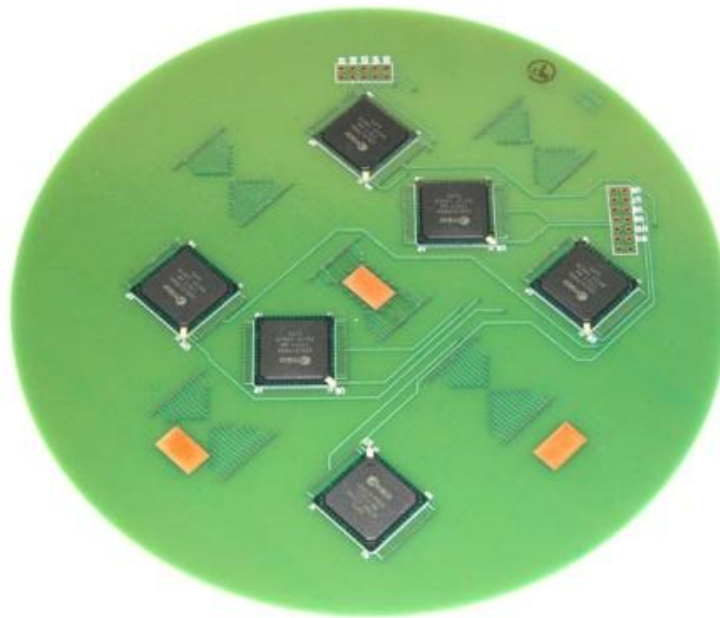
Figure 4.2.2 Round PBGA test coupon - top side
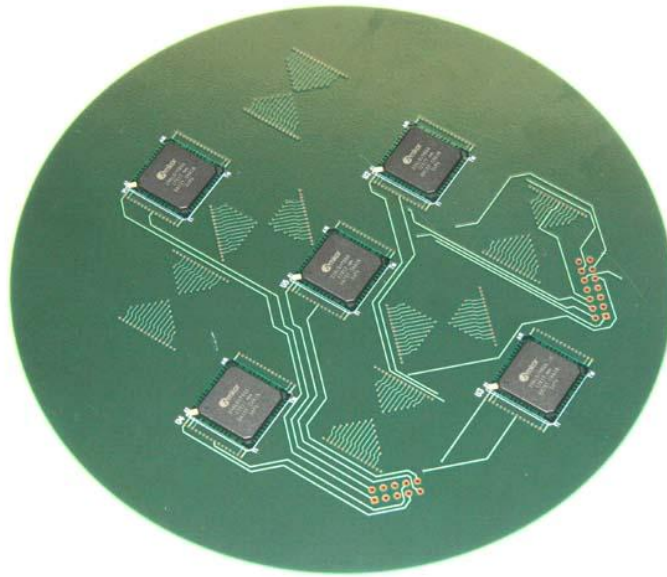
Figure 4.2.3 Round PBGA test coupon - bottom side

The coupon was designed to fit in the clamping fixture show in Figure 4.2.4. The fixture clamps ½- inch edge around the perimeter of the board. The four bolts shown were used to clamp the board in the fixture. Four separate bolts were used to secure the drop fixture to the drop table. The drop table was raised to the desired height and released. The table then strikes the impact surface once and is caught on the rebound. The magnitude and shape of the acceleration pulse is determined by the drop height and the medium placed between the impact surface and the drop table. For this test, felt was the medium used. The Figure 4.2.5 show the board attached to the drop tower. An Impac drop tower was used in this initial testing. Two accelerometers, an Endevco 7270A-20KM6 and Endevco 2255B-01, were directly attached to the drop tower table to monitor acceleration during the drop event.

Figure 4.2.4 Drop test fixture
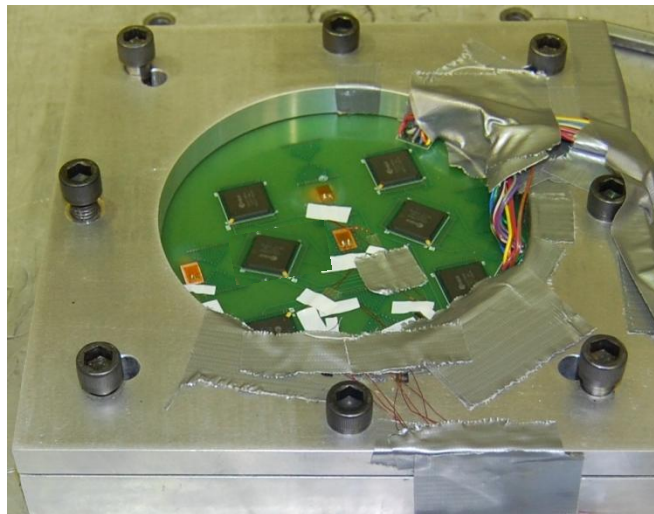
Figure 4.2.5 Test coupon and fixture attached to drop table

The initial drop pulse was approximately a 5000 G half-sine, 300 millisecond duration, acceleration pulse. This pulse gave a PWB strain rate on the order of 1 per second. An example of the acceleration pulse for the initial drops can be seen in Figure 4.2.6.
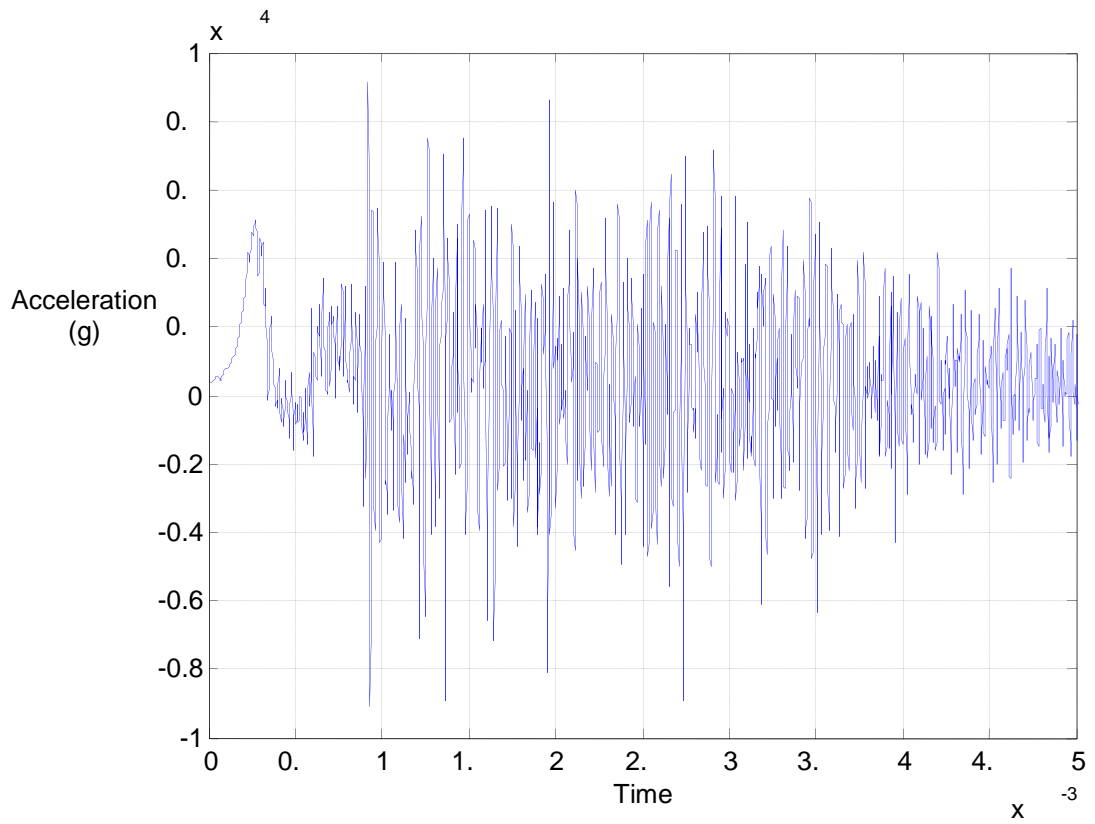
Figure 4.2.6 Acceleration pulse for initial drop
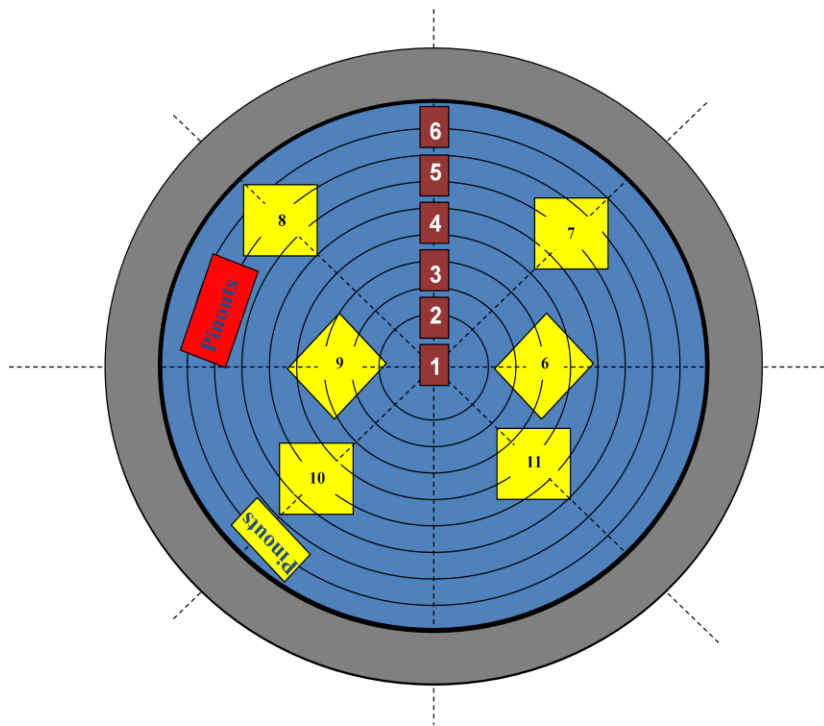
Figure 4.2.7 Strain gage placement

The continuity and strain were measured during the test. In later testing six strain gages were placed along the radius of the board as shown in Figure 4.2.7. This allowed for a better understanding of the board behavior during the test compared to the strain gage locations as shown in Figure 4.2.1.

During this first drop test with a 5,000 G pulse, three components failed, two on the bottom side and one of the top side. During the drop impact, three components were completely separated from the board; the components that remained attached to the board did not show any loss of continuity. Figure 4.2.8 shows one of the failed components that was ripped from the board. In the detailed pictures of the back of the component, shown in Figure 4.2.9, the dog bone copper traces that were once a part of the PWB are now seen attached to the back of the component. This can be further evidenced by Figures 4.2.10 and 4.2.11. These figures display the round test coupon that once held the PBGA shown in the previous figure. Here, the voids in the board where the dog bone structures once were are illustrated and the board fibers are exposed. Also shown are the dangling copper traces which have been ripped from their original location.
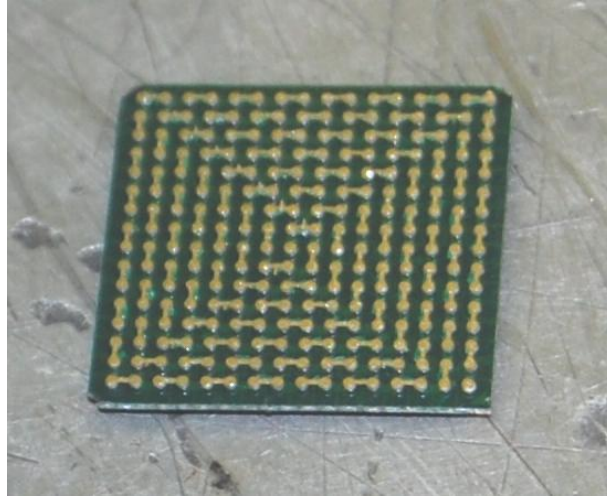
Figure 4.2.8 Back side of failed PBGA coupon

| HV | WD | Mag | Spot | Sig | Tilt | X: -0.5 mm | Pressure | ——100.0µm—— |
| 30.0 kV | 11.1 mm | 201x | 3.0 | SE | -1.1 ° | Y: -1.8 mm | 83.0 Pa | |
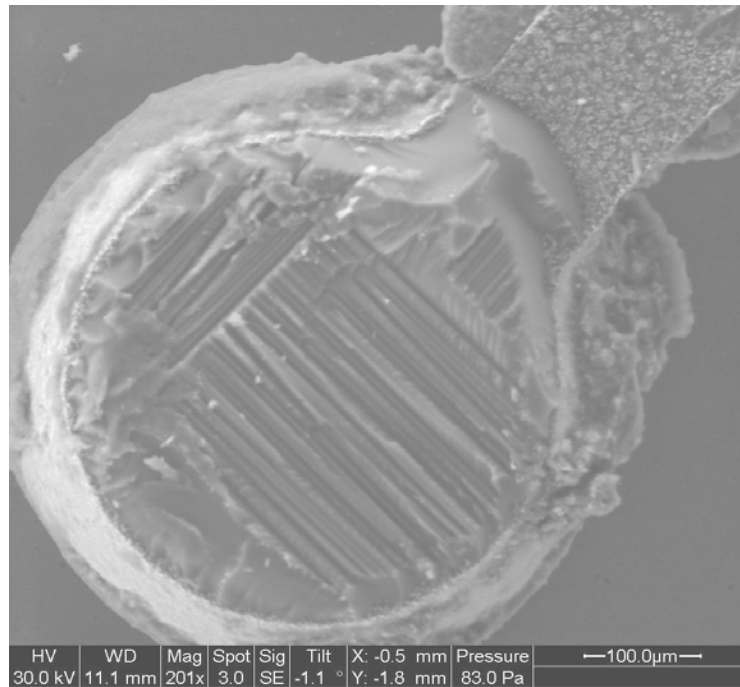
Figure 4.2.9 Close up of the back side of the failed PBGA component
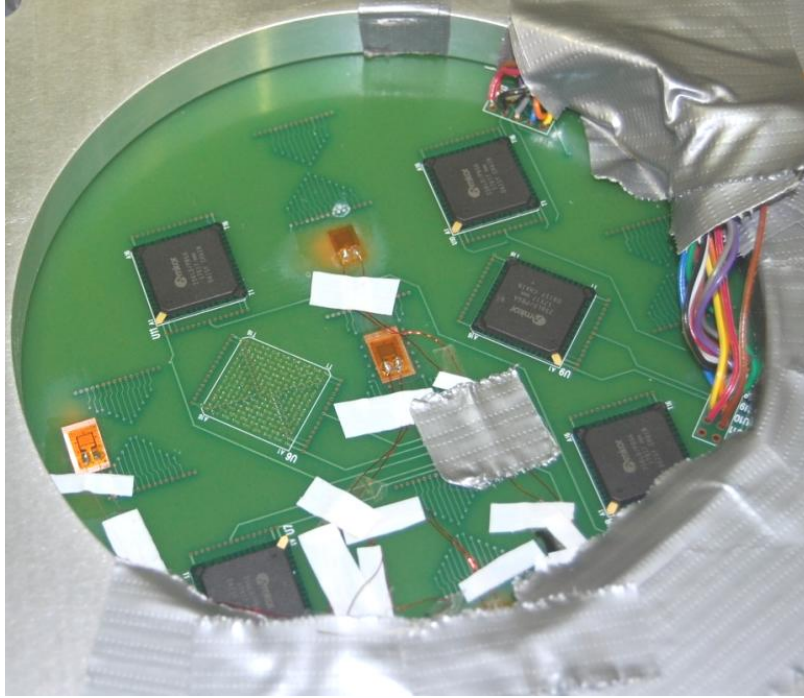
Figure 4.2.10 Post test picture of the test coupon

HV	WD	Mag	Spot	Sig	Tilt	X: -1.3 mm	Pressure	⊢———300.0µm———⊣
30.0 kV	11.4 mm	91x	3.0	BSE	-1.0 °	Y: -9.1 mm	83.0 Pa	
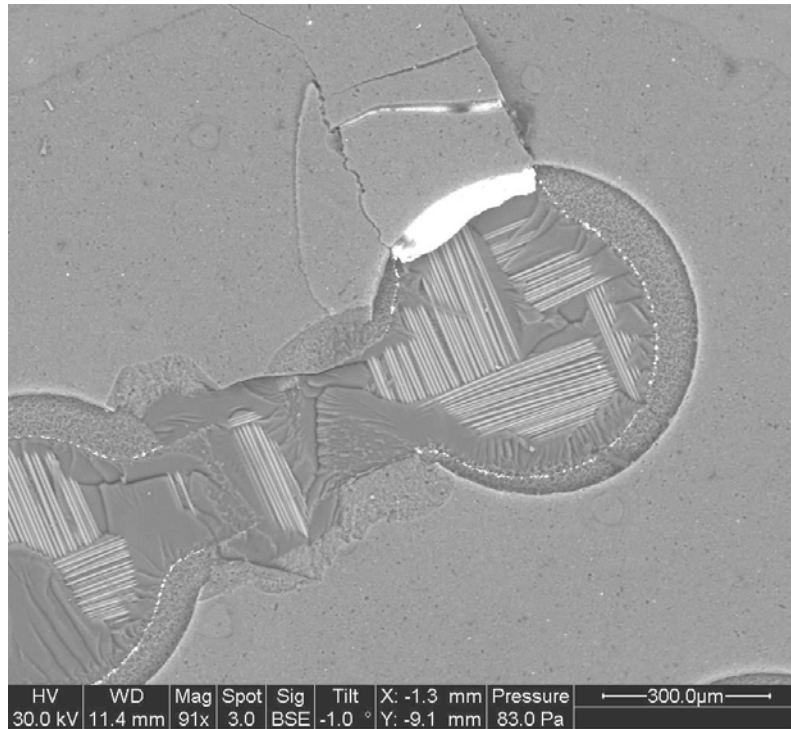
Figure 4.2.11 Post test picture of the test coupon – showing missing dog bone connector

The manner in which these components failed was unexpected. To better understand these failures, the acceleration pulse was examined using a fast Fourier transform (FFT) to see what frequencies were present in the signal. The lower frequency portion of the signal FFT is shown in Figure 4.2.12. The acceleration pulse from this initial test contained much more high frequency content than would be desired in controlled drop testing.
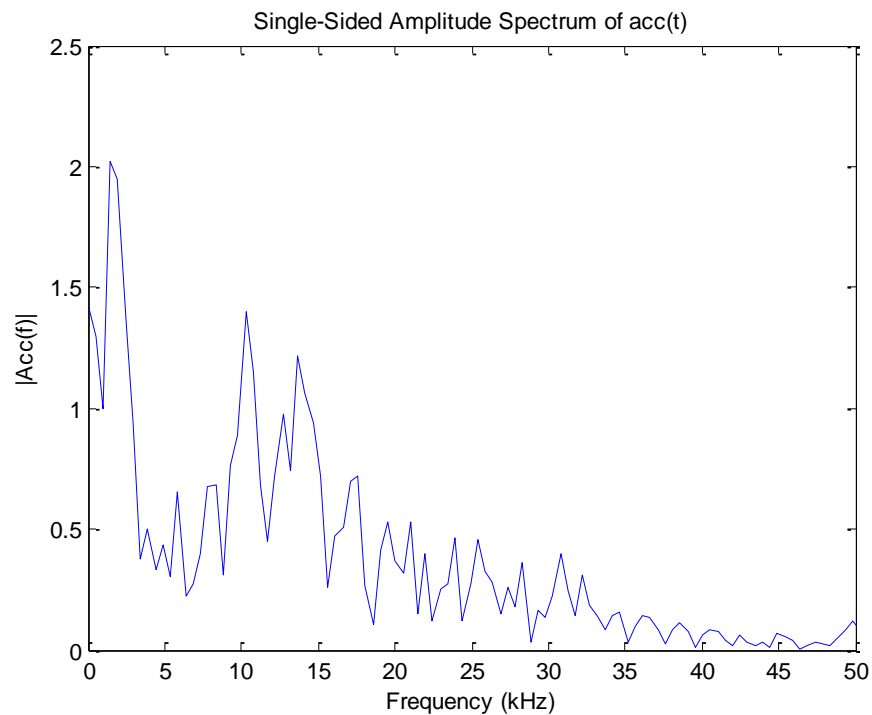
Figure 4.2.12 FFT of the acceleration pulse from the initial drop

Though this high frequency content is very common in real world applications, it is not useful in this study. This study is concerned with obtaining a fundamental understanding of how PBGAs react under higher rate loading. A classic half-sine

66

acceleration pulse is more beneficial in accomplishing this goal. To obtain a cleaner acceleration pulse that would be more like a half –sine, a Lansmont 23-D shock tester was used. An accelerometer, model 350B23-ICP® from PCB Piezotronics, was used to monitor the acceleration during the drop event. It allowed for 10,000g maximum measurement and had a high sensitivity of 0.372mV/g at 100 Hz. The data was logged using the Test Partner 3 (TP3) program from Lansmont. For this testing, a recording time of 2ms and a sampling rate of 500,000 samples per second were used. This recording time interval was selected to provide the highest sampling rate that would capture the entire pulse duration. An example of the improved acceleration pulse can be seen in Figure 4.2.13. This was a 2,400 G acceleration pulse. The FFT performed on the improved acceleration pulse shows nearly negligible high frequency input in this signal compared to what is shown in Figure 4.2.12.

The same setup of 6 strain gages was used with the Lansmont drop tower. The sampling rate was 20,000 Hz. An example of a typical strain plot can be seen in Figure 4.2.14. The PWB strain appears to be influenced by more than the first natural frequency. The plot shows two separate frequencies acting on the board. The edge, center, strain gage 2 and strain gage 3 are dominated by the first natural frequency, ~700 Hz, while strain gage 4 and 5 appear to be dominated by the second natural frequency. ~1400 Hz. The calculated natural frequencies for an unpopulated clamped circular board are 920 Hz and 1750 Hz for the first two modes. The two frequencies can be better seen in the inset shown in Figure 4.2.14. This higher order mode influence does rapidly damp out as the signal decays.
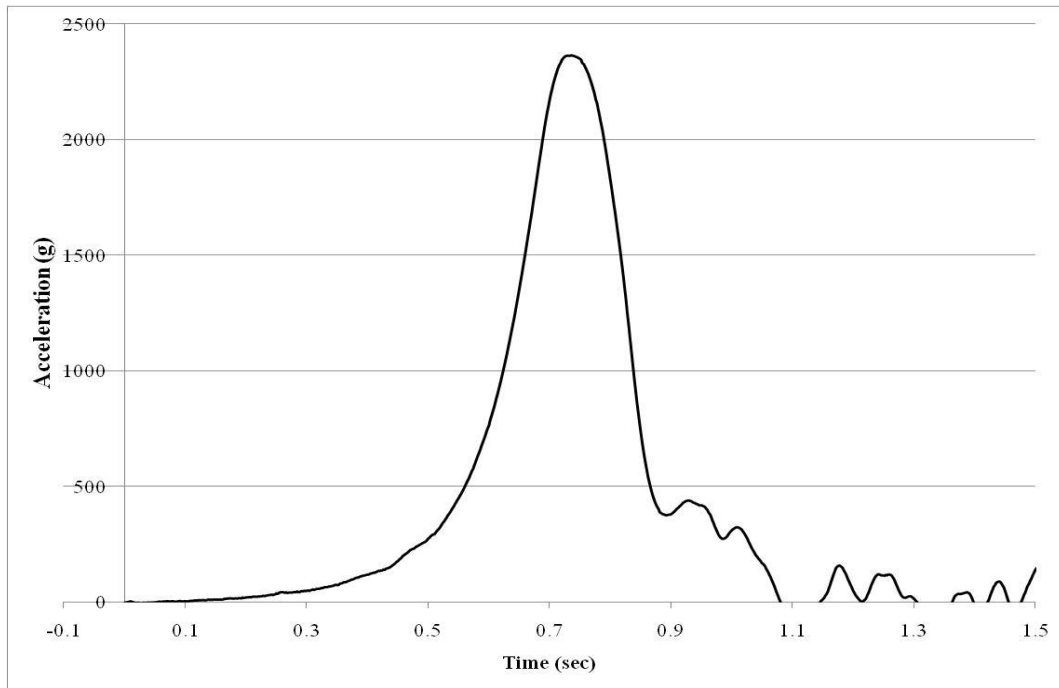
Figure 4.2.13 Improved acceleration pulse
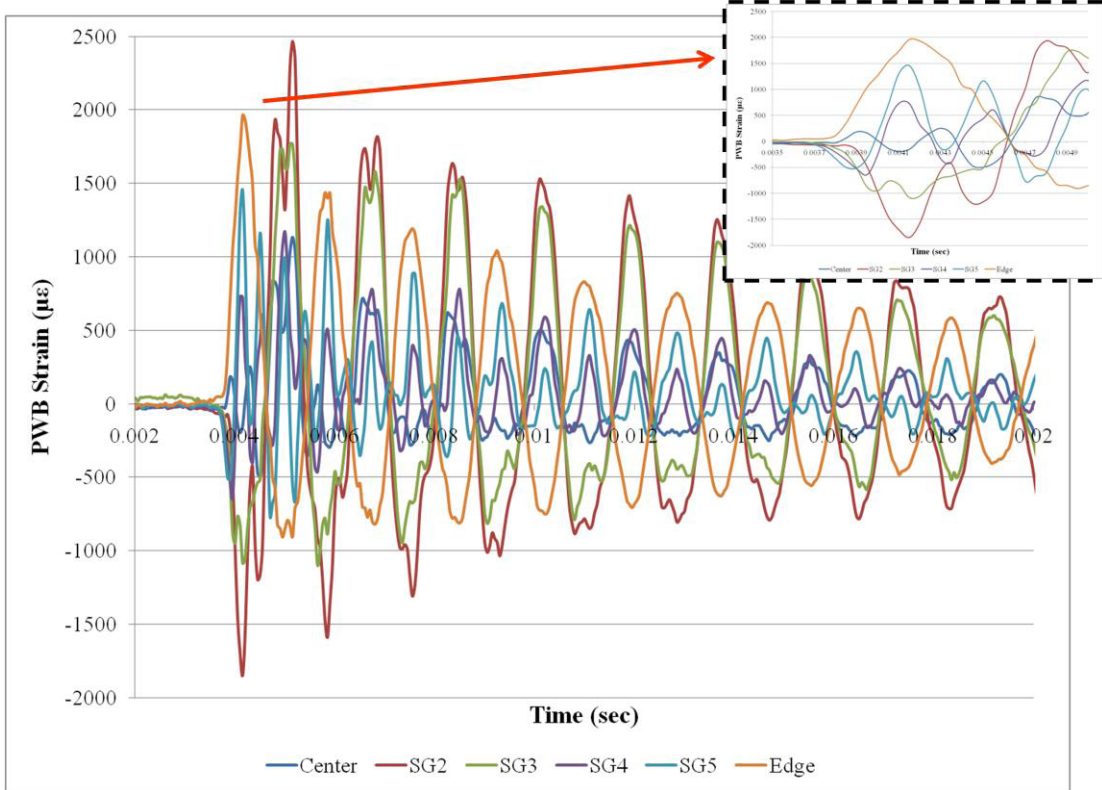
Figure 4.2.14 Sample strain plot

Figure 4.2.15 and 4.2.16 depict representatives of the failures observed after the test. The same phenomenon of the PBGA separating from the board was seen but it was not the only cause of the observed failures. Copper trace and board failure were the most prevalant failure modes though some instances of bulk solder failure were noticed. The same failures were seen for both SAC and SnPb coupons.
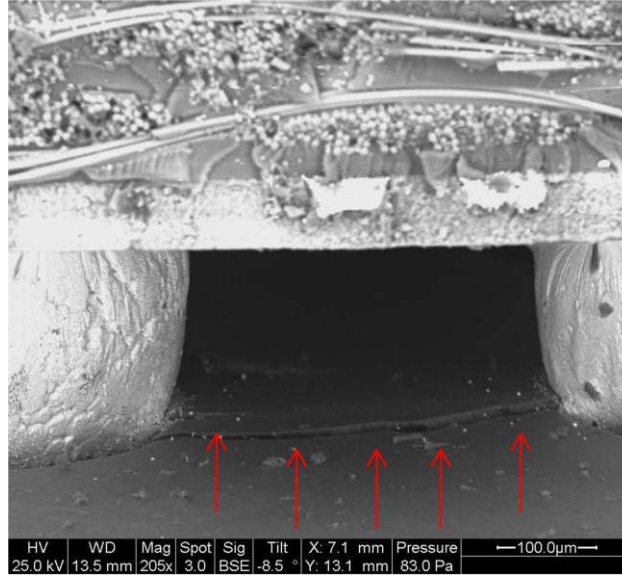
Figure 4.2.15 Drop test failure picture- trace pull up (SnPb, PBGA1)
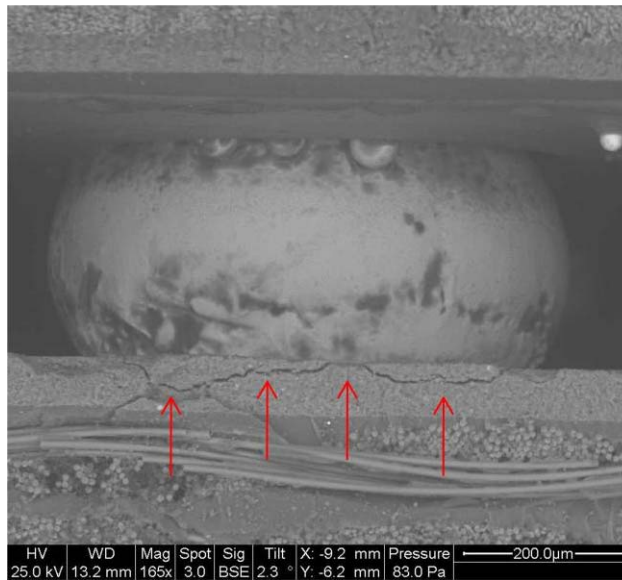
Figure 4.2.16 Drop test failure picture cracking under copper pad (SAC, PBGA6)

The failure data from this set of drop testing was added to the data obtained from the four point bend testing in Figure 4.2.17. The strain data was correlated to the location of the component on the test coupon. The PWB strain that is plotted for the high rate

data is the PWB strain for the ring in which the component is located. This is not necessarily the maximum PWB strain. There is a slight decrease in durablity in the SAC and SnPb PBGA assemblies but the data in Figure 4.2.17 counted only each drop as one cyle to failure. Each drop accounts for more than one strain reversal. To account for the multiple strain revesal per drop, the strain data was examined to determine the number of strain reversals that were seen by each component. Since the strain is a decaying signal the cycles counted for the drop data account for the first nine oscillations seen by the compnent except in the cases where the second mode was apparent. These component saw an extra three reversals (12 total). This is shown in Figure 4.2.18. The drop data corelates well with the bend test data. It was found that varying the number of strain reversals that equated to one drop did not shift the data much due to the plot being in log-log space. The PWB strain rate is indicated in Figure 4.2.19 along with the associated failure data. The graph contains failure data covering strain ranges for four orders of magnitude. This test showed that the PWB strain rate has no decernable effect on the number of cycles to failure. Yet it must be noted that others have found a strain rate dependence in while testing lead and leadfree solders [19][29][34][59][62][63][64]. These studies, however reported, failures only in the bulk solder, whereas the work here had mixed failure modes (in the PWB and bulk solder).
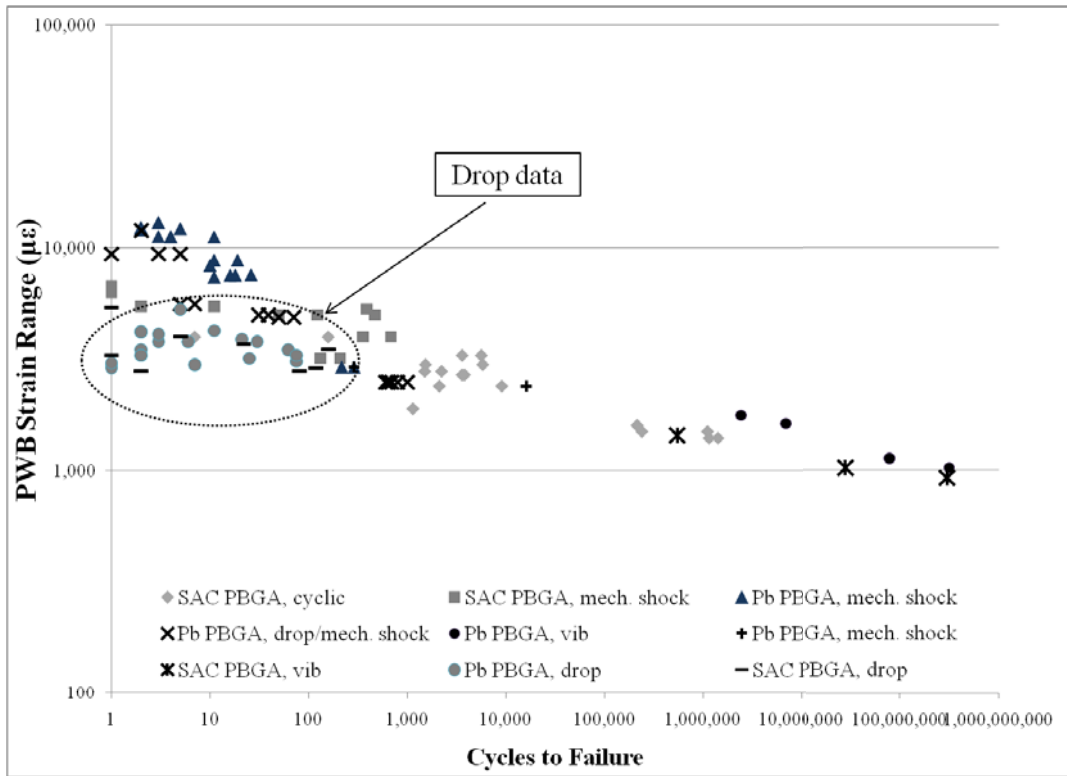
Figure 4.2.17 Unadjusted Drop Data
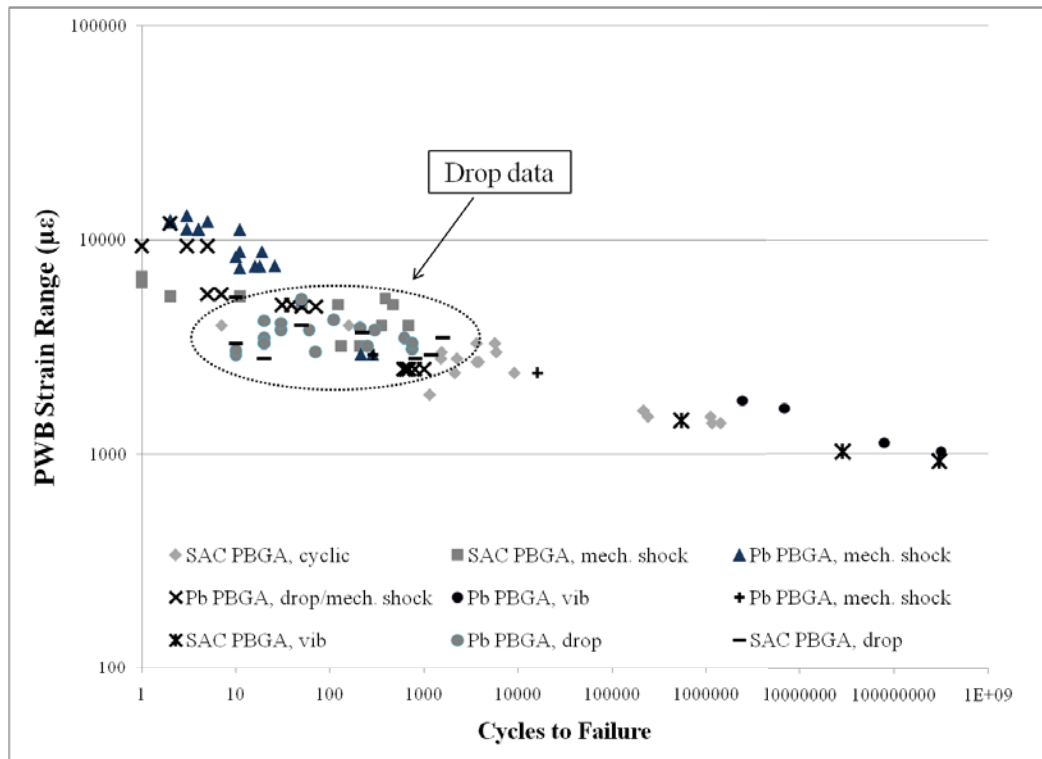
Figure 4.2.18 Adjusted Drop test results

72

Figure 4.2.19 plots the combined data from the vibration, bend and drop testing. The PWB strain rate varies from 10^{-3} to 10^{0}. The data is for SnPb eutectic and SAC305 solder assemblies. The standard error line for one and four standard errors about the y intercepts are plotted. Despite the aforementioned differences in the data, the shaded area in the figure clearly indicates a failure free area for a regon 4 standard error from the mean. This shaded area can serve as a design goal for PBGA survivablity during circuit board design, adjusting the line for the desired number of standard errors to serve as a saftey factor.
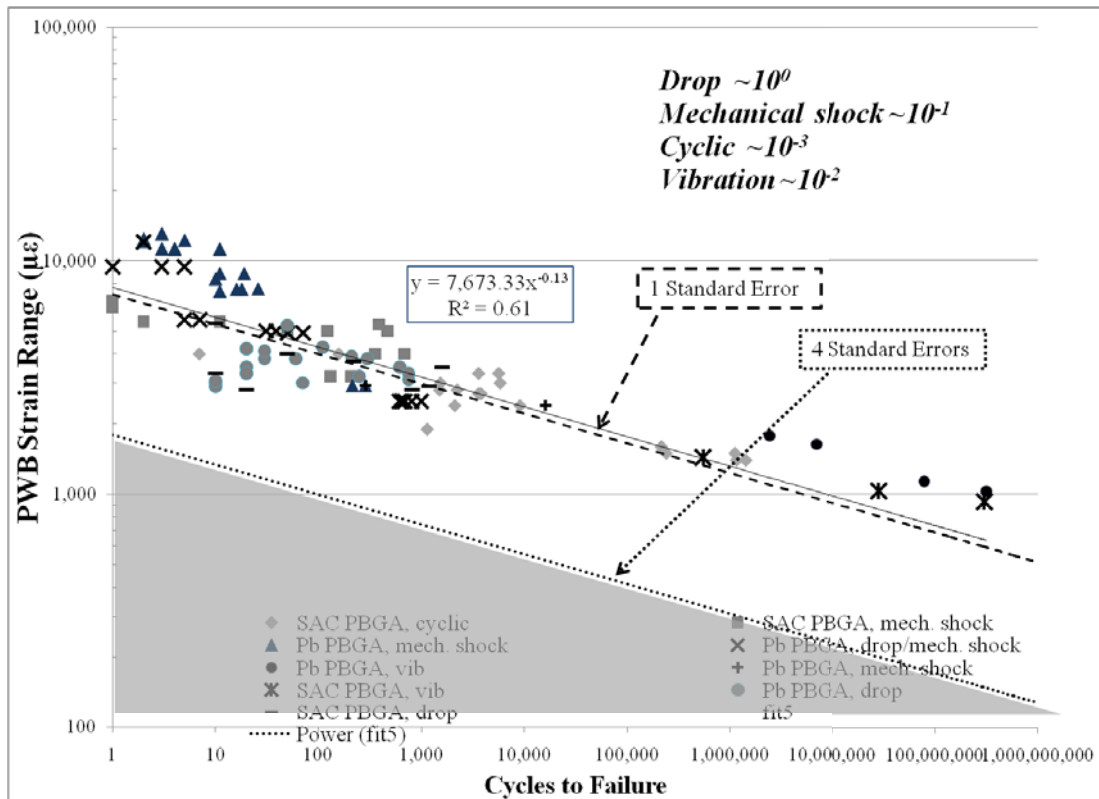
Figure 4.2.19 Combined data plot

Conclusion

This section examines the fatigue behavior of PBGA components mounted on an FR-4 printed wiring board that is subjected to bending. The PWB bending strain rate was rapid enough to assume any solder creep was negligible. By using a combination of mechanical four point bend testing and drop testing the PWB strain rate was varied from about 10^{-3} to 10^0 per second. The PBGA components were daisy chained and the board routed so that continuity could be monitored. A 300 ohm increase in the circuit resistance served as a failure indicator and from simultaneous monitoring of the PWB strain it was possible to determine to the strain level and cycles to failure.

Two different solder assemblies were compared; normal lead based Sn37Pb solder and an alternative lead free solder Sn3.0Ag0.5Cu solder (SAC 305). OSP was used on the PWB copper land finish for both solders, due to previous researchers finding that SAC 305 and ENIG copper land finish exhibited early failures in drop testing.

It was observed that the fatigue failure site for the PBGAs varied as a function of the load level. For high levels of printed wiring board strain and relatively short times to failure, on the order of 10 cycles, the failure site was within the PWB and due to breaks in the copper traces. The copper lands and traces were pulled out of the board, often along with a chunk of the board laminate material. As the PWB strain was lower and the fatigue life increased (10-100,000 cycles), failure sites were found to be a combination of copper land and trace failures along with solder fatigue cracks in the solder intermetallics. For low PWB strain levels which resulted in fatigue life of

100,000+ cycles, or in the classic high cycle fatigue life region, the failures were mainly fatigue cracks in the bulk solder and intermetallics. Despite seeing different failure sites, the SAC 305 failure data when plotted in a durability fatigue plot exhibited a linear behavior. There was no visible transition between the low cycle fatigue regime and the high cycle fatigue regime. A single power law fatigue failure model fit the complete range of failures.

There was found to be no difference in the high cycle fatigue behavior between Sn37Pb solder and SAC 305 assemblies. The conclusion was reached by comparing the failure data obtained in this study as well combining it with additional data from testing by other individuals. It was noted that the Sn37Pb soldered PBGA assemblies perform better in the ultra low cycle fatigue region.

No PWB strain rate influences were seen in the failure and fatigue data for either SAC 305 or Sn37Pb solder. The mechanical cycling and vibration yielded PWB strain rates on the order of 10^{-3} up to 10^{-1} per second. Drop testing raised the PWB strain rates up to 10^{0} or 1/s. All the drop testing failure data overlaid the other testing data in the durability plot.

A final durability plot of all the PBGA failure data clearly shows a design limit for FR-4 PWB strain range for failure free operation. This plot is a very useful tool for board designers.

Chapter 5: Comparative Fatigue Behavior for Surface Mount Components Assemblies with Sn37Pb and SAC305

In previous section, PBGAs and LCRs packages were evaluated for their survivability under bending loads. SN durability curves were developed using printed wiring board strain as the "stress/strain" parameter. Several other studies have used the PWB strain for their evaluation of electronic component durability [16][18][19][28][29][48]. Most recently Zhao, et al [46] used PWB strain to evaluate the robustness of ICs under high frequency cyclic bending for different combinations of lead free solder. Wong et al [49] performed drop and bend testing while varying the material properties and manufacturing processes and used the PWB strain as the stress parameter for SN curves to evaluate their failure data. Using PWB strain as the failure metric is very convenient for comparisons between types of solders when a single type of component is used. Using PWB strain avoids the need for performing a detailed finite element analysis (FEA) of different components and it is a very easy parameter to experimentally measure.

The problem with conducting detailed FEA models is that it requires a highly trained and experienced user. In addition the finite element analysis is a very time intensive process which includes, building the model, obtaining detailed material properties, and then post processing the analysis to determine a suitable stress or strain parameter. One of the biggest issues with conducting a detailed finite element

analysis is the extensive material, mechanical, and geometric properties required for an accurate analysis. These properties are at best difficult to obtain and sometimes just not available.

Using the PWB strain as the "stress" parameter in generating a durability curve is appropriate for evaluating the survivability of individual components with the same I/O count, size, PWB thickness, stress ratio, etc. but not for comparing one component family to another. The incorrectly plotted comparison of the fatigue life each component type as a function of PWB strain can be seen in the appendix. This section will use FEA modeling to obtain the stress in the solder for a particular component and use this solder stress to compare the behavior of the previously tested PBGA and LCR components in a master SN durability curve.

In comparing the results from different experimental tests with PBGAs and LCRs it is first necessary to remind the reader about the well know influence of mean stress on fatigue life. The effect of mean stress is commonly referenced in terms of the stress ratio, R, which is simply the ratio of the minimum alternating stress value divided by the maximum alternating stress value or R=σ_{min}/σ_{max}. As schematically shown in Figure 5.1, the mean stress has a great affect on time to failure. In the four point bend experiments previously discussed, the stress sinusoidally varies from a maximum value to approximately 0, or R = 0 and the mean stress = ½ of the stress range. In fully reversed bending ($R = \frac{\sigma_{min}}{\sigma_{max}} = -1$, zero mean stress), as seen in most vibration

environments, the fatigue life will be longer than alternating tension-zero loading

$(R = \frac{\sigma_{min}}{\sigma_{max}} = 0)$ for the same stress range.
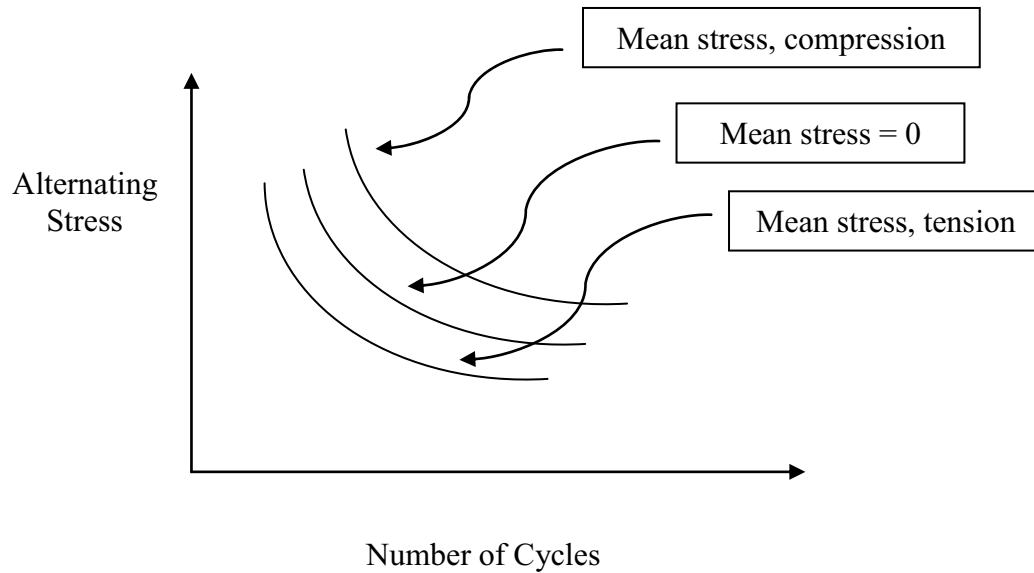
Figure 6.1. Effect of mean stress [45]

Experiments

A picture of the test coupons for the PBGAs and LCRs are seen in Figures 6.2 and 6.3, respectively. The PBGA coupons were assembled with Sn37Pb and Sn3.0Ag0.5Cu with OSP on the copper pads. The 2512 coupons were assembled with these same solders but had bare copper before reflow. These coupons were subjected to four point bend alternating tension only testing. The four point loading allowed for a constant bending moment in the area where the components are located. The printed wiring board strain and continuity were monitored during the test. SN

durability curves were developed for each family of components with PWB strain serving as the "stress/strain" parameter for the SN like durability plot.

Printed wiring board strain cannot serve as the basis for a master durability failure curve or serve as an accurate basis for comparing different component families. The results need to be shifted based upon the size of component, component solder attach size, PWB thickness etc. PWB strain is convenient to use for quick analysis of tests with common components, but for a master curve analysis needs to be based on the critical strain or stress in the solder where the fatigue crack initiates.
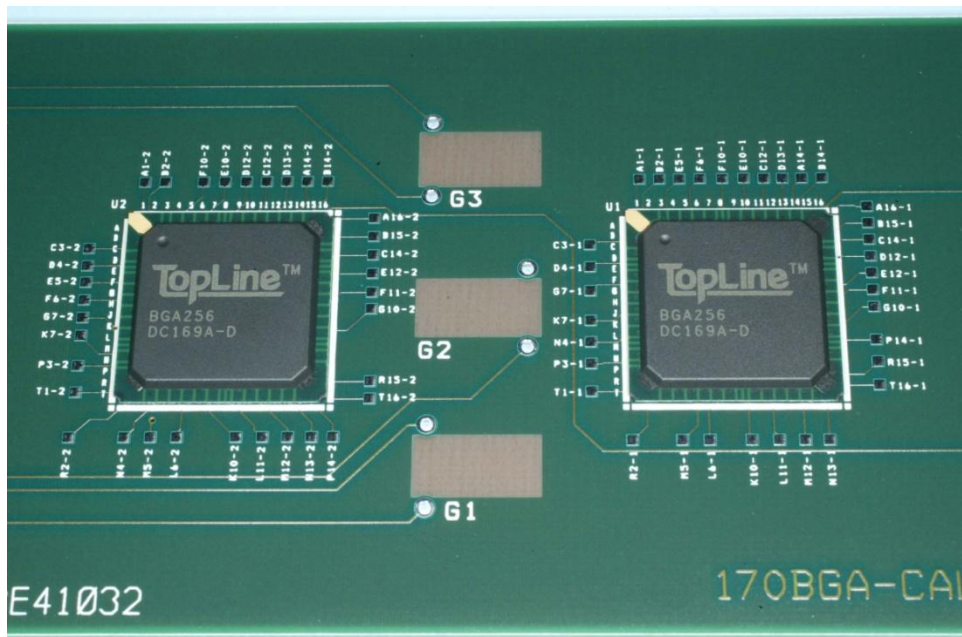
Figure 6.2. PBGA Four-point bending test coupon
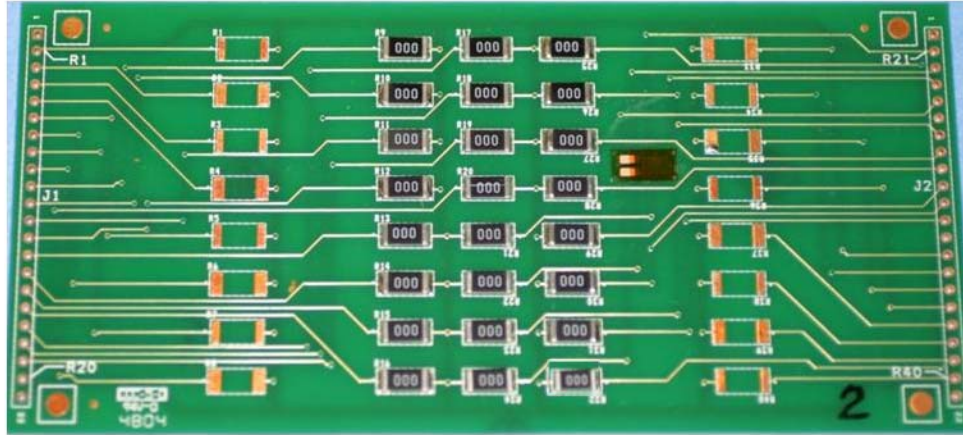
Figure 6.3. LCR Four-point bending test coupon

Discussion

In order to properly compare the PBGA test data to other test data, an FEA model was created to obtain the stress in the critical area of the solder joint. For the PBGA, that critical area is the top of the solder ball closest to the PBGA or the bottom of the solder ball closest to the PWB. The picture of the FEA model can be found in the appendix. This FEA model is a two dimensional linear elastic analysis and only uses elastic properties for all materials including the solder. A linear elastic analysis was conducted because in high cycle fatigue, the response of the solder is predominately elastic and any plastic deformation can be considered negligible. For different sized PBGAs, and for the LCRs, a stress index value in the solder needed to be determined. Neither a maximum stress nor an entire volume averaged stress in the solder is appropriate for this task. A maximum stress was too sensitive to the geometric singularities and the mesh density of the model while a complete volume averaged stress was too sensitive as to whether a solder joint was bulbous or solder starved.

The choice of the stress parameter, or method of calculating a stress value for the solder joint, follows the approach which has been developed for use in determining a stress value in solder joints for thermo-mechanical fatigue. In thermo-mechanical fatigue a volume average is calculated over 10% of the solder joint in the critical stressed region where a fatigue crack is expected to initiate. Examples of this approach can be seen in Darveaux's [20][26], Qi [50], Zhou [13] and Osterman [52]. Using the 10 percent volumetric average helps smooth out any artificial stress concentration effects that may be present in the FEA model, yet it is sensitive to the stress in the critical region of the solder joint.

For each component compared, a finite element model was created and a 10 percent volume average stress calculated. For such an elastic analysis, this calculated 10 percent volume averaged stress is directly proportional to the far field PWB strain. From the FEA it is then possible to convert all the PWB strain values in the durability plots to equivalent solder stress values. The plot in Figure 6.4 shows the result of this conversion. Figure 6.4a depicts the durability plot of the PBGA data with the PWB strain range plotted on the vertical axis and Figure 6.4b shows the durability plot of the same PBGA data with the interconnect stress index value (10% volume average) on the vertical axis. As expected, the plots are basically identical with only changes in the values of the vertical axis. The plots are nearly identical because the components in this plot are all identical sized PBGAs and with a linear elastic analysis the PWB strain is directly proportional to the solder stress. The only minor difference is between the Sn37Pb solder and the SAC305 solder, because the elastic modulus of

the two solders is not exactly equal. The elastic modulus of Sn37Pb was assumed to be 36 GPa [55] and the modulus of SAC305 was assumed to be 40 GPa [54]. For the same PBGA component and same PWB strain, the SAC305 solder stress will be about $40/36 = 1.11$ or 11 percent higher.

Basquin's power law relation, $\sigma^b N = \text{constant}$, is used here to model fatigue behavior of the PBGA coupons. The high cycle fatigue (HCF) exponent, b, for the PBGAs with Sn37Pb is 12.5, (90% CI is 10.7 to 17.5). The SAC high cycle fatigue exponent is 10 (90% CI is 9.1 to 11.1). However, the 90% confidence intervals for these two exponents overlap indicating that there is no statistical difference in their values. Performing as z test as done in chapter 3, assuming the means are equal, yields

$$-1.645 \leq z = 0.066 \leq 1.645$$

Hence, the numerical difference between the HCF exponents for the PBGA coupons with SAC305 and Sn37Pb is statistically insignificant. Thus there is no significant difference between the HCF life for PBGA assemblies with SAC305 and Sn37Pb under bend loading.
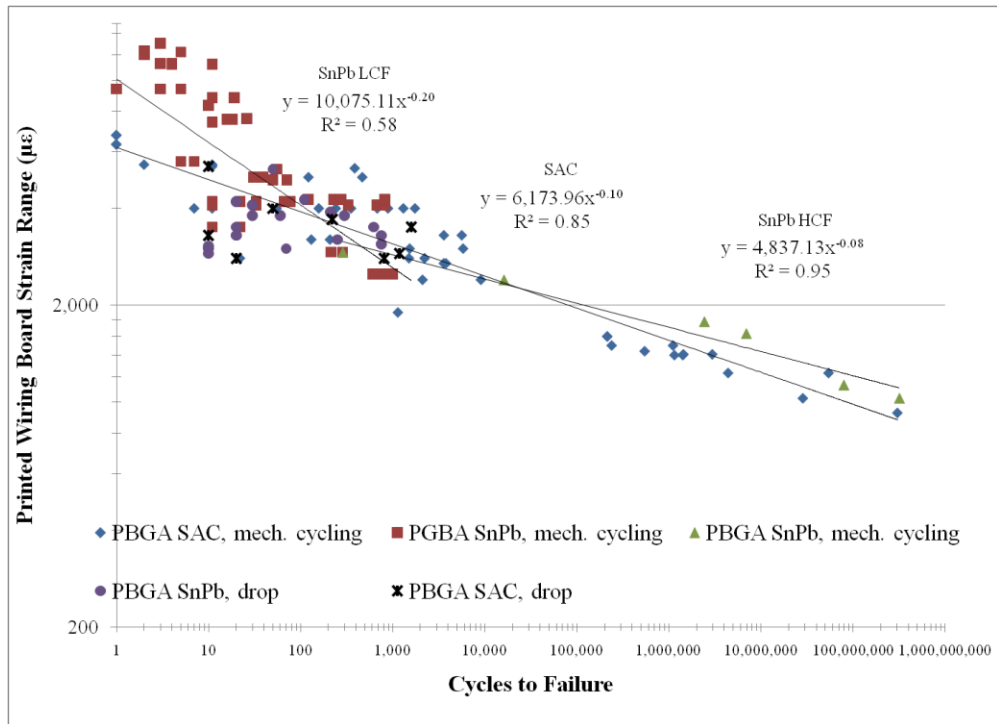
(a)
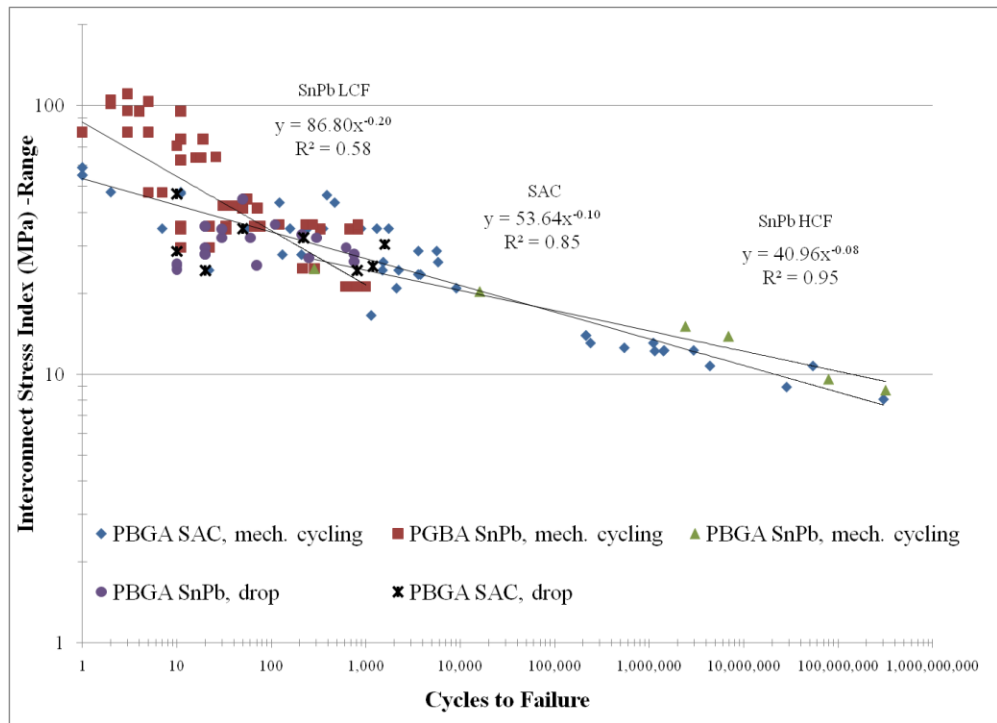
(b)

Figure 6.4. a) PBGA durability plot with PWB strain range b) PBGA durability plot with solder stress

A similar FEA analysis was conducted on the 2512 LCRs. For this component, the critical stress area is in the area beneath the copper pad. Again a 10% volume average stress was calculated as a function of PWB far field strain for both the Sn37Pb and the SAC305 solder to obtain an interconnect stress index. Figure 6.5 shows the addition of the LCR data to the previous durability plot seen in Figure 6.4(b). The addition of this LCR data further demonstrates that SAC305 and Sn37Pb have similar durability under bending loads.

Though the addition of the LCR data changed the value at which Sn37Pb regression line crosses the SAC305 regression line in the high cycle regime, the difference between the two data sets remains statistically insignificant. The fatigue exponent for SAC305 increased from 10 to 11.1, and the fatigue exponent for Sn37Pb increased from 12.5 to 14.3 but their 90% confidence interval remain overlapping. It needs to be noted that this additional LCR data consists of over 200 data points because each test coupon had 24 resistors. This addition of a large number of data points increased the spread of the failure distribution and increased the value of the fatigue exponent. The fitted power law model through a linear regression basically fits to the mean time to failure or 50% of component failure. In chapter 3, it was pointed out that using a mean time to failure results in a higher fatigue exponent than if one would fit to 1 or 10% failure percentage.
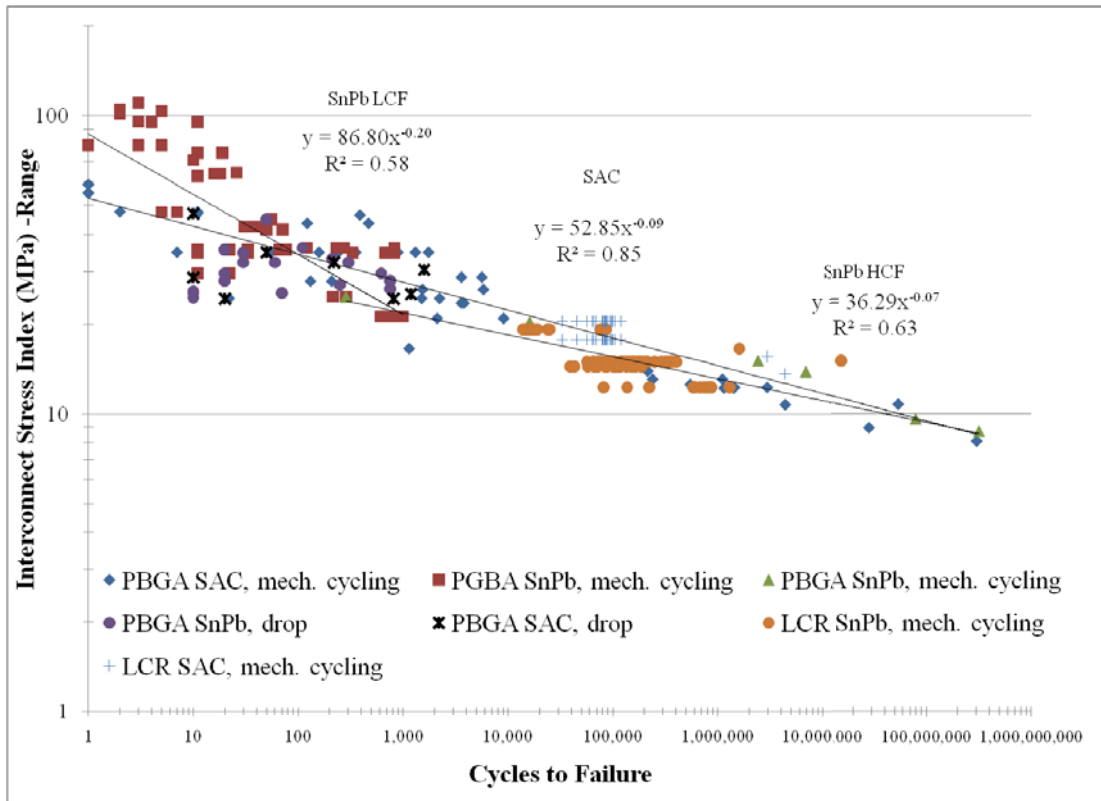
Figure 6.5. LCR Fatigue data with BGA data for stress in solder

To add further data to this master curve the PBGA data from Paquette et al [56] was investigated. Paquette performed harmonic vibration testing on partial perimeter array 160 I/O, 0.8 mm pitch Amkor brand BGAs. The strain in these tests was measured underneath the component. This caused the stiffness of the component to influence the measured PWB strain. To accurately compare the strain values from these tests to the four point bending tests, a 2D linear elastic FEA simulation was run to determine the relationship between the strain under the component to the strain away from the component on the PWB where the component stiffness is negligible. The results from this FEA simulation were used to transform the reported strain values to a strain comparable to the four-point bend PWB strain. The critical average

stress in the solder was also calculated from a FEA model of the Amkor PBGA, as described earlier. Figure 6.6a shows the PBGA data with the converted data from the Paquette experiment.
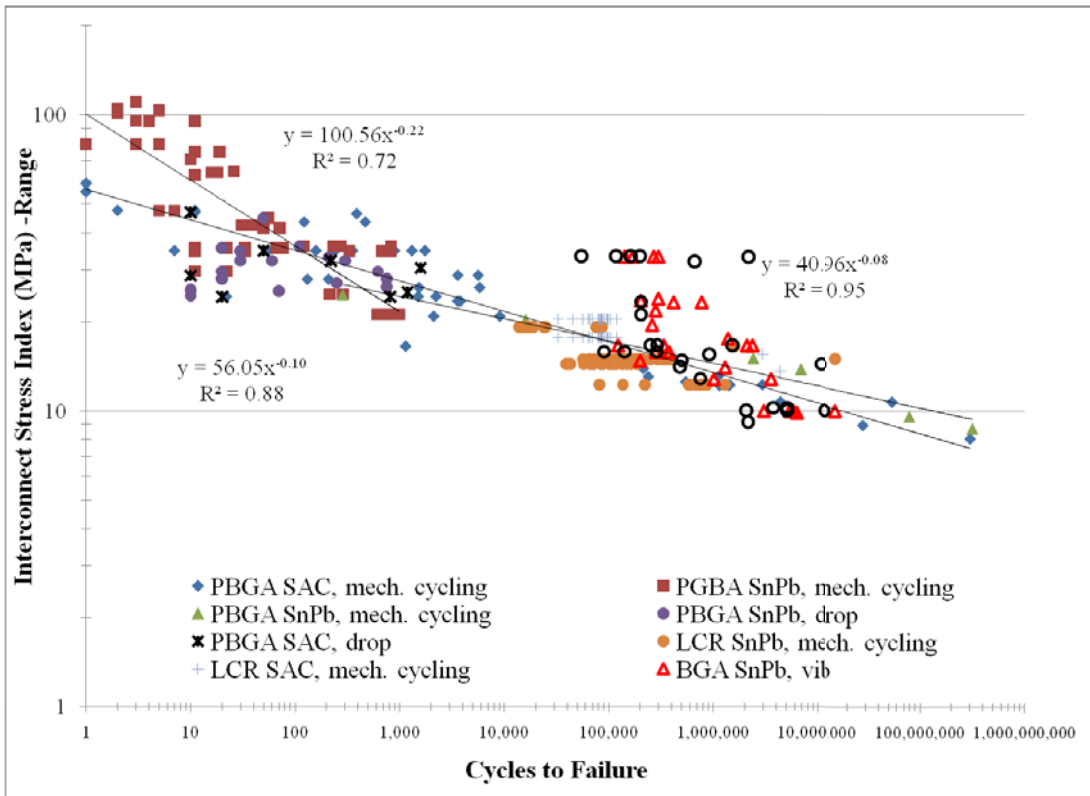
(a)
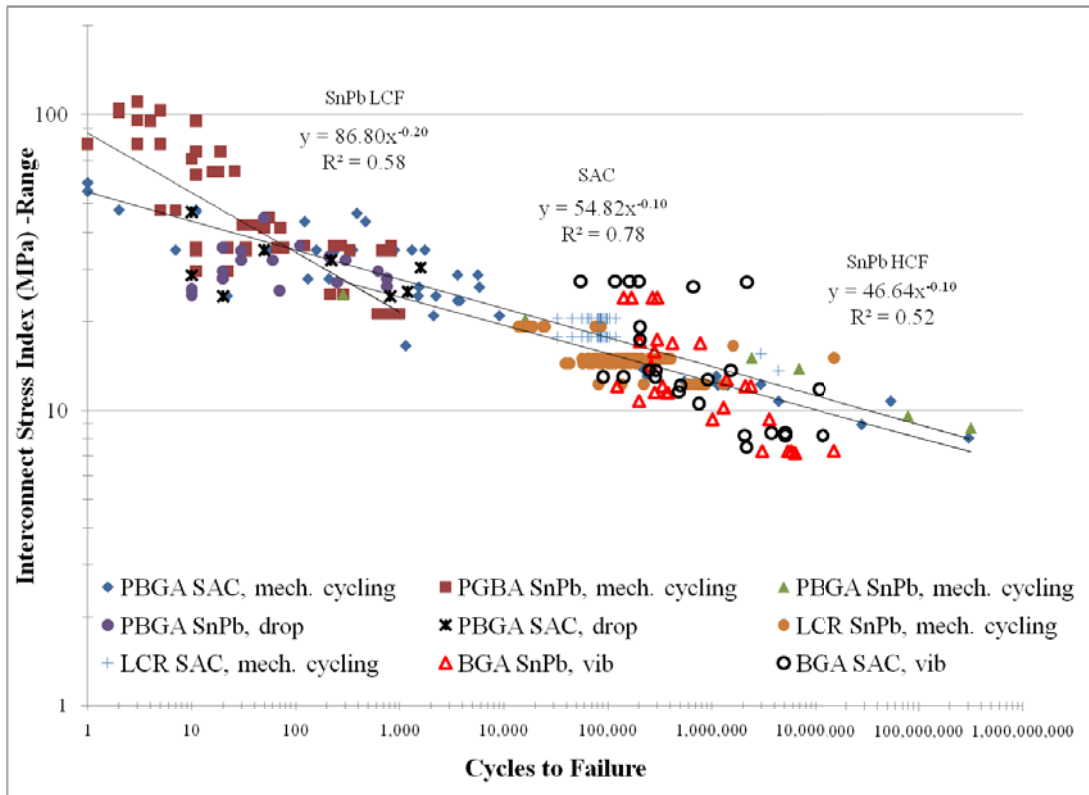
(b)

Figure 6.6. a) PBGA data with vibration data from Paquette-unadjusted a) Data adjusted to account for R-ratio effects

The vibration failure data from Paquette as seen in Figure 6.6a appears to be slightly higher than the four point bending data of the PBGAs and the LCRs. This is actually expected and is attributed to the fact that the vibration test performed by Paquette is fully reversed loading with a zero mean stress, whereas the four-point bending data is tension-tension testing with a mean stress equal to the stress amplitude or one-half the stress range. The effect of the mean stress needs to be accounted for. A simple approximate way to do this is through a modified Goodman diagram [47].
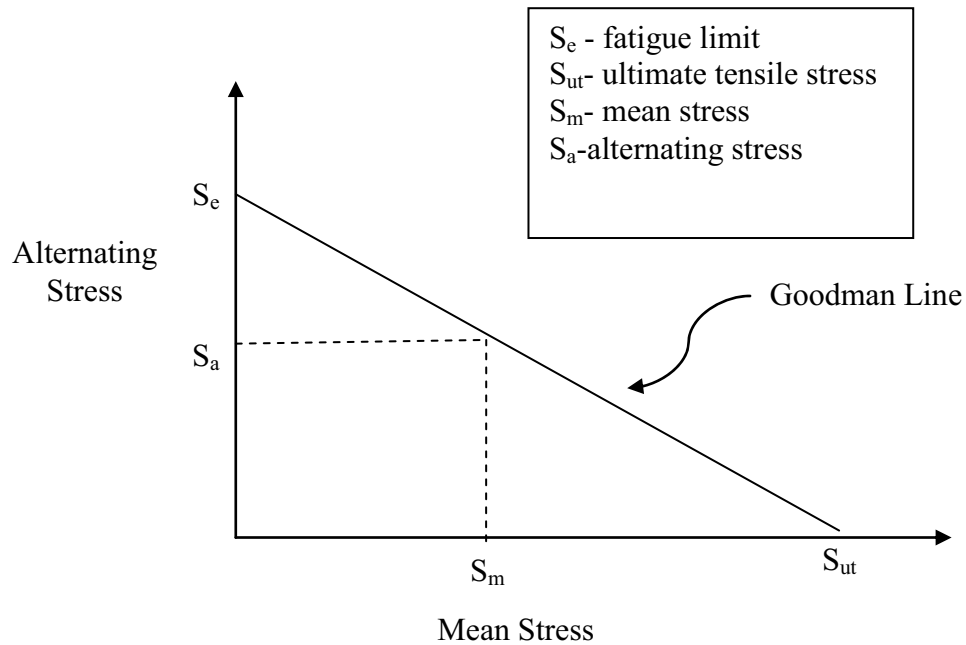
Figure 6.7. Modified Goodman diagram

A modified Goodman diagram is capable of being used account for different stress ratios in a SN curve. The Goodman diagram can be used to determine a correction factor or transform two different sets of fatigue data with different mean stresses to a common base. The following discussion will describe how we can transform the Paquette PBGA data with zero mean stress to an equivalent set of data with mean stress equal to the stress amplitude (the four point bend test results).

Figure 6.7 shows a schematic of a typical modified Goodman diagram. The mean stress is plotted along the horizontal axis and the alternating stress amplitude is plotted along the vertical axis. The Goodman diagram was originally developed to

determine an equivalent endurance limit for a material under conditions of non-zero mean stress. Rather than an endurance limit, the Goodman diagram can be used to determine the equivalent stress at some particular life under a nonzero mean stress. From Paquette's test data and the FEA analysis, the critical stress amplitude for zero mean stress can be obtained for a life of about 1 million cycles. This point, which equated to approximately 11 MPa (value obtained from durability plot), is plotted on the vertical axis, as shown in Figure 6.8. If there were no alternating stress amplitude, it can be assumed that the solder joint would fail when it reaches its critical tensile stress value. Typically in the Goodman diagram, this is taken to be the yield strength. Thus, a point is placed on the horizontal axis at the yield strength of solder 27.2 MPa [53] as shown in Figure 6.8. A straight line is drawn between these two points. This line is assumed to be the loci of all failure states between zero mean stress and zero alternating stress amplitude. For the four point bend testing, the mean stress equals the alternating stress amplitude. This condition is represented in the diagram with the dashed lines, x. From simple geometry the ration S_a/S_e can be calculated and is found to be 9/11. This ration is how much Paquette's stress values should be reduced so that they can more accurately be plotted on a SN diagram for R=0, mean stress equal to alternating stress amplitude. The plot adjusted for this R-ratio effect can be seen in Figure 6.6b. Accounting for the different mean stresses between the two experiments increased the agreement between the two data sets.
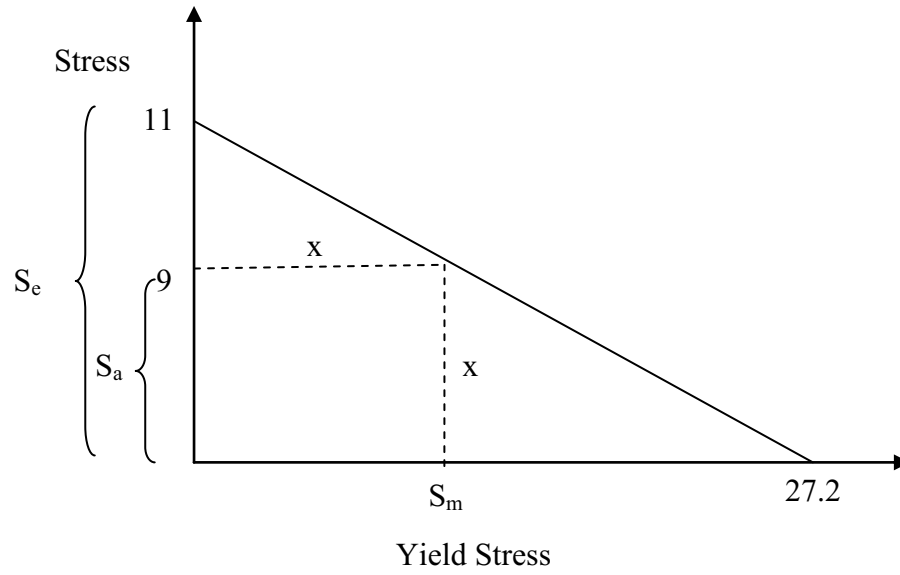
Figure 6.8 Correction factor diagram to account for fully reversed bending

The addition of the corrected data from Paquette, gives a fatigue exponent of 10 for both the SAC305 and Sn37Pb solder. The 90% confidence interval about the fatigue exponent for the Sn37Pb solder assemblies (9.2 to 12.2) contains the entire range of the 90% confidence interval for SAC305 (9.4 to 11). Performing a z-test and again assuming the means are equal yields

$$-1.645 \leq z = 0.0183 \leq 1.645.$$

Hence there is no statistical difference in the high cycle fatigue behavior of SAC305 and Sn37Pb assemblies.

Conclusion

This section creates a master fatigue curve for SAC 305 and Sn37Pb solder for components attached to a PWB subjected to bending at a fast enough rate that solder

creep can be considered negligible. The fatigue data as a function of a interconnect stress index is shown in Figure 6.9. Fatigue data from two different package types, BGAs and LCRs were initially used in the creation of a durability curve. To combine the fatigue data from different component families, an equivalent 10 percent volume averaged solder stress is calculated by FEA in the critical region of the solder joint where a fatigue crack would initiate. Additional fatigue data from vibration testing by Paquette was added. The resulting master SN durability plot clearly shows that there is no statistically significant difference in the fatigue behavior of these two solder types outside the ultra low cycle fatigue region (<10 cycles). As explained in Chapter 4, in the ultra low cycle fatigue region, Sn37Pb solder is more durable. The combined data presented in this section gives greater confidence in the modeled behavior of electronic assemblies with these solders. This section also emphasized the importance of accounting for the effect of the mean stress when comparing test results.
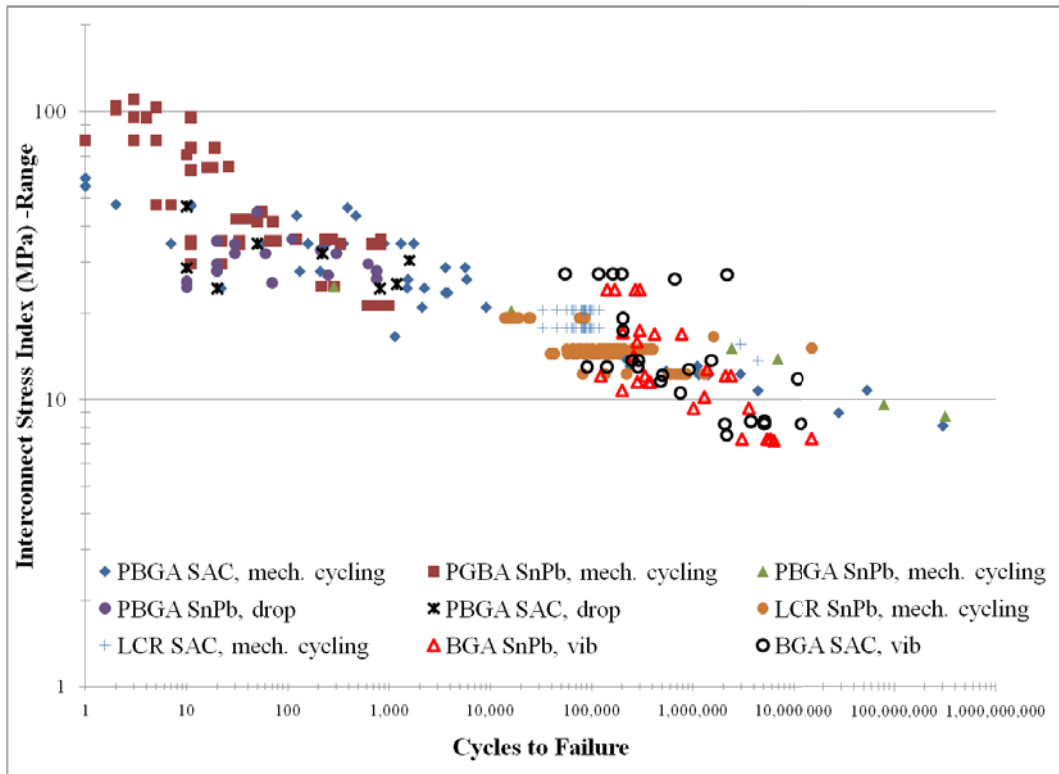
Figure 6.9. Sn37Pb and SAC305 master durability curve

Chapter 6: Conclusions, Contributions, and Future Work

Conclusions and Contributions

This work was initially motivated to assess the inclusion of electronic devices in extremely harsh shock loading conditions A typical acceleration profile includes a peak value of 10,000 – 100,000 G's applied over a timeframe of milliseconds, and 1,000 – 5,000 G's applied over a timeframe of microseconds. Such large accelerations can produce stresses and deformations that can exceed the structural limits of packaged electronic hardware. This dissertation focused on obtaining a better understanding of the mechanical behavior of Sn37Pb solder and SAC305 (Sn3.0Ag0.5Cu) at PWB strain rates between 10^{-2} and 10^{0} and obtaining an initial failure model for PBGAs under these strain rates. Once this fundamental understanding of this behavior has been achieved, this work can be extended to encompass the desired higher strain rates.

Summary Conclusions

This dissertation provides a better understanding of the mechanical loading behavior of Sn3.0Ag0.5Cu and Sn37Pb solder assemblies. The bend tests were found to be an excellent method for observing durability trends. The 2512 resister components were first evaluated to gain a larger confidence in the high cycle fatigue exponent of Sn37Pb solder and whether or not this fatigue exponent changes when a lead free SAC solder is used. It was observed that the Weibull distribution shape parameter reduces as the time to failure increases. It was also noted that the shape parameters for the Weibull distribution for samples under mechanical loading are much lower

93

than one would obtain from thermal cycling meaning the failure distribution is much wider about the mean. The fact that the Weibull shape parameter is a function of the time to failure means that it is important to calculate various failure statistics or parameters such as the high cycle fatigue exponent at the desired failure percentage. The work with the large data set of LCR components improved our confidence in the fatigue behavior of SAC305 assemblies as compared to Sn37Pb assemblies. No significant difference between the HCF fatigue lives of these solders was observed.

The leaded SOIC and SOT components were tested to understand the effects leads have on time to failure. The leaded packages assemblies were found to have a much higher fatigue life than assemblies with 2512 LCRs. The fatigue life was so long that it turned out to be impractical to do extensive testing with these components. Our test fixture and board design did not allow us to apply large enough load to accelerate the failures so that they could fail in a reasonable period of time.

The largest amount of time was spent studying the fatigue response of mounted PBGA components when the PWB was loaded in bending. PWBs were mechanically cycled in a materials testing machine, subjected to vibration loads on an electro-dynamic shaker, and shock loaded by using a drop tower. The basic PBGA used in the testing was a 256 I/O, 1 mm pitch, mounted on a 1.59 mm (1/16") thick FR-4 PWB. From this testing, a durability diagram, using PWB strain, was created. This durability plot can be used to assess the components durability and this "master

curve" is used to assess the durability of Sn3.0Ag0.5Cu soldered assemblies compared to Sn37Pb soldered assemblies.

The insight gained during the course of creating the master SN durability curve is extremely valuable. Early in the testing program, failure analysis cross sections showed that there were different failure mechanisms responsible for the detected failure. Failure was defined as an increase in circuit resistance of 300 Ohms. In the PBGA samples tested at a high strain level, failure were seen in the PWB, mainly cracking under the copper pad or copper pad pull-out. For medium strain levels, failure was still seen in the PWB but there were also cracking through the intermetallics of the solder ball. At lower strain levels, failures were mainly seen in the bulk solder.

As a designer or engineer responsible for the reliability of the system, one is primarily concerned whether the system will work or not. Thus it was decided to continue to measure failure with simple loss of continuity, and not be concerned whether the failure was due to board or trace failure, or due to a crack in the solder joint. Using this definition of failure, it was found that for SAC305 solder PBGA test assemblies there is no low cycle to high cycle fatigue transition. If one were able to separate out just the solder joint failures, this result would probably be different. But with the two competing failure mechanisms, no transition was seen. It was surprising to see this low cycle to high cycle fatigue transition as evidenced by the slope of the failure line (fatigue exponent) with Sn37Pb assemblies even though board and trace failure was

seen. This implies that Sn37Pb assemblies are more compliant that SAC305 assemblies at very high loads.

The master SN durability model using PWB strain as the "stress" parameter was created using a large amount of failure data and was correlated with independently gathered data. To further correlate this data with other data generated with different components, an equivalent stress was calculated using finite element models. The equivalent stress was the 10% volume averaged elastic stress in the critical region of the solder joint where a fatigue crack would initiate. This allowed a more detailed master curve to be created using results from LCR testing and various sized PBGAs. The final results still show that there is basically negligible difference between the high cycle fatigue behavior of Sn37Pb assemblies and SAC305 assemblies. The natural scatter in high cycle fatigue data is so large that it is impossible to determine any statistical difference. The approach of converting PWB strain to an equivalent interconnect stress index can be used for any family of electronic assemblies for determining which particular component is the most susceptible to failure.

The PBGA study also evaluated the effect of PWB strain rate on the failure of PBGA assemblies with SAC305 and SnPb. No dependence on PWB strain rate was found between strain rates in the range of 10^{-3} to 10^{0} for FR-4 PWB material. This is possibly due to the PWB being the source of the majority of the failures in this higher rate testing. The PWB material may be the most important aspect of designing

electronic assemblies for survivability under high rate loading and in the low cycle fatigue regime.

Future Work

Future work can include:

- ➤ Continue the investigation of PBGAs under higher printed wiring board strain rates ($>10^0$) using different solder and board finishes to explore if this non-rate dependence holds true. The testing can also incorporate BGAs with varying pitch, array size, and manufacturers and explore the effect ageing may have in high rate testing.

- ➤ Explore the effect different board materials (other than FR-4) has on the failure modes and durability of PBGAs under high rate loading since this study found PWB to be the main source of failure in the high rate study.

- ➤ Determine if the leaded components are as durable under bending loads with lead-free solder types.

- ➤ Create failure models for other electronic components to determine with components are most susceptible to failure under mechanical loading. The results from these new models can be incorporated onto the master durability curve after obtaining the critical stress in the solder.

Appendix

The following is a review of the literature of the four model types, equations based, analytical based, finite element based and experimental based.

2.1 Current fatigue modeling/assessment techniques

Fatigue-life models can typically be divided into four main categories. Failure models that are based on equations, models that a based on analytical methods, models that are based on numerical or finite element techniques and models that are based on experimental results.[2] These categories are often combined with some studies, but generally there tends to be a dominant method or category used in the model creation.

2.1.1 Equation Based Models

Equation based model tend to rely on only previous experience and are not derived based on any other models. The best known example of this type of modeling is Steinburg's model. He created a model for determining the life of electronic components under shock and vibration loading based on the printed circuit board critical displacement. This critical displacement was based on the size and type of package and its location on the printed wiring board. This critical displacement however is not an actual PCB displacement but rather a value based on treating the

printed wiring assembly as simple spring mass system. An expected displacement is calculated using the peak acceleration and natural frequency.   The critical displacement is then compared to the expected displacement to determine if the component will survive. Though this model has been shown work well in the estimation of fatigue life, the usability is limited because the model is only applicable to a limited number of electronic components for which the component calibration factor has been previously determined. [3]

2.1.2 Analytical Based Models

The analytical based models are commonly used equations that are adapted to their current testing conditions by finding the material constants and making any necessary assumptions. The physics of the problem is used for determining failure. The following is a summary of different models developed using this approach. The main problem with these methods is that if the physics of the problem changes then the model and model constants can no longer be used to solve the problem it was originally developed to solve.

The Coffin-Manson equation is often used as a basis for starting model development for electronics in the low cycle regime. The Coffin-Manson Equation is $N_f = A \ \Delta\varepsilon^{\ m}$, where N_f is the number of cycles to failure, $\Delta\varepsilon$ is the inelastic strain range per cycle, and m and A are material constants. These material constants must be found during testing. Guo, et al. [4] developed a model based on the Coffin-Manson equation omitting the plastic deformation portion. The model was a semi-experimental model based on random vibration. Random vibration experiments were

done using 256 I/O plastic ball grid array packages to obtain material constants for their model. The model constants developed in this analysis are unique to a particular configuration and not easily adaptable to other configurations.

There are variations of the use of the Coffin-Manson equation. It is often combined with other models and used for model building. Shetty et al [5] built a fatigue model using Basquin's equation, for the high-cycle portion, and the Coffin-Manson equation. These were combined with finite element analysis to predict cycles to failure. The model constants were found by calibrating the experimental to simulation results. The cycles to failure are calculated based on the average strain energy density using these model constants. Chip scale packages were tested under monotonic bend tests to study their overstress limits and fatigue life using accelerated bend tests. A double sided board was used but failure in the bend test were only found on the top side for the overstress tests and more were found on the top side in the cyclic bend tests. This is normal for fatigue testing because cracks propagate in tension. Fatigue cracks were found in the solder during failure analysis.

Park et al [6] used the Morrow energy model, $N_f^m \Delta W = C$, where ΔW is the plastic strain energy density, m is the fatigue exponent and C is the material ductility coefficient) to determine whether energy density can be a parameter governing the fatigue life of solder alloy under mixed-mode loading conditions. 63Sn37Pb and Sn3.5Ag0.75Cu solders were tested using BGA packages. Some of the specimens were aged two months at room temperature and others were aged 72 hours at 100ºC.

Displacement controlled test subjected the specimens to a fully reversed triangle mixed load at constant displacements. The plastic strain energy density dissipated in a solder was assumed to be related to the fatigue life of the solder joint. This density was determined from the maximum force applied hysteresis loop. It also is noted that the material constants found by this study differed from the constants found in previous tests done by others.

Barker et al [7] performed a stress on the leads and solder joints of quad leaded components to determine the critical area of the attach without performing any finite element analysis. Basquin's law is then used to calculate the fatigue life of the component. This method is said to only be usable on compliant leads and where the component does not move with respect to the board.

2.1.3 Finite Element Based Models

This category of models is based solely on finite element simulations. Some of them however employ the use of case studies to test their models. The problem with models based on FEA is that they require a highly skilled user to develop the model and without proper meshing technique erroneous results can be given. They can also be time intensive to create and run detailed models. Sidharth et al [8] developed a finite element model for determining the fatigue life of the corner lead of a leaded assembly. The original model was not based on experiments but was later correlated with experimental data and found to be a good estimator of failure.

Finite element based models tend to be very complicated in their approach and are often simplified to reduce the amount of time involved. Sun et al [9] used a finite element simulation in conjunction with low cycle fatigue test to determine the constants in the Coffin-Manson equation for Sn8Zn3Bi and Sn37Pb. The model consisted of three parts, the solder joint, copper pads and the printed circuit board. A 3D model was used to include any edge effects. The shear strain range was calculated and the elastic strain was ignored.

Shetty, et al [5] tested chip scale packages using three- and four-point bending. The exact component type was not given for proprietary reasons. Double sided board and a servo-hydraulic MTS machine were used to carry out the testing. Packages on the top side of the board failed faster than packages on the bottom side at a given curvature. A finite element model was developed to predict bending failures. The model was based on deformation energy using the average strain energy in the critical solder joint (the corner solder joint).

Wang et al [10] demonstrated the complexities involved with using highly detailed FEA. The physics of the problem can get construed when using very detailed FEA. They used FEA along with drop testing to study the drop test sequence. Flip chip packages were tested but no failures were observed in testing. They attempted to model the full drop event but scaled back to a lees complicated model because they got errors two times higher than the actual event. Wong et al [11] showed FEA to be a useful tool in studying the physics of a problem. They examined the physics of board

level drop impact using FEA. They modeled three key events to aid in their analysis, velocity impact of a PCB, velocity impact of a PCB with central mounted component, and velocity impact of the drop assembly. They were each modeled as a beam, beam, and solid element with sub elements, respectively. From the FEA it was found that there are three drivers for failure in board level drop tests, elongation and bending of the interconnect from the difference in the flexure of package and board, the inertia forces of the package, and the stress wave at impact. The first cause dominates for packages near the center of the board while the last two dominate for packages near the support. They also found the out of plane stress to increase with height of the drop, thickness of the fall plate, length of the PCB, and package stiffness and size. It decreases with increasing solder bump height, size, and number and the diameter of the impact cone. It was also discussed that high strain rates tend to suppress any plastic deformation and raise the fracture toughness of ductile materials.

FEA can also be a very useful tool in studying the fatigue life of printed wiring assemblies. Zhou et al [12, 13] used a time domain approach to characterize the behavior of SnPb eutectic and SAC305. In the low cycle regime, the components were tested under broad-band random vibration. In the high cycle regime, a narrow-band harmonic vibration test was used. Through finite element analysis, a transfer function was found to convert the printed circuit board strain to solder strain. The Coffin-Manson equation was used to explain the behavior of the solder in low cycle fatigue; Basquin's relation was used in the high cycle regime. The model constants for each solder was calculated. Again this model found material constants based

upon and a detailed finite element analysis in the model development. To use the model the board strain would have to be converted to solder strain using FEA.

2.1.4 Experimental Based Models

Though most models involve some level of testing for validation purposes, these models are driven by experiments. The use of an experimental based model can be fairly accurate assuming the models developed are used properly. Zhang et al [14] performed isothermal mechanical durability tests using Sn3.5Ag, Sn3.9Ag0.6Cu and Sn37Pb. Nine, six, and eight samples, respectively, were tested. A thermo-mechanical-microstructural (TMM) test system was developed and used. A power law model based on crack propagation was used characterize the durability. Model constants were obtained for each solder based on the total strain range (TSR), inelastic strain range (ISR), and ΔW, the cyclic inelastic work density (based on the hysteresis loop). The tests were conducted at 25ºC and at a strain rate on 3.2E-2 1/s. The model constants were found using transformation functions. These model constants were found to be in good agreement with others in literature.
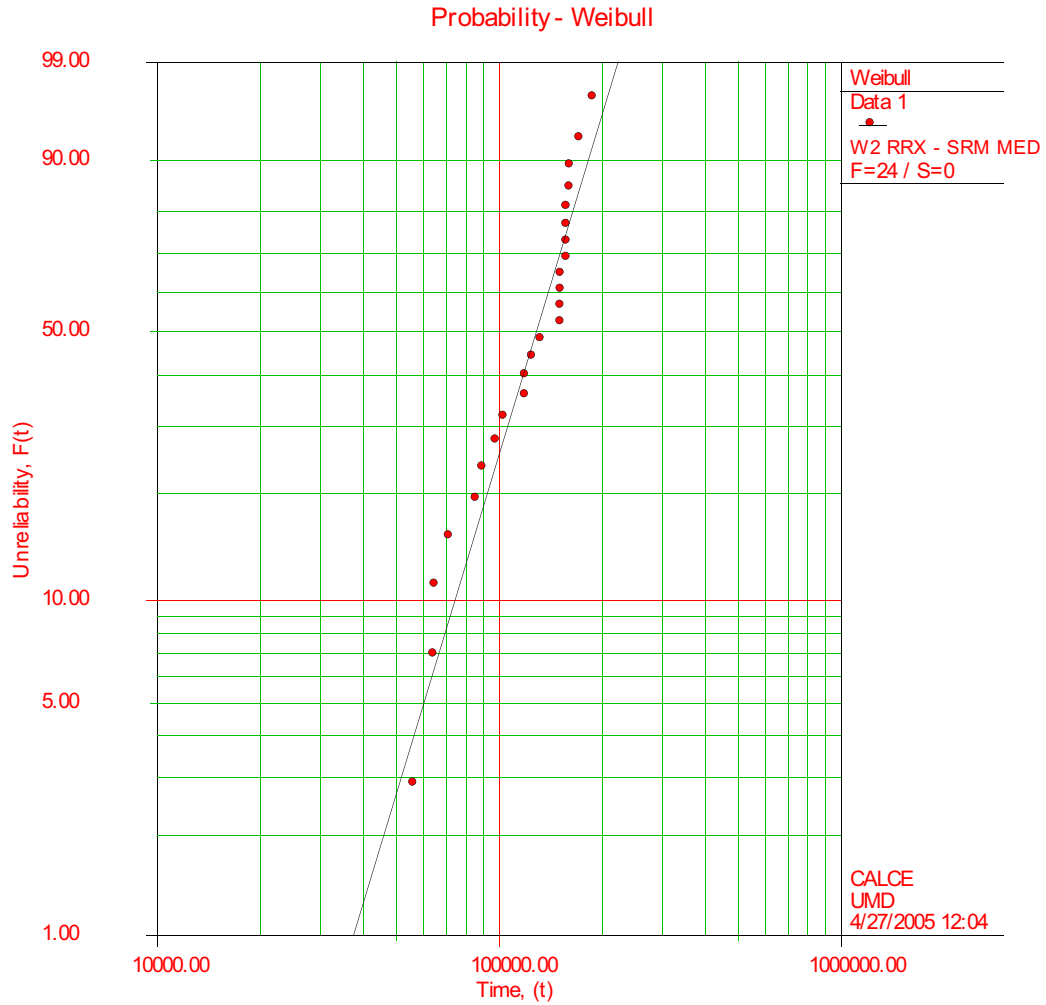
LCR Weibull distributions
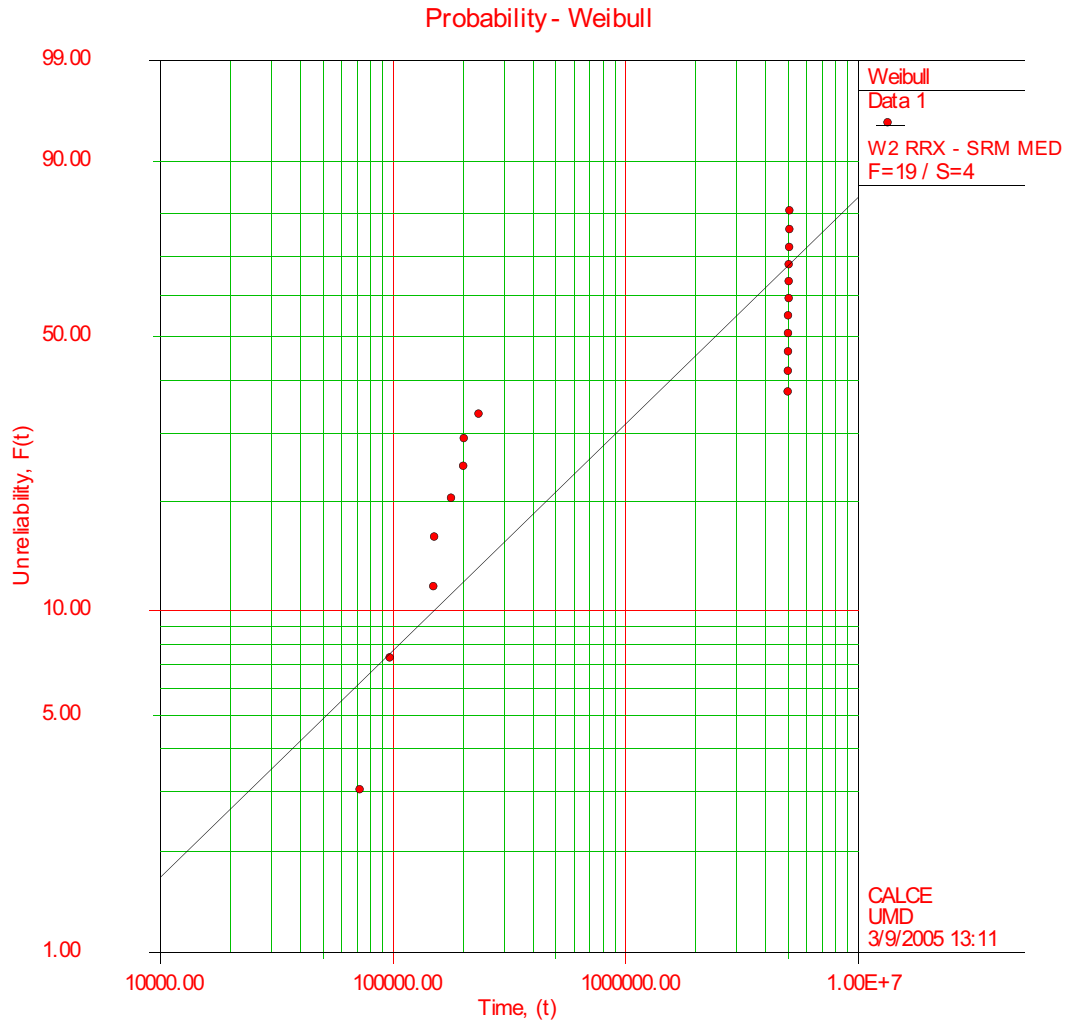
β=0.6764, η=4.1815E+6, ρ=0.8765

Figure A.1 Weibull distribution for SnPb at 850με

Figure A.2 Weibull distribution for SnPb at 1400με
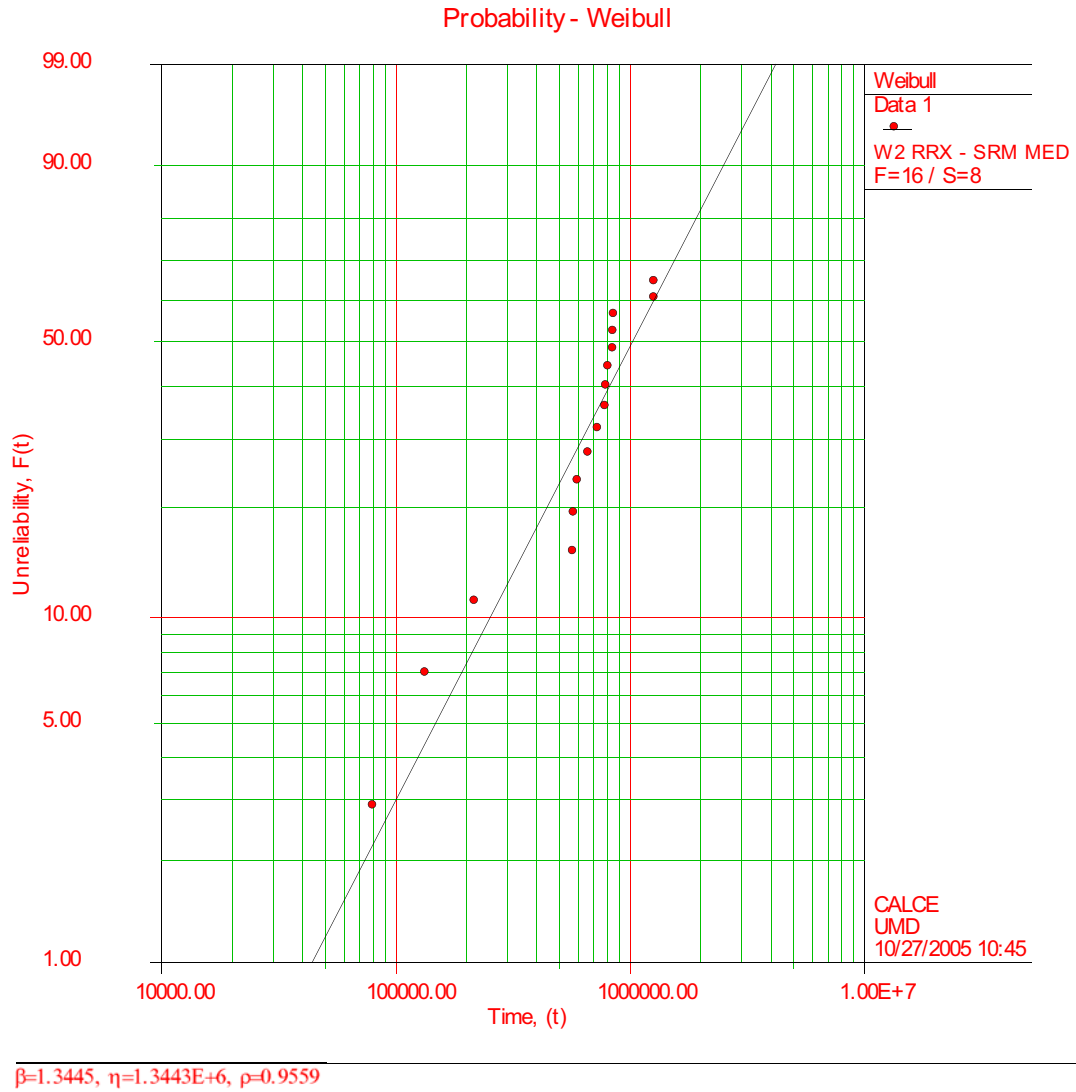
Figure A.3 Weibull distribution for SnPb at 1150με

Probability - Weibull

$\beta=2.4131,\ \eta=1.3946E+5,\ \rho=0.9859$

Figure A.4 Weibull distribution for SnPb at 1350με

Probability - Weibull
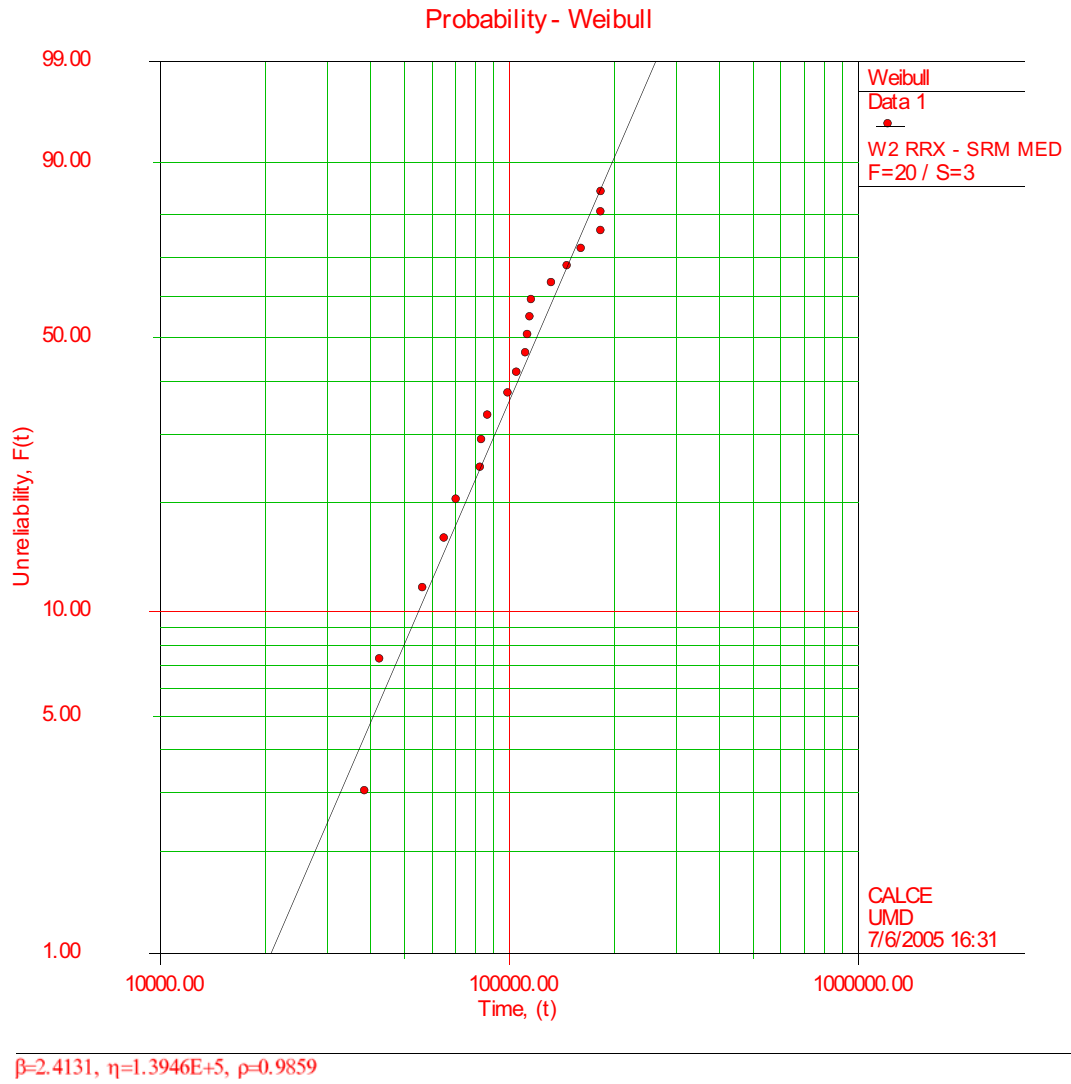

$\beta=2.1339$, $\eta=3.7628E+4$, $\rho=0.7260$

Figure A.5 Weibull distribution for SnPb at 1800µε
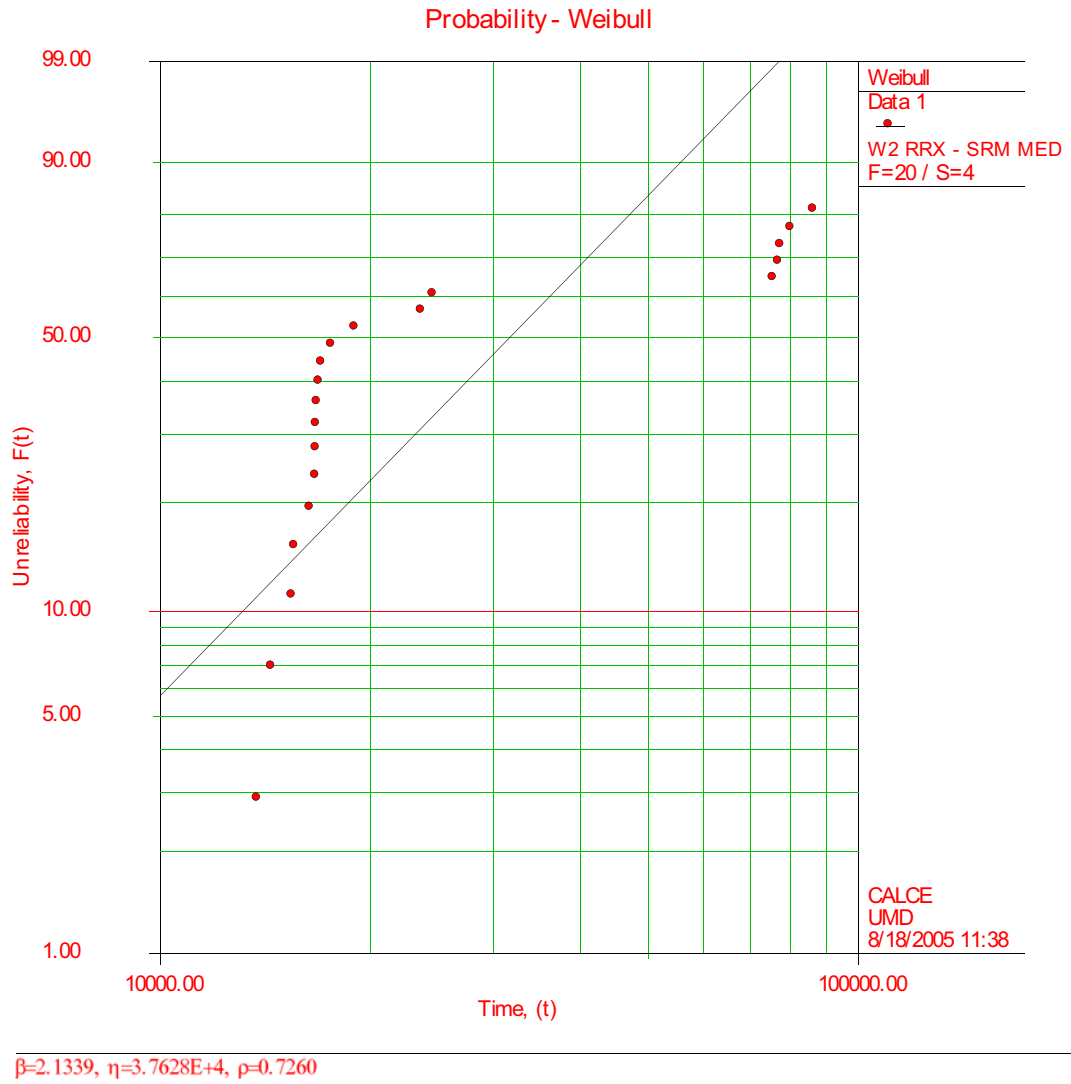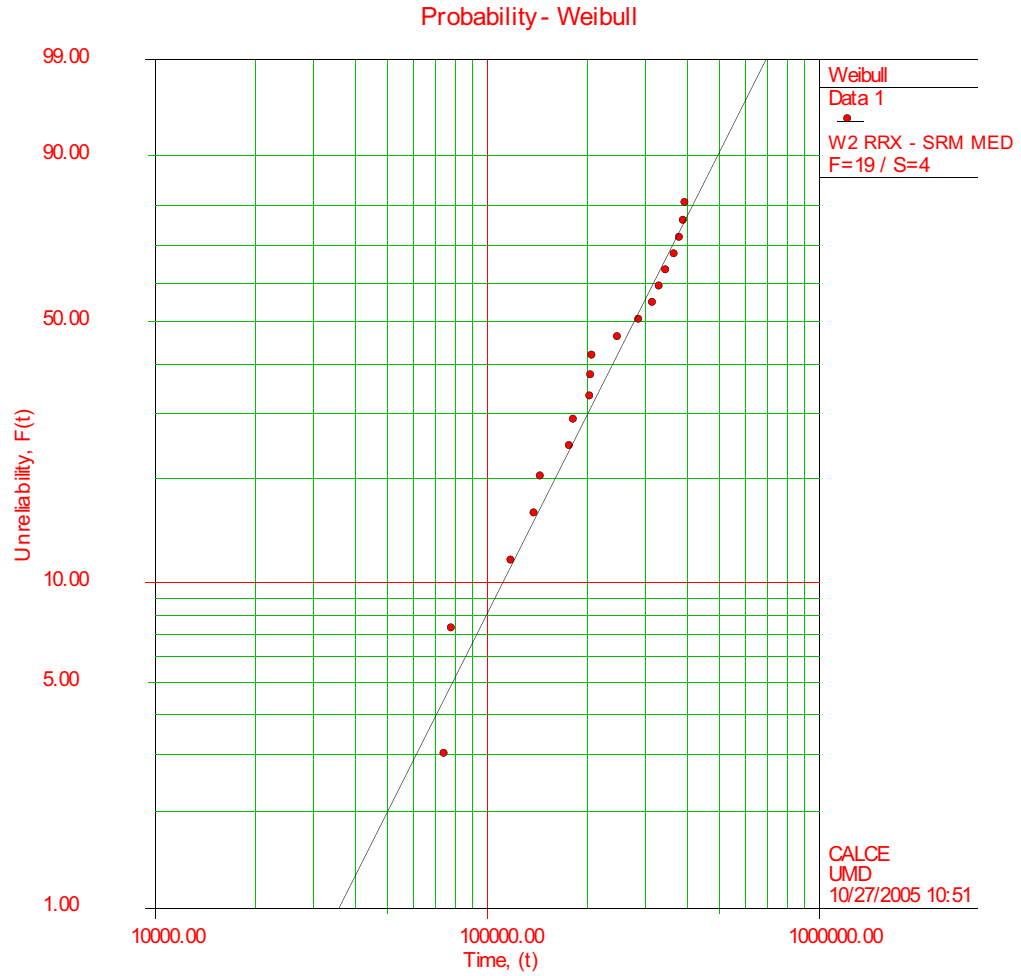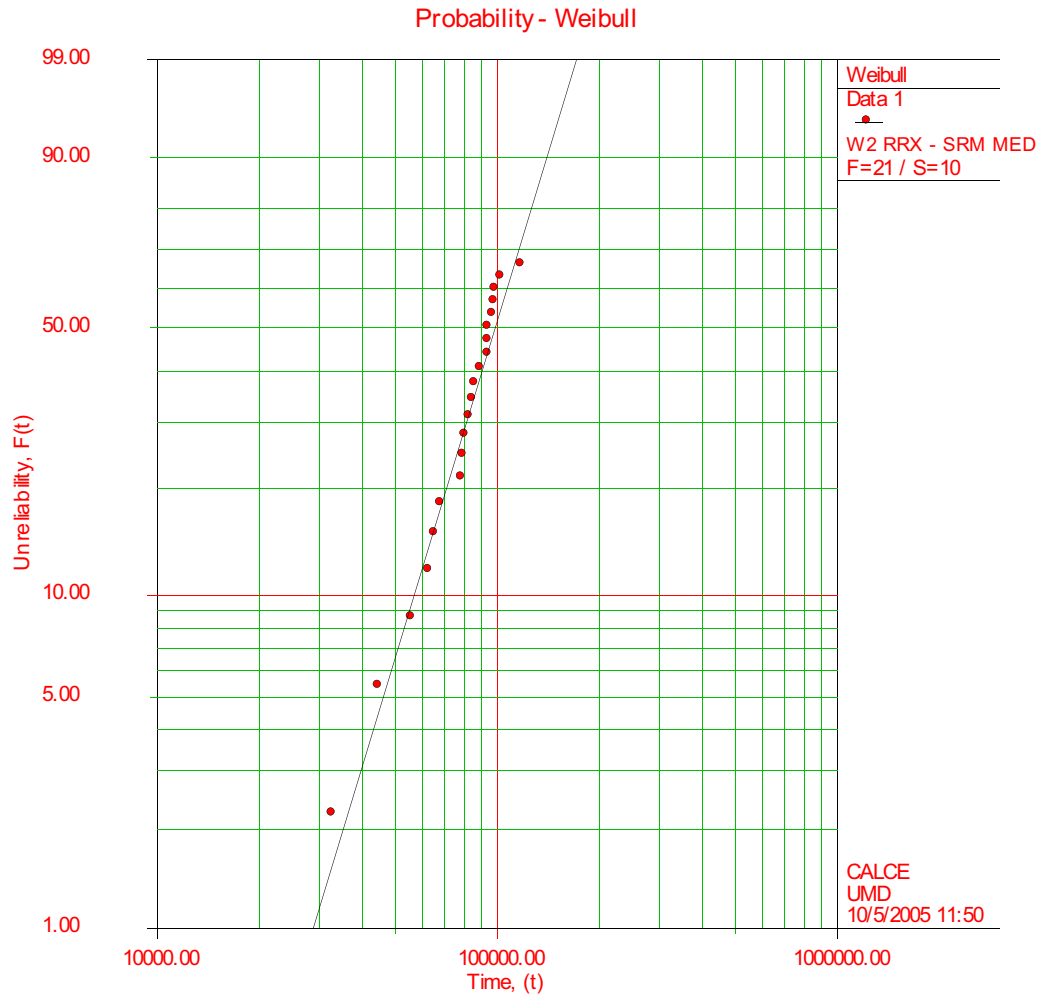
Figure A.6 Weibull distribution for SnPb at 1400με

Figure A.7 Weibull distribution for SAC at 1850 µε
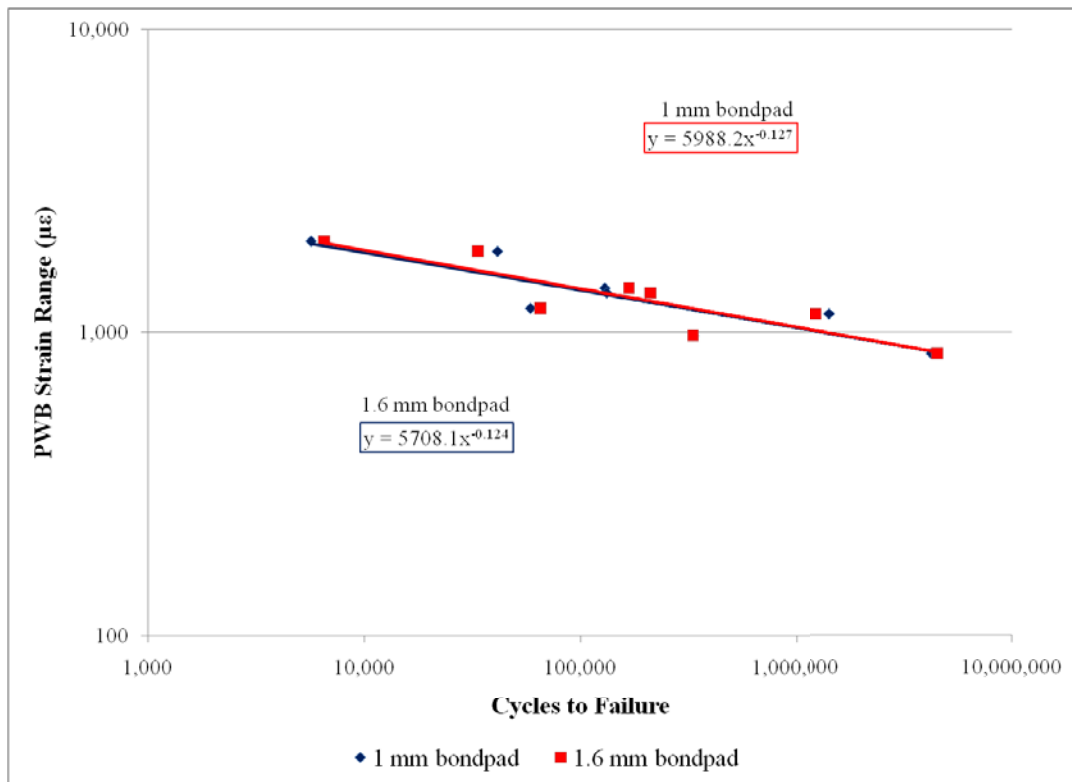
Figure A.8 Effect of bond pad size on LCRs
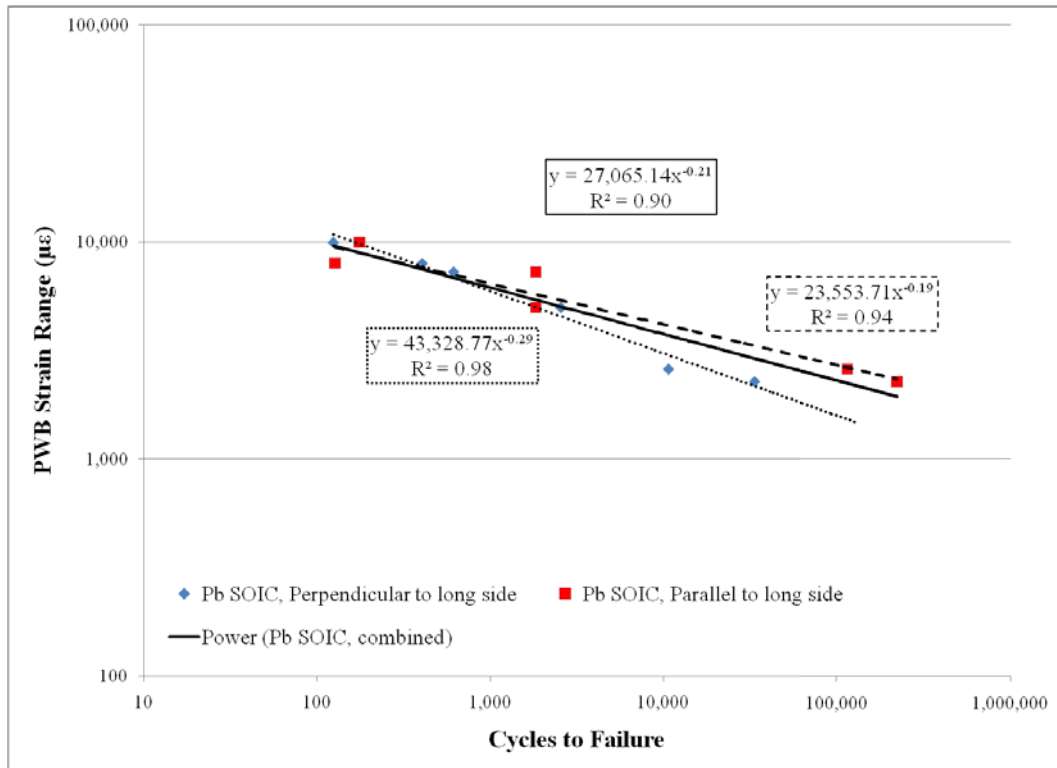
Figure A.9 Effect of component orientation of SOIC failure

PBGA Drop test data and orientation effects

Due to how each side of the drop test coupon was oriented, one side oriented along the diagonal and the other straight, a finite elment analyis was done to determine the affect of orientation on the stress in the solder. The FEA models are shown in the appendix. The stress in the solder for the diagonal model are siginificantly higher than in the straight model. The drop test results are listed in Table 3.2.1. BGAs 1 through 5 are located such that they are loaded on the straight and BGAs 6 through 11 are loaded on the diagonal. There are a total of 22 failures, 18 on the straight and 14 on the diagonal. However, ten of the failure on the straight loaded model are the center compoents. Removing the center loacted component (PBGA 5) from this analysis leaves only eight accurances of failures in the radially loaded components. Table 3.2.1 lists the PBGA that failed, the drop number on which it failed, and the orientation of each PBGA to better illustrate this.

Table A1. Drop Test Data

Solder Type	Acceleration (g)	Max Strain (με)	Failed (Drop Number)	Diagonal, Straight, or Center?	Total Drops
Sn37Pb	500	3000	BGA2 (2) BGA 5(2) BGA 6 (3)	Straight Center Diagonal	3
Sn37Pb	6400	2900	BGA 8(4)	Diagonal	8
Sn37Pb	3200	2500	BGA9 (1) BGA 5(2)	Diagonal Center	6
Sn37Pb	13000	3000	BGA7 (1) BGA 5(2) BGA 1 (2) BGA 6 (3)	Diagonal Center Straight Diagonal	6

			BGA7 (1)	Diagonal	
Sn37Pb	7500	3000	BGA 5(2)	Center	10
			BGA 6 (6)	Diagonal	
			BGA 3 (7)	Straight	
			BGA7 (1)	Diagonal	
			BGA 5(3)	Center	
Sn37Pb	4000	2300	BGA 6 (30)	Diagonal	100
			BGA 4 (62)	Straight	
			BGA 2 (75)	Straight	
			BGA5 (11)	Canter	
Sn37Pb	2900	2460	BGA 6(21)	Diagonal	100
			BGA 7 (25)	Diagonal	
			BGA 3 (71)	Straight	
Sn37Pb	3600	3300	BGA5 (5)	Center	10
SAC305	7500	3400	BGA 5 (1)	Center	6
SAC305	3200	2700	BGA 5 (2)	Center	6
			BGA8 (1)	Diagonal	
			BGA 5(5)	Center	
SAC305	2200	2500	BGA 6 (22)	Diagonal	180
			BGA 7 (81)	Diagonal	
			BGA 2 (119)	Straight	
			BGA 9 (159)	Diagonal	

PWB behavior analysis during drop event

In real world situations, a camped boundary condition does not exist. Yielding at the clamped edges eliminates the effect the clamping force and transfers the moment to the central part of the plate [61]. A good estimate of the effect of a clamped boundary condition is to average the ideal equations for clamped boundary condition and simply supported conditions. However, if the thickness divided by the radius is less than 0.1 and the deflection is less about one-half the thickness, as is in this case, then the equations for ideal clamped conditions provide a good estimate for actual plate deflection. The deflection equation for a circular plate with fixed edges subject to a uniform lateral pressure is

$$w = \frac{p_0 a^4}{64D} \left[1 - \left(\frac{r}{a}\right)^2\right]^2$$

,

where a is the radius of the plate, r is the radius of the central loaded area, h is the thickness of the plate, p is the load per unit area, D is the flexural rigidity and

$$D = \frac{Eh^3}{12(1 - v^2)}$$

where v is the Poisson ratio, and E is the Young's Modulus. The moments in the radial and theta direction are given by

$$M_{rr} = \frac{p_0 a^4}{64D} \left[1 + v - (3 + v)\left(\frac{r}{a}\right)^2\right]$$

$$M_{\theta\theta} = \frac{p_0 a^4}{64D} \left[1 + v - (1 + 3v)\left(\frac{r}{a}\right)^2\right]$$

The strain in the radial direction can then be calculated using

$$\epsilon_{rr} = M_{rr} - \nu M_{\theta\theta}.$$

This theoretical radial strain value is plotted along with strain data from test board 8 in Figure A.10. Note that this theoretical strain value is for a bare FR-4 board. The weights of the drop table and of the fixture were used to calculate a suitable value for the pressure constant for the theoretical calculations. As shown in the plot the edges of the test coupon behave in accordance with the theoretical values. The portion of the board however does not. This is possibly due to the PBGA located on the board. They act as stiffeners on the board. Also the theoretical strain behavior only accounts for the fundamental behavior of the PWB. As stated earlier, there appears to be more than the fundamental mode present during the initial dropping of the test specimen.

The location of possible inflection was calculated using beam theory. For fixed (clamped) supports under uniform loading, the inflection point is found using [60]

$$x_{infl} = 0.2113L$$

The dashed lines in Figure A.10 represent the possible location of these inflection points. However no decernable effects of these inflection point are seen in the strain data.
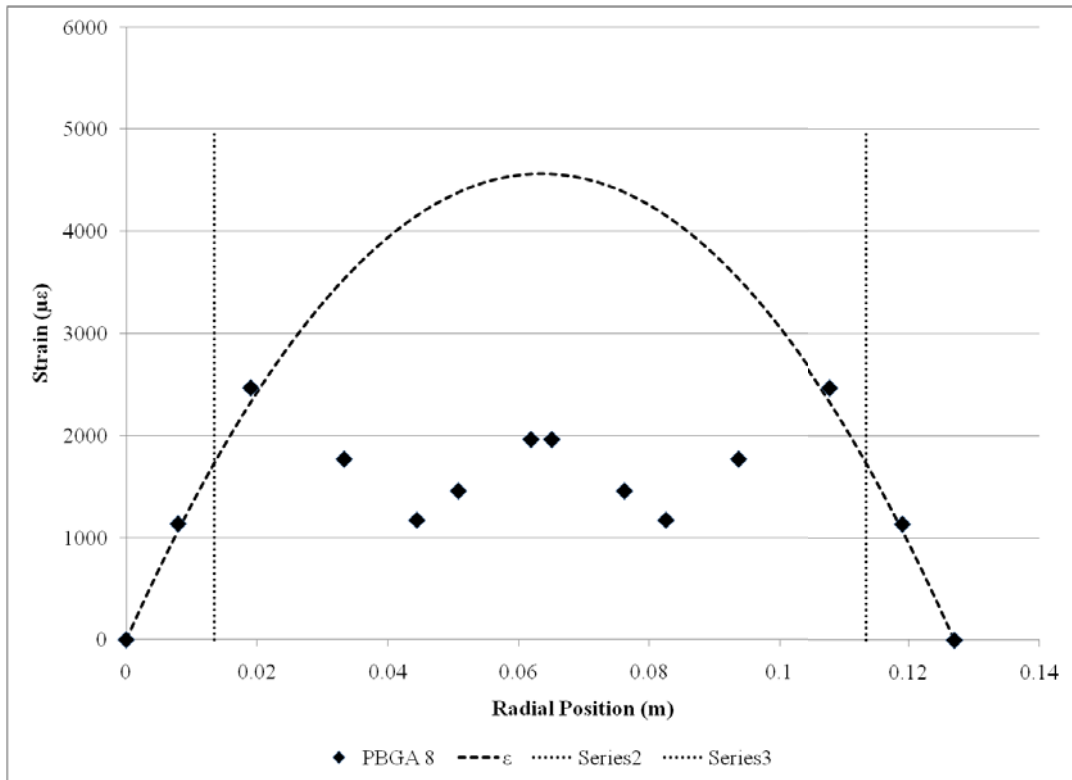
Figure A.10 Theoretical vs. actual strain during drop for clamped edge conditions

This high rate PBGA testing can also be compared with similar high rate testing done by Watkins[42]. That testing was performed on 0402, 0603, and 1206 sized capacitors to understand how they behaved under high rate loading. The same drop test fixture used by this study was used. The strains seen by Watkins were significantly lower than the strains presented here.

This strain discrepancy is possibly due to the face that Watkins grinded out a portion of the test coupon for leveling. This gave the location of the strain gages a different thickness than that of the surrounding test coupon. The Watkins study also obtained its strain data from an unpopulated test coupon. The Figure A.11 shows the

maximum strain values by location plotted from the Watkins study and this PBGA study. The strain values for the Watkins study are on the secondary vertical axis. Similar trend exists in the behavior of the PWB for the two studies despite the PBGA test coupon being populated during the strain data acquisition. The lines between the strain values are used here only to demonstrate the trend in the data.
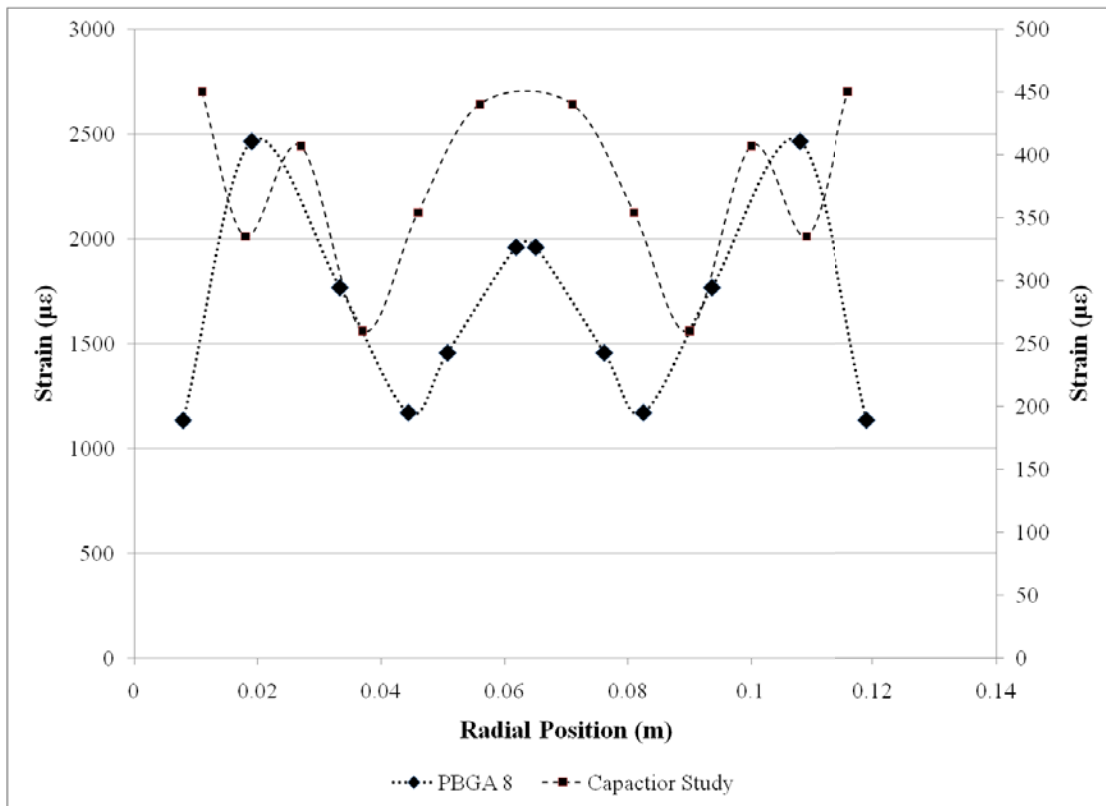

Figure A.11 Board Response Comparison

PBGA Top/Bottom Analysis

To better understand how the packages behaved under drop loading conditions, the PBGA packages were strain gaged on top of the component and on the PWB beneath the component. Figure X shows the response of the two Practical brand PBGAs. The

strain over maximum strain is plotted versus time in seconds. One is SnPb eutectic and the other is the leadfree version using Sn3.0Ag0.05Cu. Both test coupons were dropped at the same accleration of 4000 G's. This data shows that though there are different solder types being used both components behave simialarly at the same acceleration level.
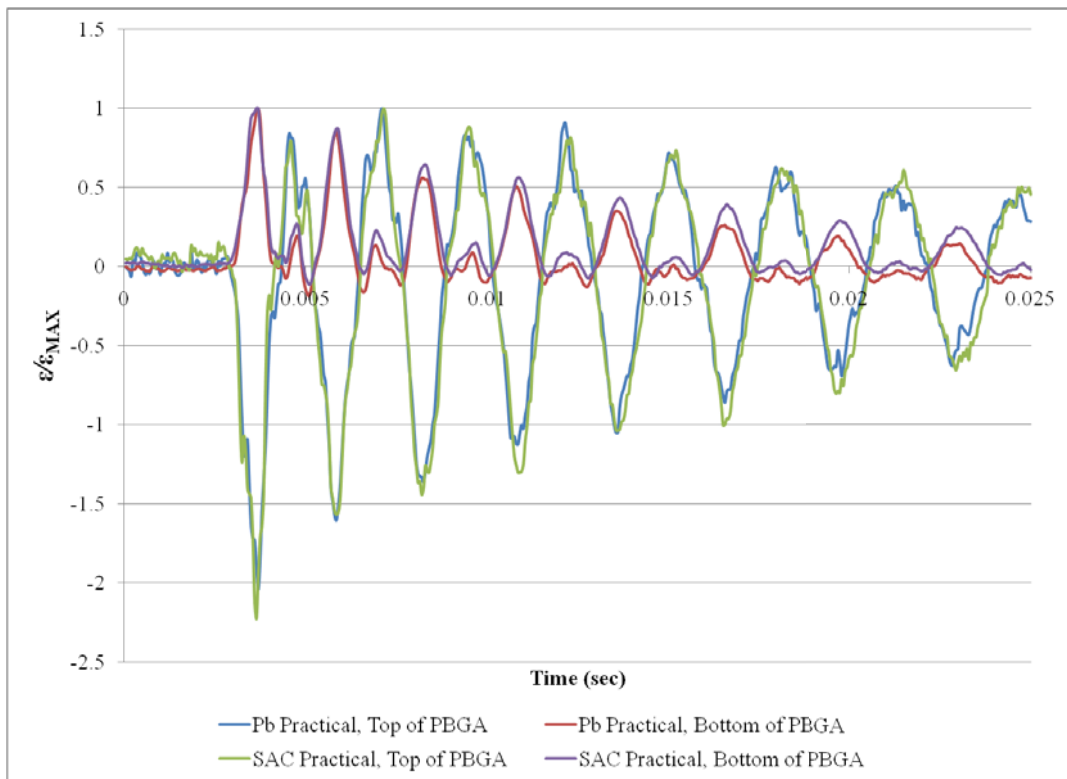
Figure A.12 Comparison of Practical lead and lead-free PBGA coupons

This same test was run for the Topline brand components used in Watkins et. al. [] and the SnPb eutectic Practical components. The dummy die size in the Topline component is 5mm by 5m; whereas, the dummy size in the Practical component is

7mm by 7mm. The response profile is the same general shape and level for both component types. There is a phase shift in the reaction of the two components. For comparison sakes, however, since the levels are the same for both tests, the values of strain response of the two component types can be compared.
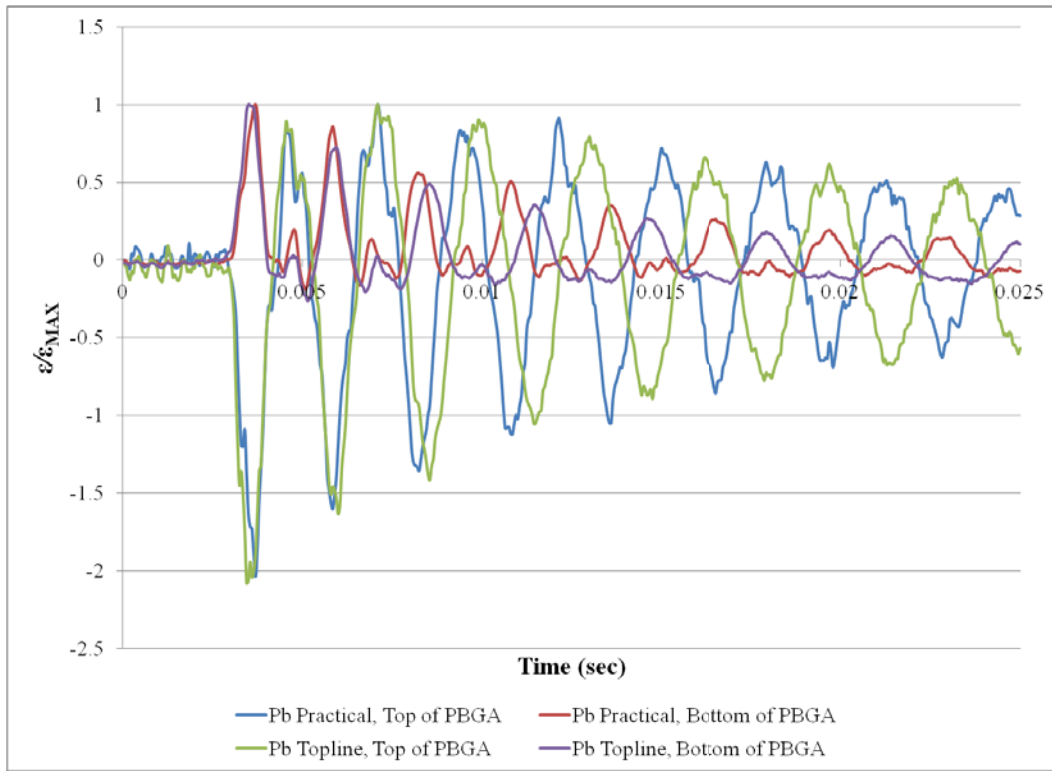
Figure A. 13 Comparison of Topline and Practical brand PBGAs

Figure A.14 Unadjusted/Incorrectly plotted LCR, BGA, and PBGA data with PWB strain

The data shown above is the LCR, BGA, and PBGA data plotted against the PWB strain. Using the PWB strain will cause incorrect inferences drawn between the different data sets. The data was shown in Chapter 6 to collapse into a closer range with the use of a interconnect stress index.
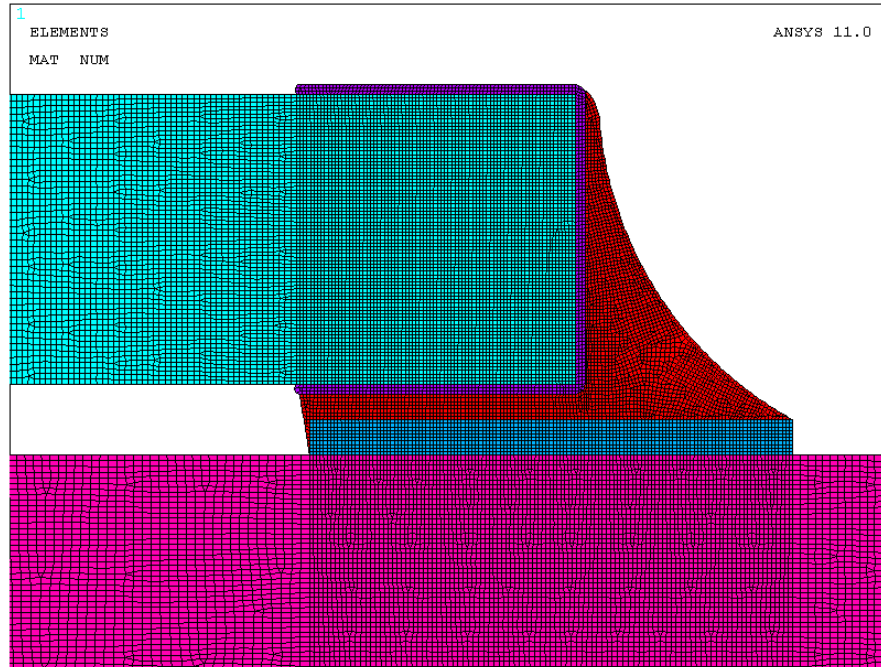
Figure A.15 2512 LCR FEA Model Mesh
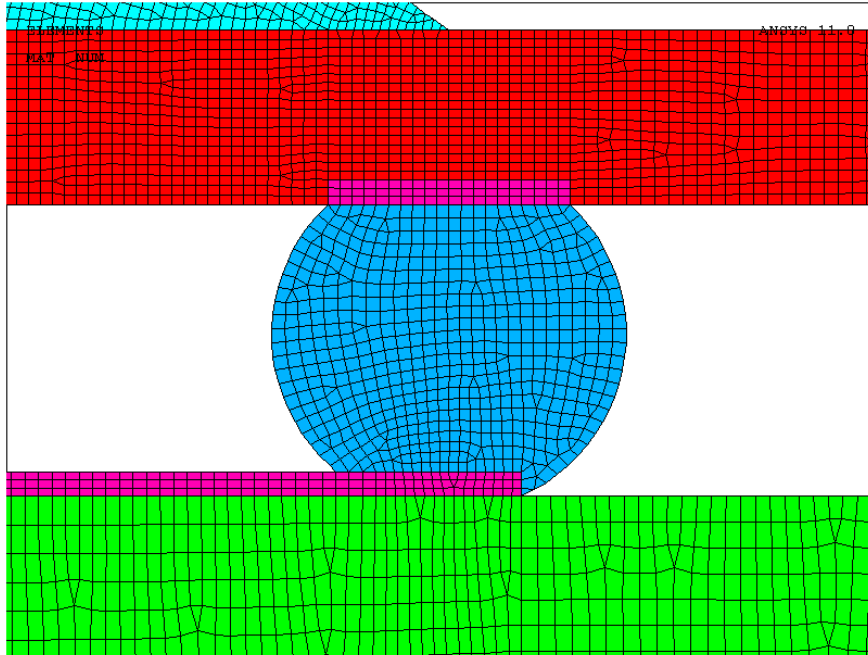
Figure A.16 PBGA 256 I/O, 1 mm pitch, Topline and Practical brand FEA Model (Mesh)
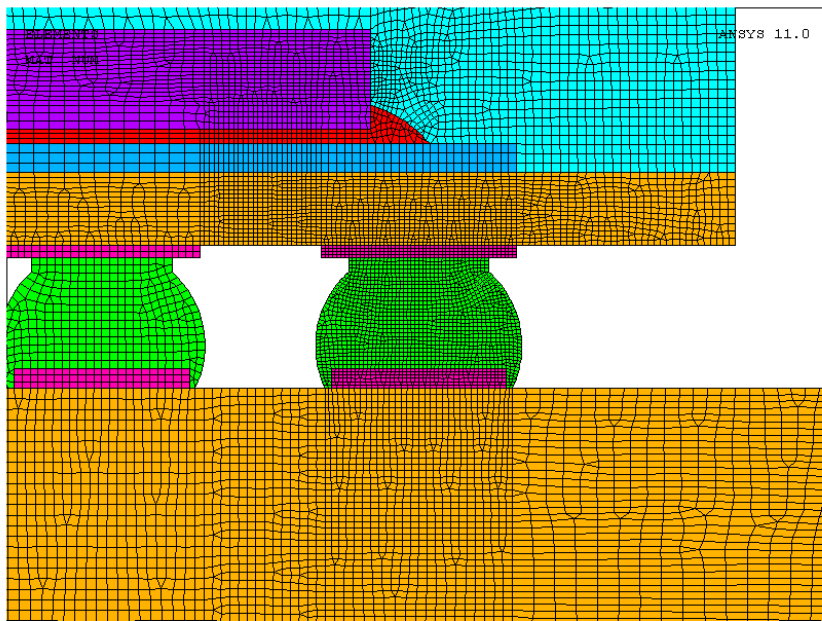
Figure A.17 BGA, 160 I/O, 0.8 mm pitch Amkor brand FEA Model (Mesh)

PBGA and LCR PWB strain and stress values from FEA

PBGA 256 I/O, 1 mm pitch, Topline and Practical brand

SAC305

 Strain=2728, Stress=22.8MPa

Sn37Pb

Strain=2728, Stress=19.8MPa

BGA, 160 I/O, 0.8 mm pitch Amkor brand

<u>4 Balls (center of BGA)</u>

SAC305

Stress=28.7MPa; Strain board=2385; Strain Bottom=1125

Sn37Pb

Stress=28.1 MPa; Strain Board=2391; Strain Bottom=1139

<u>7 Balls (perimeter of BGA)</u>

SAC305

Stress=32.6MPa; Strain board=2765; Strain Bottom=1076

Sn37Pb

Stress=32.2MPa; Strain Board=2772; Strain Bottom=1320

2512 Resistor

SAC

Strain on board= 2532

Stress(average in 10% of solder)= 26.9 MPa

Sn37Pb

Strain on board= 2532

Stress(average in 10% of solder)= 26.7 MPa

.

References

[1] Center for Advanced Life Cycle Engineering (CALCE) Electronic Products and Systems Center, project proposal, University of Maryland College Park.

[2] Wu, Mei-Ling. Rapid assessment of BGA fatigue life under vibration loading. Doctoral dissertation: University of Maryland, 2006, College Park, Md, http://hdl.handle.net/1903/3940.

[3] Steinberg, Dave S. *Vibration Analysis for Electronic Equipment*, Wiley-Interscience, New York, 1988.

[4] Guo, Quiang, Mei Zhao, HangFang Wang, "SMT solder joint's semi-experimental fatigue model," Mechanics Research Communications, Vol. 32, 2005, pp. 351-358.

[5] Shetty, Santosh, and Tommi Reinikainen, "Three- and Four-Point Bend Testing for Electronic Packages," Transactions of the ASME, Vol. 125, December 2003, pp. 556-561.

[6] Park , Tae-Sang, and Soon-Bok Lee, "Low cycle Fatigue Testing of Ball Grid Array Solder Joints under Mixed Mode Loading Conditions," Journal of Electronic Packaging, Vol. 127, September 2005, pp. 237-244.

[7] Barker, D., Y. Chen, and A. Dasgupta, Estimating the Vibration fatigue Life of Quad Leaded Surface Mount Components, Journal of Electronic Packaging, Vol. 115, Issue 2, June 1993, pp. 195-200.

[8] Sidharth and D. B. Barker, Vibration Induced Fatigue Life Estimation of Corner Leads of Peripheral Leaded Components, Journal of Electronic Packaging, Vol. 118, Iss. 4, December 1996, pp. 244-9.

[9] Sun, Peng, Cristina Anderson, Xicheng Wei, Liqiang Cao, Zhaonian Cheng, and Johan Liu, "Low cycle fatigue testing and simulation of Sn-8Zn-3Bi and Sn-37Pb solder joints." Soldering and Surface Mount Technology, 2005, pp. 38-44.

[10] Wang, Y. Y., C. Lu, J. Li, X. M. Tan, Y. C. Tse, "Simulation of drop/impact reliability for electronic devices," Finite Element in Analysis and Design, Vol. 41, 2005, pp. 667-680.

[11] Wong, E. H., K. M. lim, N. Lee, S. Seah, C. Hoe, J. Wong, "Drop Impact Test-Mechanics & Physics of Failure," ECTC Conference 2002, pp. 327-333

[12] Zhou, Y., E. Scanff, and A. Dasgupta,Vibration Durability Comparison of Sn37Pb vs SnAgCu Solders, 2006 ASME International Mechanical Engineering Congress and Exposition, Chicago, Illinois, November 5-10, 2006.

[13] Zhou, Y., and A. Dasgupta, Vibration Durability Assessment of Sn3.0Ag0.5Cu & Sn37Pb Solders under Harmonic Excitation, 2007 ASME International Mechanical Engineering Congress and Exposition, Seattle, Washington, November 11-17, 2007.

[14] Zhang Qian, Abhijit Dasgupta, Peter Haswell, and Michael Osterman, "Isothermal Mechanical Fatigue of Pb-free Solders: Damage Propagation Rate & Time to Failure," *34th International SAMPE Technical Conference*, Baltimore, MD, November 4-7, 2002.

[15] Lund, Eivind and Terje G. Finstad, Design and construction of a four-point bending based set-up for measurement of piezoresistance in semiconductors, Rev. Sci. Instrum., Vol. 75, Iss. 11, 2004.

[16] Harada, Kozo, Shinji Baba, Qiang Wu, Hironori Matsusshima, Toshihiro Matsunaga, Yasumi Uegai, and Michitaka Kimura, "Analysis of Solder Joint Fracture under Mechanical Bending Test," 2003 Electronic Components and Technology Conference, pp. 1731-1737.

[17] Ilho, Kim and Lee Soon-Bok, "Reliability Assessment of BGA Solder Joints under Cyclic Bending Loads," 2005 International Symposium on Electronics Materials and Packaging (EMAP2005), December 11-14, 2005, pp 27-32.

[18] Shetty, Santosh, and Tommi Reinikainen, "Three- and Four-Point Bend Testing for Electronic Packages," Transactions of the ASME, Vol. 125, December 2003, pp. 556-561.

[19] Lall, Pradeep, Dhananjay Panchagade, Deepti Iyengar, and Jeff Suhling, "Life Prediction and Damage Equivalency for Shock Survivability of Electronic Components," Thermal and Thermomechanical Phenomena in Electronics Systems, May 30- June 2, 2006, pp. 804- 816.

[20] Darveaux, Robert, Coery Reichman, and Nokibul Islam, "Interface Failure in Lead Free Solder Joints," 206 Electronic Components and Technology Conference, pp. 906-917.

[21] Chong, Desmond Y. R., F. X Che, John H. L. Pang, Kellin Ng, Jane Y. N. Tan, and Patrick T. H. Low, "Drop impact reliability testing for lead free and

lead based soldered IC packages," Microelectronics Reliability, Vol. 46, 2006, pp1160-1171.

[22] Suhir, E. "Could Shock Tests Adequately Replace Drop Tests?" 8th International Symposium on Advanced Packaging Materials, 2002, pp. 67-81.

[23] Seah, S. K. W., E. H. Wong, Y. W. Mai, R. Rajoo, and C. T. Lim, "Failure Mechanism of Interconnections in Drop Impact," ," 2006 Electronic Components and Technology Conference, 2006, pp. 1484-1492.

[24] Wong, E. H., P. Rajoo, Y. W. Mai, S. K. W. Seah, K. T. Tsai, and L. M. Yap, "Drop Impact: Fundamentals & Impact Characterisation of Solder Joints," 2005 Electronic Components and Technology Conference, 2005, pp. 1202-1209.

[25] Marjamäki, P., T. T. Mattila, and J. K. Kivilahti, "A Comparative Study of the Failure Mechanisms Encountered in Drop and Large Amplitude Vibration Tests," 2006 Electronic Components and Technology Conference, 2006, pp. 95-101.

[26] Darveaux, R., and K. Banerji, Constitutive relations for tin-based solder joints, IEEE Transactions on Components, Hybrids, and Manufacturing Technology, Vol. 15, Iss, 6, December 1992, pp. 1013-1024.

[27] Rooney, Daniel T., N. Todd Castello, Mike Cibulsky, Doug Abbott, and Dongji Xie, "Materials characterization of the effect of mechanical bending on area array package interconnects," Microelectronics International, Vol. 20, Iss. 1, Apr 2003, pp. 34 – 42.

[28] Jonnalagadda, Krishna, Fangjuan Qi, and Jim Liu, "Mechanical Fatigue Reliability of PBGA Assemblies with Lead-free Solder and Halogen-free PCBs," 2004 Inter Society Conference on Thermal Phenomena, 2004, pp. 165-170.

[29] Varghese, J, and A. Dasgupta, "An Experimental Approach to Characterize Rate-dependent Failure Envelopes and Failure Site Transitions in Surface Mount Assemblies," Microelectronics Reliability, 2006.

[30] Woodrow, Thomas A., JCAA/JG-PP No-Lead Solder Project: Vibration Test, Boeing Electronics Materials and Processes Report, 2005, pp. 771-806.

[31] American Competitiveness Institute, Mechanical Shock Environmental Testing of Tin-Lead and Lead-Free Circuit Boards, JCAA/JG-PP lead-free solder project NASA Contract No. NAS10-0329, Final Report.

[32] Zhang, Q., P. Haswel,l and A. Dasgupta, "Isothermal Mechanical Creep and Fatigue of Pb-free Solders," International Brazing & Soldering Conference, San Diego, CA, February 16-19, 2003.

[33] Qi, H., G. Plaza, S. Ganesan, M. Osterman, and M. Pecht, Reliability Assessment on Insertion Mount Assembly under Vibration Conditions, 2007 Electronic Components and Technology Conference, May 29-June 1, 2007, Reno, Nevada, pp. 407-414.

[34] Seah, S. K. W., E. H. Wong, Y. W. Mai, R. Rajoo, and C. T. Lim, "High Speed Bend Test Method and Failure Prediction for Drop Impact Reliability," 2006 Electronic Components and Technology Conference, 2006, pp. 1003-1008.

[35] Qi,, H., S. Ganesan, J. Wu, M. Pecht, P. Matkowski, and J. Felba, Effects of Printed Circuit Board Materials on Lead-free Interconnect Durability, 5th International Conference on Polymers and Adhesives in Microelectronics and Photonics, October 23-26, Wroclaw, Poland, 2005 , pp. 140-144.

[36] Vianco, Paul T. An Overview of Surface Finishes and Their Role in Printed Circuit Board Solderability and Solder Joint Performance. *Circuit World,* March 1999, Vol. 25 Iss. 1, pp. 6 – 24.

[37] Watkins, James. Evaluating the Susceptibility of Electronic Components to Flexural Failures with High Rate Considerations for Sn37Pb Solder, Doctoral dissertation: University of Maryland, 2008, College Park, Md.

[38] Blattau, Nathan and Craig Hillman, "A Comparison of the Isothermal Fatigue Behavior of SnAgCu to SnPb Solder", Surface Mount Technology Association International Conference, Chicago, IL, September 29, 2005

[39] Zhou, Y and A. Dasgupta, "Vibration Durability Assessment of Sn3.0Ag0.5Cu & Sn37Pb Solders under Harmonic Excitation", 2007 ASME International Mechanical Engineering Congress and Exposition, Seattle, Washington, November 11-17, 2007.

[40] Varghese, Joseph, Effect of Dynamic Flexural Loading on the Durability and Failure Site of Solder Interconnects in Printed Wiring Assemblies, Dissertation, University of Maryland College Park, 2007.

[41] Yu, Alan, Prognostics Demonstration of Electronic Components Subjected to Vibration Environment of a Light Military Tactical Vehicle, Masters Thesis, University of Maryland College Park, 2007.

[42] Watkins, James, Evaluating the Susceptibility of Electronic Components Assembled with Leaded Solder to Flexural Failures, with High Rate Considerations, PhD Dissertation, University of Maryland College Park, 2008.

[43] Song, Bo, Reliability evaluation of stacked die BGA assemblies under mechanical bending loads, Masters Thesis, University of Maryland College Park, 2006.

[44] Gu, Jie, Prognostics of Solder Joint Reliability Under Vibration Loading Using Physics of Failure Approach, PhD Dissertation, University of Maryland College Park, 2009.

[45] Fuchs, H. O. and R. I. Stephens, *Metal fatigue in engineering*, New York : Wiley, 1980.

[46] Zhao, X.J.; Caers, J.F.J.M.; Wong, E.H.; Seah, S.K.W.; Driel, W.D.v.; Owen, N.; Lai, Y.-S.; , "Frequency dependent S-N curves for predicting drop impact robustness of Pb-free solder interconnects," *Electronic Components and Technology Conference, 2009. ECTC 2009. 59th* , vol., no., pp.93-99, 26-29 May 2009.

[47] Shigley, Joseph E. and Charles R. Mischke, *Mechanical Engineering Design*, Magraw-Hill, 1989, pp.297-299.

[48] Tan, L. B, S. K. W. Seah, E. H. Wong, Xiaowu Zhang, V. B. C. Tan, and C. T. Lim, "Board Level Solder Joint Failures by Static and Dynamic Loads," 2003 Electronics Packaging Technology Conference, 2003, pp. 244-251.

[49] Wong, E.H. , S.K.W. Seah, C.S. Selvanayagam, R. Rajoo, W.D. van Driel, J.F.J.M. Caers, X.J. Zhao, N. Owens, M. Leoni, L.C. Tan, Y.-S. Lai and C.-L.

Yeh7, High-Speed Cyclic Bend Tests and Board-Level Drop Tests for Evaluating the Robustness of Solder Joints in Printed Circuit Board Assemblies, Journal of Electronic Materials ,Volume 38, Number 6, June 2009, pp 884-895.

[50] Qi, Haiyu Qi, Mikyoung Lee, Michael Osterman, Kyujin Lee, Seyong Oh, and Tim Schmidt, Simulation Model Development for Solder Joint Reliability for High Performance FBGA Assemblies, 20th IEEE SEMI-THERM Symposium, 2004

[51] Osterman, Michael and Michael Pecht, Strain range fatigue life assessment of lead-free solder interconnects subject to temperature cycle loading, Soldering & Surface Mount Technology, Vol 19, Issue 2, 2007, pp 12–17.

[52] Osterman, Michael and Abhijit Dasgupta, Life expectancies of Pb-free SAC solder interconnects in electronic hardware, Journal of Materials Science: Materials in Electronics, Volume 18, Numbers 1-3, March, 2007, pp 229-236.

[53] Technical Reports for the Lead Free Solder Project: Properties Reports: "Room Temperature Tensile Properties of Lead-Free Solder Alloys;" Lead Free Solder Project CD-ROM, National Center for Manufacturing Sciences (NCMS), 1998.

[54] Wiese S. and S. Rzepka ,Time-independent elastic-plastic behaviour of solder materials (2004) Microelectronics Reliability, 44 (12), pp. 1893-1900.

[55] Rodney J. McCabe and Morris E. Fine, "Athermal and Thermally Activated Plastic Flow in Low Melting Temperature Solders at Small Stresses," Scripta Materialia 39(2), 189 (1998).

[56] Paquette, Beth, D. Barker, and M. Osterman, Long-term Vibration Fatigue Life of Pb-free Interconnects, CALCE EPSC Technical Review Meeting, Fall 2009.

[57] Keat, Loh Wei, Lee Yung Hsiang, Ajay A/l Murugayah, and Tay Tiong We, "Nonlinear Dynamic Behavior of Thin PCB Board for Solder Joint Reliability Study under Shock Loading," 2005 International Symposium on Electronic Materials and Packaging, December 11-14, 2005, pp. 268-274.

[58] Ma, Hongtao, Constitutive models of creep for lead-free solders, Journal of Material Science, 2009, Vol 44 pp. 3841–3851.

[59] Ma, Hongtao, and Jeffrey C. Suhling, A review of mechanical properties of lead-free solders for electronic packaging, Journal of Material Science, 2009, Vol 44 pp. 1141–1158.

[60] Shigley, J. E., Mischke, C. R., Mechanical Engineering Design, 5 th ed., McGraw-. Hill, New York, 1989

[61] Boresi , Arthur P. and Richard J. Schmidt, Advanced Mechanics of Materials, Wiley; 6 edition (October 22, 2002)

[62] Meier, K, S. Wiese, M. Roellig, K. –J. Wolter, "Mechanical Characterisations of Lead Free Solder Alloys under High Strain Rate Loads," 2009 Electronic Components and Technology Conference, pp. 1781-1787.

[63] Wang, B. and S. Yi, "Dynamic plastic behavior of 63 wt% Sn wt%Pb eutectic solder under high strain rates," Journal of Material Science Letters, Vol 21, 2002, pp. 697-8.

[64] Geng, Phil, Philip Chen, and Yun Ling, "Effect of Strain Rate on Solder Joint Failure Under Meachincal Load," 2002 Elcetronic Components and Technology Conference, pp. 974-978.

[65] Keat, Loh Wei, Lee Yung Hsiang, Ajay A/l Murugayah, and Tay Tiong We, "Nonlinear Dynamic Behavior of Thin PCB Board for Solder Joint Reliability Study under Shock Loading," 2005 International Symposium on Electronic Materials and Packaging, December 11-14, 2005, pp. 268-274.